

UNIVERSITY OF STRATHCLYDE
FACULTY OF ENGINEERING
DEPARTMENT OF CIVIL AND ENVIRONMENTAL ENGINEERING



Elodie Coudert

**USE OF ALKALI ACTIVATED FLY ASH BINDER FOR SOIL
STABILISATION: A MULTI-SCALE APPROACH**

Thesis for the Ph.D. degree in
Civil and Environmental Engineering
2019

TUTORS

Prof. Giacomo Russo

Prof. Alessandro Tarantino

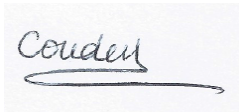
Dr. Dimitri Deneele

Declaration of Authenticity and Author's Rights

This thesis is the result of the author's original research. It has been composed by the author and has not been previously submitted for examination which has led to the award of a degree.

The copyright of this thesis belongs to the author under the terms of the United Kingdom Copyright Acts as qualified by University of Strathclyde Regulation 3.50. Due acknowledgement must always be made of the use of any material contained in, or derived from, this thesis.

Signed:

A handwritten signature in cursive script, appearing to read "Couder", is written on a light-colored rectangular background. A horizontal line is drawn underneath the signature.

Date: 4th June 2019

This study addresses the use of alkali activated fly ash-based binder to improve engineering characteristics of soils, and as a substitute to usual high-carbon footprint stabilisers such as lime and Ordinary Portland Cement. In particular, it examines the use of a calcium-rich fly ash from coal combustion binder activated by a sodium-based alkaline solution for kaolin treatment. The global aim is to explore the feasibility of using this binder as a potential soil stabiliser. To do so, a multi-scale analysis that conjointly explores the physicochemical evolution of the system, its microstructure and mechanical performances was carried out.

At a particle level, calcium-rich particles from fly ash constitute the reactive part of the mix. Their dissolution releases calcium that subsequently combines with silicon and potentially aluminium to form chains whose structure resembles the one of Calcium Silicate Hydrate encountered in Portland Cement and responsible of a mechanical improvement. At a microstructural level, a denser material is consequently formed over time because of the filling of pores by the new compounds. Different heterogenous matrices of various porosity and arrangement are however observed across the material and owed to the high heterogeneity of fly ash whose particles locally react differently. Finally, at a macroscopic level, those changes lead to an improvement of the treated soil resistance to compression and shear forces. The maximum stability is achieved after 28 days for 10 % of added binder, and with an effectiveness suitable for field applications. This study hence confirms a positive feasibility potential of using calcium-rich fly ash-based alkali activated binder for kaolin soil stabilisation.

Keywords:

Soil stabilisation

Alkali activated material

Kaolin

Fly ash

Preface and Acknowledgements

I am extremely grateful to all and every unique persons that crossed my path during the PhD. I have learnt so much from everyone and feel deeply enriched equally from hardships to laughers to sharing.

Thank you, Grazie & Merci.

Table of Contents

Chapter 1	Introduction.....	1
Chapter 2	Literature review	7
2.1	Introduction to Alkali Activated Material and Geopolymer	8
2.1.1	How to create Alkali Activated Material and Geopolymer products?	8
2.1.2	History of wordings: Alkali Activated Material vs. Geopolymer	8
2.1.3	Mechanism.....	9
2.1.3.1	Low-calcium systems.....	9
2.1.3.2	High-calcium systems.....	11
2.1.4	Structure.....	12
2.1.4.1	N–A–S–H and K–A–S–H gels.....	12
2.1.4.2	Geopolymer structure	13
2.1.5	Properties.....	14
2.1.6	Experimental tools adapted	15
2.2	Synthesis conditions.....	17
2.2.1	Aluminosilicate source.....	17
2.2.1.1	Chemical composition.....	17
2.2.1.2	Mineralogical characteristics.....	18
2.2.2	Alkaline activating solutions	19
2.2.2.1	Alkali hydroxides.....	19
2.2.2.2	Alkali silicates.....	20
2.2.2.3	Mix of alkali silicate and hydroxide.....	21
2.2.2.4	Influence of alkali cation type: potassium and sodium.....	21
2.2.3	Water demand.....	23
2.2.4	Other synthesis conditions.....	24
2.2.4.1	Temperature	24
2.2.4.2	Curing time	25
2.2.4.3	How to stop alkali activation reactions?.....	25
2.3	Use of Alkali Activated Materials for soil stabilisation.....	25
2.3.1	Global context and key issues	25
2.3.2	Alkali activation of naturally occurring clay minerals at ambient temperature	26
2.3.3	Overview of research on alkali activated soils	27

2.3.4	Choice of a reactive aluminosilicate	29
2.3.4.1	Possibilities.....	29
2.3.4.2	Coal fly ash.....	29
2.4	Summary and conclusions	30
2.5	References	32
Chapter 3 Use of alkali activated fly ash binder for kaolin clay soil stabilisation: Physicochemical evolution..... 37		
3.1	Abstract	39
3.2	Introduction	40
3.3	Material and methods	41
3.3.1	Materials.....	41
3.3.2	Sample preparation.....	42
3.3.3	Methods	43
3.4	Results and discussion	44
3.4.1	Alkali activated fly ash binder.....	44
3.4.1.1	X-ray diffraction (XRD)	44
3.4.1.2	Derivative thermogravimetric analysis (DTG).....	45
3.4.1.3	Fourier Transform Infrared spectroscopy (FTIR)	46
3.4.1.4	Scanning Electron Microscopy (SEM)	48
3.4.1.5	Nuclear Magnetic Resonance (NMR).....	50
3.4.1.6	pH evolution.....	52
3.4.2	Interaction between the alkali activated fly ash binder and kaolin	53
3.4.3	Comparison with lime treated kaolin	60
3.4.3.1	Reactivity of initial phases	61
3.4.3.2	Reactivity timescale.....	62
3.4.3.3	Stability and structure of the compounds formed.....	62
3.5	Conclusions	65
3.6	References	66
Chapter 4 Use of alkali activated fly ash binder for kaolin clay soil stabilisation: Microstructural evolution..... 70		
4.1	Abstract	72
4.2	Introduction	73
4.3	Material and methods	75
4.3.1	Materials.....	75
4.3.2	Sample preparation.....	75

4.3.3	Methods	76
4.4	Results and discussion	76
4.4.1	Raw fly ash.....	76
4.4.2	Alkali activated fly ash binder.....	78
4.4.2.1	Optical Microscopy	78
4.4.2.2	Scanning Electron Microscopy (SEM)	79
4.4.2.3	Mercury Intrusion Porosimetry (MIP)	86
4.4.3	Interaction between the alkali activated fly ash binder and kaolin	88
4.4.4	Comparison with Portland cement.....	92
4.4.4.1	Processes generating the microstructure.....	92
4.4.4.2	Pore network characteristics	93
4.4.4.3	Macroscopic behaviour according to the microstructure evolution	93
4.5	Conclusions	95
4.6	References	96
Chapter 5 Use of alkali activated fly ash binder for kaolin clay soil stabilisation:		
Mechanical behaviour		98
5.1	Abstract	100
5.2	Introduction	101
5.3	Material and methods	102
5.3.1	Materials.....	102
5.3.2	Sample preparation.....	102
5.3.3	Methods	103
5.4	Results and discussion	105
5.4.1	One-dimensional compression.....	105
5.4.2	Shear strength.....	110
5.4.3	Link between the microscopic and macroscopic scales	114
5.5	Conclusions	117
5.6	References	118
Chapter 6 Conclusions		120
List of Figures		124
List of Tables		127

Introduction

Soft clay-rich soils are frequently encountered in construction sites. Their poor mechanical performance represents a critical issue in engineering projects. These soils cannot be directly used as earthfill materials and may cause excessive settlements of foundation structures. To improve their engineering characteristics Ordinary Portland Cement and lime are commonly used and whose stabilisation mechanisms have been widely reported (Pomakhina et al., 2012; Lemaire et al., 2013; Chemedda et al., 2015; Deneele et al., 2016; Maubec et al., 2017; Vitale et al., 2017; Guidobaldi et al., 2017). Nevertheless, those conventional stabilisers are associated with high carbon dioxide emissions and energy intensive processes significantly increasing the worldwide carbon footprint (Scrivener and Kirkpatrick, 2008).

As an alternative and to address the competitiveness challenge of the construction industry to develop carbon-efficient geotechnical infrastructure, the use of Alkali Activated Material as a soil stabiliser is gaining more and more attention over the past ten years. Alkali Activated Materials could constitute a viable sustainable soil binder because of their much lower CO₂ emission process compared to traditional Portland cement. Furthermore, recent studies have shown a positive potential and feasibility results of using alkali activated binders for soil improvement, and this not only for different types of soil i.e. clayey soil (Wilkinson et al., 2010; Singhi et al., 2016), sandy clay (Cristelo et al., 2011), marl, marlstone (Cristelo et al., 2012), silty sand (Rios et al., 2016) or else road aggregates (Tenn et al., 2015); but also for different applications i.e. in deep soft soil (Cristelo et al., 2011), at shallow depth (Zhang et al., 2013) or in rammed earth construction (Silva et al., 2013).

Alkali Activated Materials derive from the reaction between a solid aluminosilicate powder (usually metakaolin, fly ash, blast furnace slag or natural pozzolan), and an alkali metal source (most commonly alkali hydroxide and/or alkali silicate solutions) (Buchwald et al., 2003; Shi et al., 2006). The resulting material is a binder system cured at room temperature with durability and mechanical properties potentially suitable for Portland cement replacement.

Works on alkali activated binder treated soils are recent and constitute a novel domain of application. Consequently, very few studies on clay soil treatment using this type of binders have been conducted (Wilkinson et al., 2010; Singhi et al., 2016). The present work therefore constitutes an innovative experimental study whose main aim is to assess the feasibility of using this novel soil binder for clay soil treatment.

Considering the broad range of possibilities in the process regarding the choice of the soil to stabilise but also the solid aluminosilicate powder, the alkali activator, the water content and finally the proportions to mix those various ingredients it exists various axis of investigation.

The present study specifically focusses on one system: the use of a calcium-rich fly ash from coal combustion activated by a sodium-based alkaline solution as a binder for clay kaolin stabilisation. Kaolin was selected as its reactivity to alkaline activation at ambient temperature is negligible, and hence does not interfere in the reaction sequence allowing a study of the binder effect only. Besides, kaolin represents a wide class of clays encountered in engineering projects and so it is considered here as a model soil. Because Kaolin constitutes a few reactive solid aluminosilicate source, another reactive aluminosilicate source was added to the system and corresponds to fly ash. It was selected in a context of resource-saving as it is an industrial waste. Finally, a sodium-based alkaline solution was selected as it is the most common and less expensive solution available.

When dealing with the feasibility of using a class of material for a novel application, there are some important parameters to explore such as its composition, microstructure and processing which all affect the performances and cost of a material (Askeland et al., 2011). The work strategy was hence designed to develop a detailed comprehension of our alkali activated treated soil across various scale levels i.e. particle, microstructural and mechanical levels.

The work comprises six chapters. After an overview of the research work (Chapter 1), Chapter 2 reviews the literature relevant to the understanding of alkali activated systems. Especially, it deals with the role and influence of each ingredients constituting an Alkali Activated Material on the reaction sequence. It further provides guidelines regarding the required proportions of each ingredients to obtain optimal properties.

Chapter 3, 4 and 5 deals with the study of the treated soil using a calcium-rich fly ash. In particular, Chapter 3 investigates the first scale level i.e. the particle level by dealing with the physicochemical evolution of the treated soil. To this end, a set of complementary techniques have been used including X-ray diffraction, Derivative thermogravimetric analysis, Fourier Transform Infrared spectroscopy, Scanning Electron Microscopy, ^{29}Si and ^{27}Al Nuclear Magnetic Resonance. It gives an insight into the reactivity of the alkali activated fly ash binder by itself, including (i) which phases are present and which phases are accessible during alkaline activation, (ii) which compounds are subsequently formed, and (iii) reactivity timescale. Another key point addressed in this chapter is whether the presence of kaolin affects the reactivity of the binder. The reaction sequence has therefore been investigated by considering the binder alone and the binder mixed with kaolin. To end with, the physicochemical evolution occurring in the alkali activated fly ash is compared with one occurring in the same kaolin stabilised by i) lime or ii) a mix of lime and the same fly ash used in this experimental programme. This is aimed at assessing the potential benefit of fly ash-based binder compared to the more traditional lime.

Chapter 4 investigates the next microstructural level i.e. the arrangement of phases within the treated soil. To this end, a combination of completing techniques has been used

including Optical microscopy, Scanning Electron Microscopy and Mercury Intrusion Porosimetry in order to gain an overview of the complex pore structure. It especially gives an insight into the microstructural evolution of the alkali activated fly ash binder by itself during the first 28 days of curing, including (i) a description of the dispersion and arrangement of phases, (ii) an understanding of which processes generate the microstructure over time and (iii) a pore network characterisation. Another point addressed is the influence of kaolin mixed with the fly ash-based binder on the microstructural evolution. Because of its small size kaolinite acts as a filler of the porosity and undoubtedly plays a role on the microstructural evolution.

Chapter 5 focusses on the macroscopic level by investigating the mechanical behaviour of the treated soil. To this end, one dimensional compression test and direct shear test have been performed. It gives an insight of the evolution of the compressive strength, yield stress and shear strength over time. It also addresses the time interval for which the improvement is effective. In addition, along this whole chapter a conjoint understanding of those mechanical data in view of the knowledge gained about the physicochemical and microstructural evolution of the system was carried out.

To end with, Chapter 6 provides general conclusions of the overall work along with further potential developments.

References

Askeland, D.R., Fulay, P.P., Wright, W.J., 2011. The science and engineering of materials, 6th ed. ed. Cengage Learning, Stamford, CT.

Buchwald, A., Kaps, C., Hohmann, M., 2003. Alkali-activated binders and pozzolan cement binders—complete binder reaction or two sides of the same story, in: Proceedings of the 11th International Conference on the Chemistry of Cement. Portland Cement Association Durban, South Africa, pp. 1238–1246.

Chemed, Y.C., Deneele, D., Christidis, G.E., Ouvrard, G., 2015. Influence of hydrated lime on the surface properties and interaction of kaolinite particles. *Appl. Clay Sci.* 107, 1–13. <https://doi.org/10.1016/j.clay.2015.01.019>

Cristelo, N., Glendinning, S., Fernandes, L., Pinto, A.T., 2012. Effect of calcium content on soil stabilisation with alkaline activation. *Constr. Build. Mater.* 29, 167–174. <https://doi.org/10.1016/j.conbuildmat.2011.10.049>

Cristelo, N., Glendinning, S., Teixeira Pinto, A., 2011. Deep soft soil improvement by alkaline activation. *Proc. Inst. Civ. Eng. - Ground Improv.* 164, 73–82. <https://doi.org/10.1680/grim.900032>

- Deneele, D., Le Runigo, B., Cui, Y.-J., Cuisinier, O., Ferber, V., 2016. Experimental assessment regarding leaching of lime-treated silt. *Constr. Build. Mater.* 112, 1032–1040. <https://doi.org/10.1016/j.conbuildmat.2016.03.015>
- Guidobaldi, G., Cambi, C., Cecconi, M., Deneele, D., Paris, M., Russo, G., Vitale, E., 2017. Multi-scale analysis of the mechanical improvement induced by lime addition on a pyroclastic soil. *Eng. Geol.* 221, 193–201. <https://doi.org/10.1016/j.enggeo.2017.03.012>
- Lemaire, K., Deneele, D., Bonnet, S., Legret, M., 2013. Effects of lime and cement treatment on the physicochemical, microstructural and mechanical characteristics of a plastic silt. *Eng. Geol.* 166, 255–261. <https://doi.org/10.1016/j.enggeo.2013.09.012>
- Maubec, N., Deneele, D., Ouvrard, G., 2017. Influence of the clay type on the strength evolution of lime treated material. *Appl. Clay Sci.* 137, 107–114. <https://doi.org/10.1016/j.clay.2016.11.033>
- Pomakhina, E., Deneele, D., Gaillot, A.-C., Paris, M., Ouvrard, G., 2012. ²⁹Si solid state NMR investigation of pozzolanic reaction occurring in lime-treated Ca-bentonite. *Cem. Concr. Res.* 42, 626–632. <https://doi.org/10.1016/j.cemconres.2012.01.008>
- Rios, S., Cristelo, N., Viana da Fonseca, A., Ferreira, C., 2016. Structural Performance of Alkali-Activated Soil Ash versus Soil Cement. *J. Mater. Civ. Eng.* 28, 4015125. [https://doi.org/10.1061/\(ASCE\)MT.1943-5533.0001398](https://doi.org/10.1061/(ASCE)MT.1943-5533.0001398)
- Scrivener, K.L., Kirkpatrick, R.J., 2008. Innovation in use and research on cementitious material. *Cem. Concr. Res.* 38, 128–136. <https://doi.org/10.1016/j.cemconres.2007.09.025>
- Shi, C., Krivenko, P.V., Roy, D.M., 2006. Alkali-activated cements and concretes. Taylor & Francis, London ; New York.
- Silva, R.A., Oliveira, D.V., Miranda, T., Cristelo, N., Escobar, M.C., Soares, E., 2013. Rammed earth construction with granitic residual soils: The case study of northern Portugal. *Constr. Build. Mater.* 47, 181–191. <https://doi.org/10.1016/j.conbuildmat.2013.05.047>
- Singhi, B., Laskar, A.I., Ahmed, M.A., 2016. Investigation on Soil–Geopolymer with Slag, Fly Ash and Their Blending. *Arab. J. Sci. Eng.* 41, 393–400. <https://doi.org/10.1007/s13369-015-1677-y>
- Tenn, N., Allou, F., Petit, C., Absi, J., Rossignol, S., 2015. Formulation of new materials based on geopolymer binders and different road aggregates. *Ceram. Int.* 41, 5812–5820. <https://doi.org/10.1016/j.ceramint.2015.01.010>
- Vitale, E., Deneele, D., Paris, M., Russo, G., 2017. Multi-scale analysis and time evolution of pozzolanic activity of lime treated clays. *Appl. Clay Sci.* 141, 36–45. <https://doi.org/10.1016/j.clay.2017.02.013>

Wilkinson, A., Haque, A., Kodikara, J., 2010. Stabilisation of clayey soils with industrial by-products: part A. *Proc. Inst. Civ. Eng. - Ground Improv.* 163, 149–163. <https://doi.org/10.1680/grim.2010.163.3.149>

Zhang, M., Guo, H., El-Korchi, T., Zhang, G., Tao, M., 2013. Experimental feasibility study of geopolymer as the next-generation soil stabilizer. *Constr. Build. Mater.* 47, 1468–1478. <https://doi.org/10.1016/j.conbuildmat.2013.06.017>

Literature review

2.1 Introduction to Alkali Activated Material and Geopolymer

2.1.1 How to create Alkali Activated Material and Geopolymer products?

To create either an alkali activated material or a geopolymer product requires three components: (i) an alumino-silicate material, (ii) an alkaline activating solution and (iii) water (Figure 1). It gives a hardened material at room temperature with mechanical properties potentially suitable for Portland cement replacement. Various alumino-silicate materials and alkaline activating solutions can be selected leading to materials with different properties as explained more in details in section 2.2.

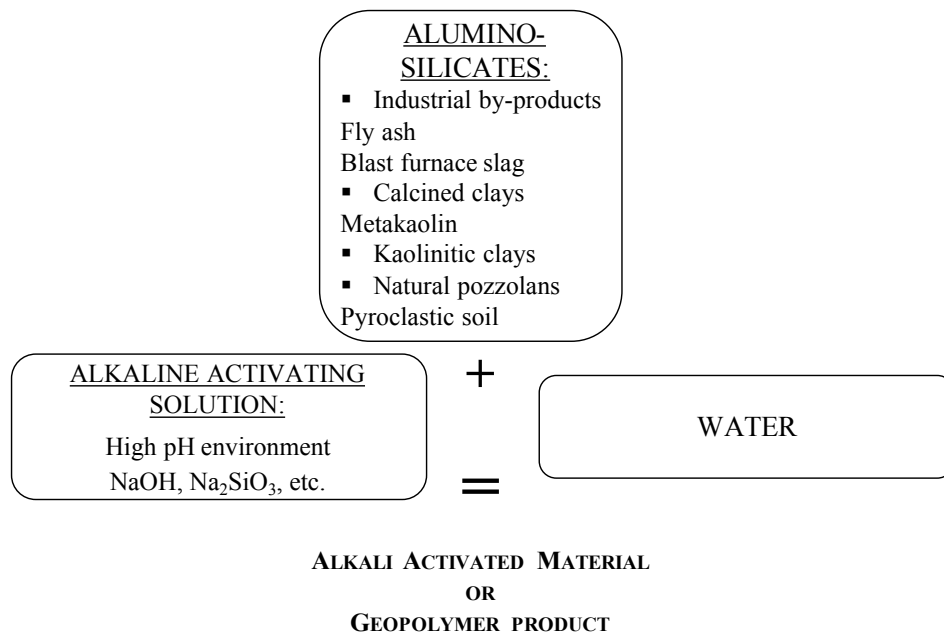


Figure 1: Components of alkali activated material and geopolymer products

2.1.2 History of wordings: Alkali Activated Material vs. Geopolymer

The wording Alkali Activated Material refers to the studies of V.D. Glukhovsky during the mid 1950s in the former Soviet Union. At that time, Glukhovsky discovered the possibility of producing binders using low-calcium aluminosilicate (clays) and solutions containing alkali metals (V.D. Glukhovsky, 1959). On this basis, he combined various types of aluminosilicate enlarging his studies to various potential alkali activated systems. Those materials were originally known as “soil cements” and “soil silicate concretes” because of their similarity to natural minerals.

Whereas, the word Geopolymer was introduced almost 30 years later by Davidovits in 1979 to design advance inorganic polymer compounds (Davidovits, 2005). Their first mineral polymer resin invented in 1977 resulted from the reaction of metakaolin (burnt kaolin) with soluble silicate (Davidovits, 2011).

Consequently, the systems studied by V.D. Glukhovsky and Davidovits strongly resemble which created a lot of confusion in wordings and terminologies among the scientific community. To date it especially exists a controversy about the use of either geopolymer or alkali activated material. In fact, some literature considers alkali activated material as the broadest classification encompassing geopolymer system (Provis and van Deventer, 2014). Whereas, Davidovits clearly states that alkali activated materials are not geopolymer, explaining that the difference lies in the final variable chemistry of those two materials which strongly influence the properties especially the durability (Davidovits, 2017).

In this report the word Geopolymer will be employed to designate the high molecular, macromolecules, polymers presenting a three-dimensional network structure, and referring to Davidovits terminology. While Alkali Activated Materials will be employed otherwise.

More details on wordings and terminologies used can be found in the next sections of this introductory part.

In order to better understand those differences the reaction mechanism will be described first followed by a description of the binding structures potentially formed.

2.1.3 Mechanism

2.1.3.1 Low-calcium systems

Once the aluminosilicate powder is mixed with the alkaline solution, a paste forms which quickly transforms into hard materials. Due to the quickness of reactions, the mechanism of low-calcium alkali activated systems is complex to study and therefore not yet fully understood.

Alkali activated system mechanisms have been initially discussed during the 1950s by Glukhovsky. His first model has been completed by the knowledge acquired on formation mechanism of zeolites (Fernández-Jiménez et al., 2006), as zeolites are crystallized analogous of amorphous to semi-crystalline geopolymer matrices. Finally, this model has been summarized by Duxson et al. (Duxson et al., 2007) (Figure 2).

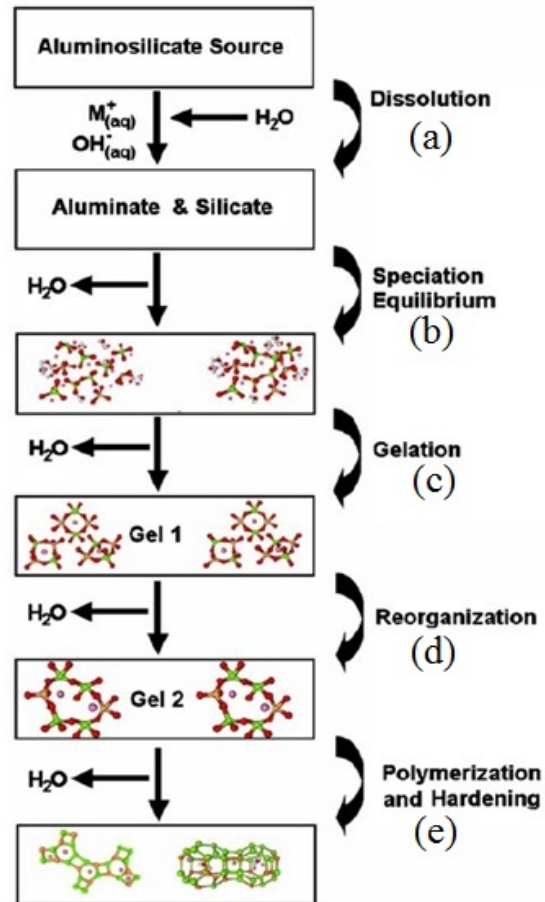


Figure 2: Conceptual model for geopolymerisation from Duxson et al. (2007)

This conceptual model shows the main steps observable in geopolymerisation. Although presented linearly, the different steps are largely coupled and occur simultaneously.

The first step (Figure 2a) is the dissolution of the solid aluminosilicate source by alkaline hydrolysis (consuming water) producing aluminate and silicate species probably as monomers (Duxson et al., 2007).

Once in solution the species released by dissolution form a complex mixture of silicate, aluminate and aluminosilicate whose speciation equilibria have been studied extensively (Swaddle, 2001) (Figure 2b).

These monomers inter-react to form dimers, which in turn react with other monomers to form trimers, tetramers and so on. When the solution reaches saturation, an aluminosilicate gel precipitates (Figure 2c) (Provis and Deventer, 2009). The time for the

supersaturated aluminosilicate solution to form a continuous gel varies considerably with raw material, solution composition and synthesis conditions (Aiello et al., 1991; Ivanova et al., 1994). Despite this, some systems never gel i.e. typically dilute systems.

Initially, an aluminium-rich gel denominated Gel 1 (Figure 2) is formed (this is an intermediate reaction product). Its formation may be explained by the higher Al^{3+} ion content in the alkaline medium in the early stages of the process, since reactive aluminium dissolves more rapidly than silicon because Si-O-Al bonds are weaker than Si-O-Si and therefore easier to sever (Fernández-Jiménez et al., 2006). As the reaction progresses, more Si-O-Si groups from the initial aluminosilicate solid source dissolve, increasing the silicon concentration in the medium and gradually raising the proportion of silicon in the gel then called Gel 2 (Figure 2) (Provis and Deventer, 2009).

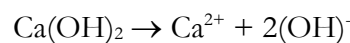
After gelation the system continues to rearrange and reorganize as the connectivity of the gel network increases (Figure 2d). Polymerisation processes (gradual attachment of monomers to each other by covalent bonds) continue resulting in the formation of a three-dimensional aluminosilicate network commonly attributed to geopolymers (Figure 2e). These processes of structural reorganization determine the microstructure and pore distribution of the material, which are critical in determining many physical properties (Duxson et al., 2007).

Finally, during the process, the water initially consumed by dissolution is partially eliminated outside while the other part resides within pores of the network (as it will be described later in section 2.2.3).

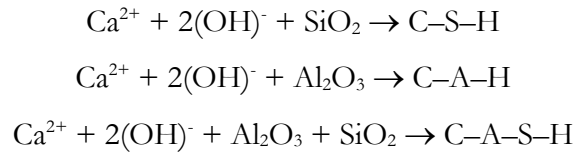
2.1.3.2 High-calcium systems

If a substantial amount of a reactive calcium source is present initially Calcium Silicate Hydrate (C-S-H) gel found in Portland Cement may also form and according to the following reactions.

First a dissociation reaction of the calcium source occurs. Taking as an example portlandite $Ca(OH)_2$ or else calcium carbonate $CaCO_3$ as a reactive source the dissociation reactions are as follows:



Dissolved calcium species Ca^{2+} then react with silicate and aluminate to form various forms of calcium silicate hydrates C–S–H, calcium aluminium hydrates C–A–H and calcium aluminium silicate hydrates as follows:



In a lime treated soil, these hydrate gels firmly bond soil particles together giving rise to an increased compressibility of the soil.

Moreover, some studies showed that the coexistence of the three-dimensional aluminosilicate network formed in low-calcium systems (see section 2.1.3.1) with calcium silicate hydrates C–S–H is possible (Yip et al., 2005). Therefore, in high-calcium systems several potential reactions may happen. Their occurrence depends notably on the reactivity of the raw products selected and the alkalinity of the system. In fact, at higher alkalinity, the dominating binder component is always the three-dimensional gel (van Jaarsveld and van Deventer, 1999).

2.1.4 Structure

As the reactions occur quickly, there is not sufficient time and space for the gel or paste to grow into a well crystallised structure. Thereby, the binding phases formed display an amorphous, disordered structure.

Following the extent of the reaction sequence different products of distinct structures can be found in the binding phase i.e. N–A–S–H and K–A–S–H gels or geopolymer product.

2.1.4.1 N–A–S–H and K–A–S–H gels

When the reaction mechanism is incomplete i.e. when the last geopolymerisation step does not occur, the main chemical reaction is the polycondensation of monomers leading to the formation of an oligomer or small molecule (Figure 3). The product formed in that case is a hydrate or precipitate. Thus, it can be considered as an alternative to calcium silicate hydrate C–S–H commonly found in Portland cement, as they both display a similar linear two-dimensional structure. However, calcium ions Ca^{2+} in C–S–H structure are in the case of alkali activated systems substituted by alkali cations such as sodium Na^+ or potassium K^+ .

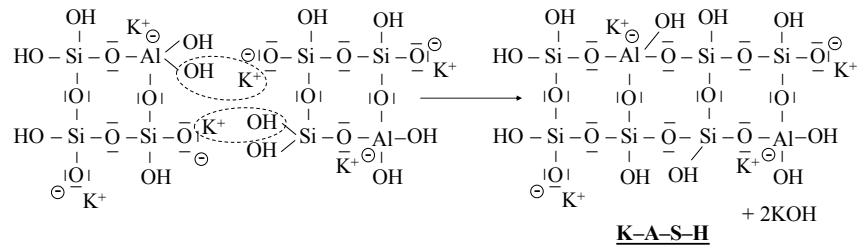


Figure 3: Polycondensation reaction of monomers leading to the formation of K-A-S-H type phases (Davidovits, 2017)

That is why a comparable terminology to C-S-H is used in that case as followed:

- For Portland cement, hydration reactions lead to the formation of calcium silicate hydrate i.e. C-S-H i.e. $\text{CaO} \cdot \text{SiO}_2 \cdot \text{H}_2\text{O}$;
- While hydrates resulting from alkaline activation correspond to $\text{Na}_2\text{O} \cdot \text{SiO}_2 \cdot \text{Al}_2\text{O}_3 \cdot \text{H}_2\text{O}$ i.e. sodium-silico-aluminate-hydrate i.e. N-A-S-H; or else $\text{K}_2\text{O} \cdot 2\text{SiO}_2 \cdot \text{Al}_2\text{O}_3 \cdot \text{H}_2\text{O}$ i.e. potassium-silico-aluminate-hydrate i.e. K-A-S-H.

2.1.4.2 Geopolymer structure

By contrast when geopolymerisation does occur i.e. when all the steps of the reaction mechanism presented in the section above happen the final chemistry differs as polymerisation continues leading to the formation of a three-dimensional network as presented in Figure 4.

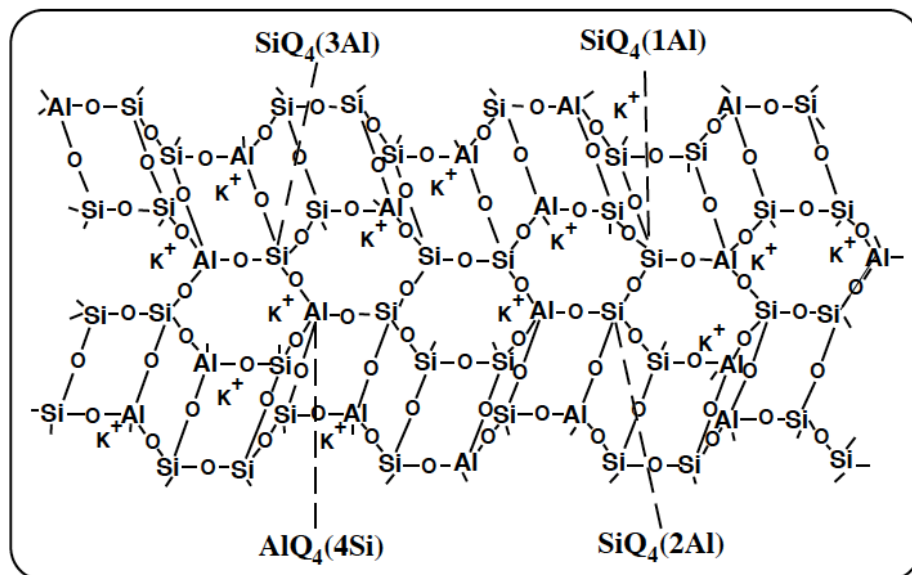


Figure 4: Proposed structural model for K-Poly(sialate-siloxo) Geopolymer (Davidovits, 1994)

This three-dimensional highly disordered, highly cross-linked aluminosilicate network is made of an assembly of SiO_4 and MAlO_4 tetrahedron, where M is an alkali cation (generally sodium Na^+ or potassium K^+) (K^+ on Figure 4) balancing the negative charge of AlO_4 tetrahedron. This structure is characteristic of geopolymer products.

Contrary to C–S–H, N–A–S–H and K–A–S–H, the geopolymer structure is a polymer structure i.e. a three-dimensional network of mineral molecules linked with covalent bonds.

2.1.5 Properties

The understanding of which structure is formed is crucial since it strongly influences the properties of the final material.

At an early stage N–A–S–H and K–A–S–H gels provide higher strength compared to geopolymer product. Nevertheless, geopolymer strength continues to increase over time reaching similar value of N–A–S–H and K–A–S–H gels (Davidovits, 2017). Besides, two-dimensional structure such as C–S–H, N–A–S–H and K–A–S–H structures are generally less stable over time than three-dimensional networking such as geopolymer which corresponds to bigger branched molecule, and therefore more stable molecule.

Moreover, although N–A–S–H and K–A–S–H gels display high early strength, their structures are not stable because of the presence of the alkali outside the structure (see potassium K^+ on Figure 3). In fact, as K^+ cations are outside the structure, they are free to move which constitutes a danger in terms of physicochemical properties. For instance, alkali such as sodium and potassium are very soluble in water. Consequently, they are migrating very fast in contact with water leading to a lot of leachates. Additionally, if exposed to the air the free alkali carbonates giving rise to high carbonation (Davidovits, 2017).

By contrast, geopolymer are stable material because of the presence of a networking element interacting with the free alkali. In fact, the alkali is strongly attached to aluminium which is itself surrounded by silicon in a three-dimensional environment (see Figure 4). Thereby, the structural alkali will not undergo leaching nor carbonation. Due to this particular structural characteristic, geopolymer products are known to present excellent durability properties i.e. very high acid, sulphate, chloride, carbonation, water and fire resistance.

Regarding C–S–H phases found in Portland cement, although they are hydrates of similar structure that N–A–S–H and K–A–S–H gels, calcium being insoluble in water, few leaching occurs.

For all those reasons it is primordial to investigate the structure of the binding phase in order to better understand durability and strength properties of the final material.

2.1.6 Experimental tools adapted

Calcium Silicate Hydrate C–S–H gel, Alkali Silico Aluminate-Hydrate (N–A–S–H and K–A–S–H gels) and geopolymer are amorphous to semi-crystalline structures. Their identification by standard method such as X-ray diffraction is therefore hardly achievable as it gives mineralogical information about crystalline phases. For that reason, the most adapted tool to distinguish small differences in structure as described above is Nuclear Magnetic Resonance (NMR).

Si-NMR

Using Si-NMR it is possible to probe the local environment (first and second neighbours) of silicon atoms within the structure. To describe the local environment of silicon atoms the Q^n notation is used, where Q represents a silicon atom and n its degree of connectivity i.e. its number of Si–O–Si types bound (Figure 5).

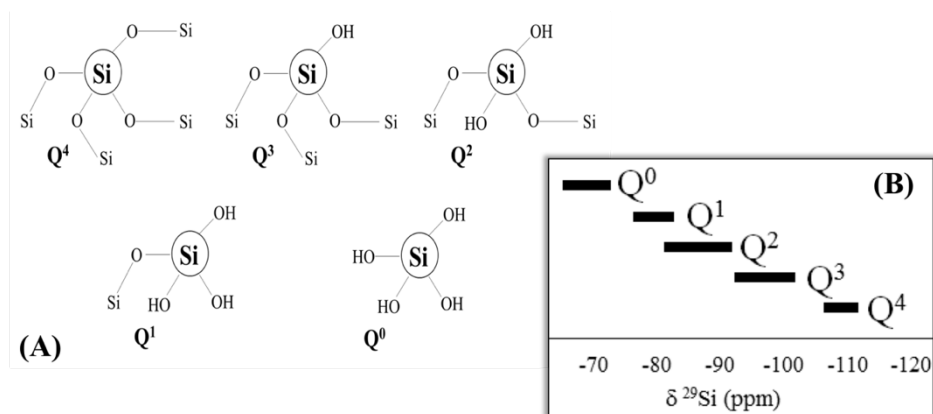


Figure 5: Local environments of silicon described by the Q^n notation

For C–S–H gel as well as N–A–S–H and K–A–S–H gels, their two-dimensional structures imply a degree of connectivity of 2, also referred as Q^2 species for which the chemical shift $\delta^{29}\text{Si}$ presents a value in the range of -80 to -90 ppm (Figure 5B). Whereas, the three-dimensional network characteristic of geopolymer corresponds to a degree of connectivity of 4 also referred as Q^4 species with a higher chemical shift.

Therefore, probing the local environment of silicon by Nuclear Magnetic Resonance allows to recognize a two-dimensional from a three-dimensional network i.e. hydrates from geopolymer products as shown in Figure 6.

Al NMR

Similarly, looking at Al-NMR it is possible to probe the local environment of aluminium atoms. When aluminium is in a three-dimensional configuration with potassium strongly attached to it i.e. in geopolymer structure the chemical shift presents a specific value of 55 ppm (Figure 7).

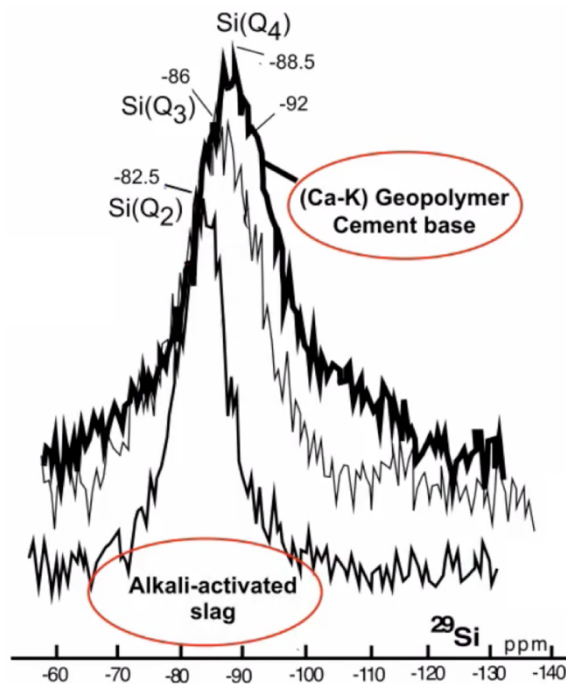


Figure 6: Si-NMR of alkali activated material vs. geopolymer product (Davidovits, 2017)

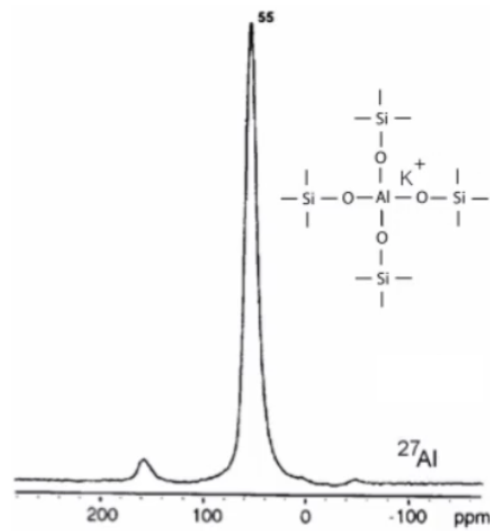


Figure 7: Al-NMR of geopolymer product (Davidovits, 2017)

Using Nuclear Magnetic Resonance, it is therefore possible to finely describe the structure of the binding phase and assess the resulting properties.

2.2 Synthesis conditions

This section will discuss how to choose the different ingredients of the mix and how their characteristics can influence the evolution of the system.

2.2.1 Aluminosilicate source

The aluminosilicate source has to consist of a certain amount of silicate and aluminate phases which can be dissolved by the alkaline medium (Buchwald et al., 2009).

In addition, its chemical composition and mineralogical characteristics are determinants in the formation of the main reaction products (Pacheco-Torgal et al., 2015).

Hence, this part addresses the influence of physico-chemical properties of the aluminosilicate source on alkali activated system in order to better understand what makes a suitable source, and gives effective mechanical strength following the alkaline attack.

2.2.1.1 Chemical composition

The silica and alumina content of the raw aluminosilicate material unquestionably plays an essential role in the degree of reaction, as well as in the composition and structure of the gel formed and, consequently in the mechanical strength and durability of the end material (Pacheco-Torgal et al., 2015).

Hence, it is central to know the $([\text{SiO}_2]/[\text{Al}_2\text{O}_3])_{\text{reactive}}$ ratio. Reactive signifying the silica and alumina content of the aluminosilicate material that takes part in the formation of cementitious gel, and does not account for non-reactive phases i.e. phases unaffected by alkali activation.

A sufficient content of reactive silica is required to achieve a structural integrity of the final network. Nevertheless, it should be bear in mind that the reactive content of silica is a less critical parameter than the reactive content of alumina. Since, the availability of silica can be balanced by the supply of an alkali silicate activating solution such as Na_2SiO_3 (as it will be mentioned in a following section 2.2.2.2). Whereas, the aluminosilicate material is the only source of aluminium in the alkali-activated system.

Besides, the reactive aluminium content controls the setting time. In fact, the aluminium present in the solution initially favours the formation of a metastable Gel 1 rich in aluminium. Over time, Gel 1 evolves into a highly silicon gel, denominated Gel 2 (as previously described in section 2.1.3). The absence of a sufficient amount of reactive aluminium retards the conversion of Gel 1 into Gel 2, affecting the mechanical strength (Pacheco-Torgal et al., 2015).

As a conclusion studies showed that the binders exhibiting the highest mechanical strength are obtained with materials whose starting $([\text{SiO}_2]/[\text{Al}_2\text{O}_3])_{\text{reactive}}$ ratio range from 2 to 4 (Fletcher et al., 2005; Criado et al., 2010; Pimraksa et al., 2011).

2.2.1.2 Mineralogical characteristics

The interrelationship between mineralogy and reactivity of individual minerals is usually extremely complex (Xu and Van Deventer, 2000). Some tendencies can however be observed.

Crystallinity

The reactivity of the aluminosilicate source is as much elevated as its amorphous phase content is high. This is the case of metakaolin, fly ash or blast furnace slag commonly used as an aluminosilicate source and whose crystallinity is low. Such amorphous materials exhibit a low chemical stability due to their disorganized structures. As a result, silica and

alumina are present in an unstable state and are consequently readily accessible to form an aluminosilicate gel.

By contrast, well crystallised aluminosilicate source such as clay minerals are much less reactive to form alkali activated binder (as explained in a following section 2.3.2).

Specific surface area

Knowledge about surface area properties of an aluminosilicate source provides also an insight into its potential cementitious gel formation (Pacheco-Torgal et al., 2015). The higher the specific surface area the higher the reactivity of the raw material following the alkaline attack.

Specific surface area depends on several factors such as particle size, morphology and surface, and mineralogical composition. For instance, finer particles having a higher specific surface area are more reactive.

The crystallinity of the aluminosilicate source however plays a dominant role. As an example, montmorillonite clay minerals which display a very high specific surface area (about 800 m²/g), but present as well a crystallized structure are unreactive following alkaline attack (as discussed in section 2.3.2).

2.2.2 Alkaline activating solutions

Alkaline activators are the second essential component in alkali-activated system development.

It exists two main types of alkaline activating solutions: alkali hydroxides and alkali silicates (which will be the only ones addressed).

The aim of this part is to understand the role of each activating solution, and thus be able to identify the most relevant alkaline activating solutions in terms of type, concentration and relative amount following the type of raw aluminosilicate material selected.

2.2.2.1 Alkali hydroxides

Sodium and potassium hydroxides (NaOH and KOH respectively) are traditionally used because of their cost and availability.

Use of alkali hydroxide solutions results in hydroxyl OH^- anions supply. Hydroxyl anions catalyse the dissolution of Si^{4+} and Al^{3+} cations by inducing the hydrolysis of Si-O-Si and Si-O-Al bonds of the raw material. Besides, the presence of OH^- ions also raises the pH to the values required for initial precursor dissolution and the subsequent condensation reactions (Pacheco-Torgal et al., 2015).

Consequently, the hydroxide concentration must be high enough for a complete dissolution of Si^{4+} and Al^{3+} from the aluminosilicate material (Rowles and O'Connor, 2003). Nevertheless, too high concentration of alkali hydroxide may be detrimental by increasing efflorescence, which corresponds to the reaction between excess alkali and atmospheric CO_2 (leading to the formation of white carbonate or bicarbonate crystals). The efflorescence process will possibly render the material more brittle (Pacheco-Torgal et al., 2015).

Considering all those aspects, it was shown that compressive strength increases along with the increase of concentration of NaOH solution within 4-12 mol/L (Wang et al., 2005).

Aside from the role of OH^- ions, the low viscosity of alkali hydroxides constitutes a marked advantage over silicate solutions (as mentioned in the following section 2.2.2.2). Indeed, high viscosity implies a need for longer time or higher temperature to evaporate the excess water of the resultant gel and therefore to gain full strength (Xu and van Deventer, 2003).

2.2.2.2 Alkali silicates

Use of a silicate solution Na_2SiO_3 is generally as well needed given that the availability of soluble silica is of cardinal importance in the material development (affecting workability, both gel composition and microstructure, and mechanical strength of the material formed) (Pacheco-Torgal et al., 2015).

Silicate solutions are made of SiO_2 and alkali oxides M_2O , where M is a monovalent alkali cation (generally sodium and potassium that will be the only ones addressed here). Silicate solutions are partially crystalline mixture, highly viscous which constitutes a drawback when used as previously mentioned.

Two important factors must be considered when soluble silica is added:

- The $\text{SiO}_2/\text{M}_2\text{O}$ molar ratio (1) and;
- The silica concentration (2).

(1) Silicate solution with a low $\text{SiO}_2/\text{M}_2\text{O}$ molar ratio (1/1) consists primarily of monomers SiO_4^{4-} and dimers $\text{Si}_2\text{O}_7^{6-}$, while a solution with a high molar ratio (3.3/1) has a higher proportion of polymeric species (Pacheco-Torgal et al., 2015). Thereby, soluble

silicate catalyses alkali activated reactions by providing self-polymerising species (monomers, dimers and larger oligomers), and initiating polymerisation between silicate oligomers and/or between AlO_4^- and silicate oligomers (Xu and Van Deventer, 2000). The greater or lesser degree of polymerisation has a triple effect on reaction kinetics and the nature of the gel initially formed (Pacheco-Torgal et al., 2015). Optimal value of $\text{SiO}_2/\text{M}_2\text{O}$ molar ratio for aluminosilicate alkaline activation was shown to be around 1-1,5 (Duxson et al., 2005; Criado et al., 2008).

(2) Although, increasing the silica ion concentration in solution (with similar concentration of Na_2O) induces greater silicate unit polymerisation (Criado et al., 2008), a very high concentration of silica in the activating solution lowers pH and raises solution viscosity, inducing a decline in the degree of reaction of the aluminosilicate material (Duxson et al., 2005).

Finally and similarly to alkali hydroxides, an excess of alkali from silicate solution to the system could cause severe efflorescence.

2.2.2.3 Mix of alkali silicate and hydroxide

Luz Granizo et al. (Granizo et al., 2007) support the idea that alkali activation of metakaolin with both sodium silicate and sodium hydroxide solutions produces materials with higher mechanical strength than activation with sodium hydroxides alone. This is why, activation solutions often consist of a mixture of hydroxide and silicate solutions. In addition, Hardjito and Rangan (Hardjito and Rangan, 2005) have shown that the higher the ratio of sodium silicate solution to sodium hydroxide solution ratio by mass the higher the compressive strength of geopolymer concrete.

2.2.2.4 Influence of alkali cation type: potassium and sodium

Alkali metal cation controls and affects almost all stages of alkali activated system as highlighted by van Jaarsveld and van Deventer (van Jaarsveld and van Deventer, 1999). They are particularly known to:

- Catalyse the reaction;

- Maintain the pH values of the aqueous phase;

- Form part of the gel structure;

- Compensate the electrical charge induced by AlO_4^- tetrahedron.

Optimum properties are usually obtained when the alkali concentration is sufficient to provide a charge-balancing of the negative AlO_4^- tetrahedron charge, but not in sufficient excess to promote efflorescence (formation of sodium carbonate by atmospheric carbonation) that may disrupt the polymerisation process (Barbosa et al., 2000). An alkali excess also creates a greater affinity for water, resulting in a longer time to evaporate excess water, and hence, may require a heating stage to achieve the desired set. This is why, the $([\text{M}_2\text{O}]/[\text{Al}_2\text{O}_3])_{\text{reactive}}$ ratio is generally set at 1 in order to fully compensate the negative charge induced by tetrahedral aluminium sites without creating any alkali excess.

Finally, efflorescence is generally more marked in the presence of sodium than potassium.

Effect of alkali cation type on hydroxide solution

Given that the first stage of the reaction is controlled by the rate at which the alkaline compound dissolves the solid network of aluminosilicates to form small, reactive aluminate and silicate species (as seen in 2.1.3), the more alkaline potassium hydroxides might induce a greater degree of dissolution than the less alkaline sodium hydroxides. Nonetheless, studies have shown that sodium releases silicate and aluminate monomers more effectively than potassium (Pacheco-Torgal et al., 2015).

Additionally, potassium hydroxide solutions display a lower viscosity than sodium hydroxide solutions. Samples synthesised from KOH solution thus show a faster evaporation of the excess water (Xu and van Deventer, 2003).

Effect of alkali cation type on silicate solution

Similarly, potassium silicate solutions display a lower viscosity than sodium silicates of comparable composition. Sodium silicates are also very much stickier than potassium silicates which could be problematic issues in the use of sodium silicates.

Structural effect of alkali cation type

It is during the final polycondensation process that alkali cations are thought to play a major role in determining the final structure (van Jaarsveld and van Deventer, 1999). Because of its larger size potassium ion benefits the polymerisation between silicate species as well as between silicate and aluminate species to form larger precursors in the gel phases. These larger precursors result in faster and more extensive polymerisation

(Pacheco-Torgal et al., 2015), explaining higher compressive strength after alkali activation with potassium compared with sodium.

Potassium ions additionally have a smaller hydration sphere than sodium resulting in a denser polycondensation reaction also supporting the higher compressive strength observed for potassium system.

Finally, McCormick and Bell (McCormick and Bell, 1989) observed that small alkali cations produce the highest rates of zeolite nucleation. Thus, sodium-based systems are more prone to form unwanted zeolite.

As a conclusion, there are pros and cons for both using sodium or potassium as alkali cation. Nevertheless, sodium hydroxide solutions are predominantly used because of their cost and availability.

In the light of the discussion of the previous parts, the composition, structure, microstructure and properties of the alkali activated material formed depends on the characteristics of the aluminosilicate source as well as the concentration, volume and type of activator used. Both the raw material and the activator must consequently be chosen very carefully. Moreover, the weight ratio of aluminosilicate powder to alkaline solution is usually chosen between 3.0 and 5.5 in geopolymerisation.

2.2.3 Water demand

During alkali activation water is one of the reactants and it is also one of the products. Indeed, on one hand the dissolution of the aluminosilicate source consumes water, while on the other hand the polymerisation between dissolved aluminium and silicon species produces water. Thereby, a higher extent of water loss in the later stage of reaction indicates a higher extent of polymerisation. Some of the expelled water during the curing and further drying periods leaves behind discontinuous nano-pores (Provis and Deventer, 2009).

Hence, the water in the alkali activated mixture provides a reaction medium and assures the workability of the mixture during mixing and handling (Slaty et al., 2013). To obtain

an optimal composition it is required to know the effective water content in term of H_2O/M_2O molar ratio (where M corresponds to sodium or potassium).

A high H_2O/M_2O ratio has a negative effect on the degree of polymerisation since an excess of water prevents condensation reactions. The effect of excess water may be to dilute the reaction or to leach the more soluble components and transport them away from the reaction zone (Barbosa et al., 2000). A high H_2O/M_2O ratio also results in the presence of excessive pores and microcracks within the matrix leading to low compressive strength (Yusuf et al., 2014).

Nevertheless, a small quantity of non-evaporable structural water must always be present in the matrix in order to preserve a structural integrity. In fact, the presence of a discontinuous nanopores network in the matrix provides benefits to the performance of alkali activated concrete (Provis and Deventer, 2009).

No optimum range of the H_2O/M_2O ratio will be given as it highly depends on the characteristics of the aluminosilicate source especially its fineness.

Remark: For synthesis at ambient temperature without any curing stage at elevated temperature (as for the application targeted herein), the H_2O/M_2O ratio should be chosen carefully as water will evaporate slowly resulting in higher time to gain full strength.

2.2.4 Other synthesis conditions

2.2.4.1 Temperature

Heat curing is generally recommended since it substantially assists the chemical reaction that occurs in the geopolymer paste (Provis and Deventer, 2009). In effect, temperature noticeably increases the reaction rate. For instance, early investigations showed that increasing the temperature up to 60 °C shortened the dissolution time from 90 days (at 20 °C) to about 14 days (at 60 °C) (Buchwald et al., 2009).

However, some data indicate excellent mechanical properties under ambient conditions, contradicting the requirement of extended periods of heat curing for satisfactory mechanical strength development (Wang et al., 1994; Shi and Li, 1989; Provis and Deventer, 2009). Rather, an adequately controlled and designed formulation can certainly

harden and develop excellent mechanical properties under ambient conditions (Provis and van Deventer, 2014).

2.2.4.2 Curing time

In the same way as Portland cement, alkali activated materials develop short and long-term properties. Moreover, compressive strength increases along with increase of curing time.

Nonetheless, reaction times can be very long for alkali activated materials despite elevated curing temperature. Indeed, progress of alkali activated reactions have shown to be fast during the first hours but then significantly slower.

2.2.4.3 How to stop alkali activation reactions?

As discussed above reaction times in alkali activated systems can be very long, polymerisation reaction occurring as long as soluble species and water are present within the structure.

Yet, in order to study samples at a given curing time alkali activated reactions must be stopped.

As a solution, samples can be freeze dried which allow the removal of water preventing any further reactions. In the specific case of studying the microstructure, a quick freeze drying should be performed in order to avoid any disturbance of the pore networks. It consists in immersing the sample in a liquid (such as isopentane) that has been cooled to its melting point in liquid nitrogen (Mitchell and Soga, 2005).

Another possible treatment consisting in a combination of water treatment to extract soluble species, and solvent treatment to extract water was seen to stop the reaction sequence for at least one week so that the material can be characterised within this time range (Chen et al., 2014).

2.3 Use of Alkali Activated Materials for soil stabilisation

2.3.1 Global context and key issues

To date, several applications of geopolymer products and alkali activated materials have already been industrialised in various areas such as the cement, ceramic and automobile industries (Davidovits, 2002). Nevertheless, very few researches have been carried out on soil stabilisation application, the oldest study dating back to only 2008.

It exists several limiting factors to its application. For instance, the complexity of soils which contains various mineral phases of different particle size, shape and composition renders difficult to predict soil behaviour following alkaline attack. Besides, each family of minerals reacts differently under alkaline condition. A first stage of studying individual mineral behaviour is thus necessary.

Another key issue is the corrosive character of alkaline solutions with specific concentration. Such solutions are User-hostile, dangerous for both workers and the soils, and cannot be implemented in mass applications without the appropriate safety procedures (Davidovits, 2011). Consequently, there is an additional need to develop user-friendly reactive alkaline solution.

Finally, soil stabilisation techniques are designed at room temperature. In those conditions clay minerals even if they constitute an aluminosilicate source are weakly reactive during alkaline activation (as described in the following section 2.3.2). The addition of a more reactive aluminosilicate material at ambient temperature is therefore required for such application (see section 2.3.3 and 2.3.4).

2.3.2 Alkali activation of naturally occurring clay minerals at ambient temperature

As shown in various studies and detailed below clay minerals are crystalline aluminosilicates and hence very stable matter resistant to alkaline attack.

1:1 clays (T-O clays)

Although 1:1 clays show the highest reactivity, their reaction following the alkaline attack is incomplete (Yousef et al., 2012).

Moreover, Mackenzie et al. (MacKenzie et al., 2007) confirmed the inability of 1:1 halloysite clay mineral (Figure 8a) to form a viable geopolymer albeit some degree of reaction was observed. The samples set to some extent but did not achieve the texture and hardness of a well-formed geopolymer product.

2:1 clays (T-O-T clays)

By contrast with the 1:1 aluminosilicate clays, it is much more difficult to alkali activate the corresponding 2:1 clays.

In effect, MacKenzie et al. (MacKenzie et al., 2008) proved that the crystallinity of pyrophyllite (2:1 analogous of kaolinite), and the protection of its octahedral layers by the enclosing tetrahedral layers typical of the 2:1 structure (Figure 8b) prevent its alkali activation.

On the basis of this structural reasoning, similar difficulties might be encountered in alkali activated material formation from other types of 2:1 clay minerals such as montmorillonite, muscovite and illite.

However, the reactivity of a clay mineral is as well influenced by the degree of substitution in its tetrahedral layers; a mineral containing a higher degree of tetrahedral aluminium for silicon substitution showing higher leaching rates in acid (MacKenzie et al., 2004). Thereby, smectitic clays with a higher extent of substitutions are slightly more reactive materials of the 2:1 type clay family.

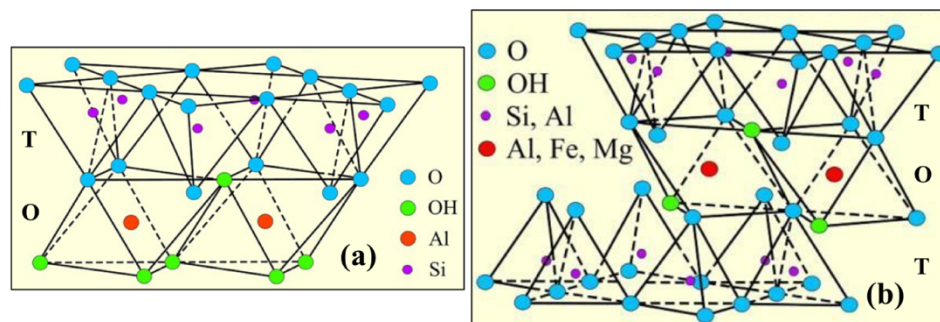


Figure 8: Schematic representation of (a) 1:1 layer, (b) 2:1 layer type clay

As a conclusion, naturally occurring clays are generally few reactive or unreactive to alkali attack, and their use as a raw material generally requires pre-treatment. Such a pre-treatment can consist of a thermal dehydroxylation between 550 °C and 800 °C or a high energy grinding (Provis and Deventer, 2009).

It also exists chemical pre-treatments to render clay minerals more reactive to alkali activated synthesis without the expenditure of additional energy. For instance, pre-treatment of a 1:1 halloysite unheated clay with 0,1M NaOH up to 24 hours gives a set and hardened final material (MacKenzie et al., 2007).

The main objective of these pre-treatments is to render the aluminium of the clay mineral more soluble under the alkaline synthesis environment (MacKenzie et al., 2007).

However, considering the targeted domain of application that is soil stabilisation a high temperature or grinding pre-treatment of the local soil are not practicable. While using sodium hydroxide NaOH as a pre-treatment represents a hostile alternative as NaOH is a corrosive solution.

2.3.3 Overview of research on alkali activated soils

By contrast to naturally occurring clays calcined source materials such as metakaolin and fly ash usually display a higher reactivity during alkaline activation because they contain certain quantities of amorphous high-energy phase (Buchwald et al., 2009). Therefore, to date, except one particular study (Verdolotti et al., 2008) any known studies on the use of alkali activated materials for soil stabilisation required the use of an additional reactive aluminosilicate source under ambient temperature. Those studies are detailed below.

In situ alkali activation of pozzolanic soils by reaction with strong hydroxide NaOH solution or an alkaline solution of NaAlO₂ has been addressed by Verdolotti et al. (Verdolotti et al., 2008). The final product sets to give a strong material. However, this study represents a specific case as pozzolanic soils have already been subjected to elevated temperatures and therefore constitute a reactive material.

Other works on alkali activated soil are recent and aim to stabilise different types of soil from clayey soil (Wilkinson et al., 2010; Singhi et al., 2016), sandy clay (Cristelo et al., 2011), marl, marlstone (Cristelo et al., 2012), silty sand (Rios et al., 2016), road aggregates (Tenn et al., 2015) to mixed soil synthesised in laboratory (Sargent et al., 2013; Zhang et al., 2013).

The type of aluminosilicate material needed in the alkali activation process varies as well. Most of the studies were conducted on the use of fly ash (Wilkinson et al., 2010; Cristelo et al., 2011; Cristelo et al., 2012; Sargent et al., 2013; Silva et al., 2013; Singhi et al., 2016; Rios et al., 2016). Nevertheless, Zhang et al. (Zhang et al., 2013) also examined the feasibility of metakaolin based alkali activated soil and some other studies on slag-based alkali activated soil are as well existing (Wilkinson et al., 2010; Sargent et al., 2013; Singhi et al., 2016).

The overall works showed the potential of alkaline activation for soil improvement and this for different designed applications. Cristelo et al. (Cristelo et al., 2011), for instance, demonstrated that alkaline activation is a viable technique to be applied in deep soft soil improvement, more specifically to jet grouting columns. Their use of fly ash and alkaline activator resulted in a soil strength improvement up to 11.4, 16.7 and 43.4 MPa at 28, 90 and 365 days curing, respectively.

While Zhang et al. (Zhang et al., 2013) described a different potential application of alkali activated soil stabilisation at shallow depth (i.e. subgrade, sub-base, shallow foundation, embankment etc.).

Or else, Silva et al. (Silva et al., 2013) proved the use of alkaline activation of fly ash as a stabilisation technique to be capable of improving the performance of rammed earth construction.

2.3.4 Choice of a reactive aluminosilicate

2.3.4.1 Possibilities

As seen above it exists different possibilities of reactive aluminosilicate. In the context of resource-saving the use of industrial wastes such as fly ash and blast furnace slag could however be preferred over metakaolin which is made from burnt kaolin, and hence requires energy to be produced.

To date, most of the studies on the use of alkali activated materials in soil stabilisation use metakaolin, fly ash and slag as reactive sources as they are well known and have already been extensively studied to produce alkali activated materials.

However, other possibilities of industrial waste can be envisaged such as silica fume or rice husk ash depending on the availability of local waste in a given area.

Or else, in Italy the use of locally available volcanic pyroclastic soil as a reactive aluminosilicate can also be envisaged.

In this study and as a preliminary stage, an industrial waste namely coal fly ash has been selected.

2.3.4.2 Coal fly ash

Coal fly ash is obtained by electrostatic or mechanical precipitation of dust-like particles during coal combustion (Lea and Hewlett, 2004). The constituents of fly ash consequently depend on the type of coal and combustion process. The coal being inhomogeneous, the resulting fly ash is a highly inhomogeneous material. In fact, fly ash chemical composition may differ between two or even within one single particle, making of fly ash a complex multi-phase material.

This inhomogeneity is problematic as the alkali activation process depends on the individual ash source selected. The knowledge of which phases the fly ash contains and which are accessible during alkali activation is therefore essential to enable a correct mechanistic analysis to be applied to each source (Provis and Deventer, 2009).

Additionally, two main classes of fly ash can be distinguished following their chemical composition (ASTM Standard C 618-85)(Lea and Hewlett, 2004):

- Class F fly ash: generally produced from burning anthracite or bituminous coal, and for which the sum of silica, alumina and ferric oxide present is at least equal to 70 %;
- Class C fly ash: generally produced from lignite or sub-bituminous coal. In that case the sum of silica, alumina and ferric oxide present is at least equal to 50 %. Class C fly ash are also referred to as calcium-rich fly ash.

The chemical composition of fly ash greatly influences the reaction sequence. Especially, it is worth noted that in the case of Class C fly ash rich in calcium, the introduction of an additional calcium source introduces further complexity into the range of phases that can be formed in the reaction system (Provis and Deventer, 2009). Namely it exists a competition between the formation of a three-dimensional alkali aluminosilicate framework structure characteristic of geopolymer, N–A–S–H gel and calcium silicate hydrate (C–S–H) typical of Portland cement.

Some studies reported the possible coexistence of those phases within a single binder (Granizo et al., 2002; Yip and Van Deventer, 2003; Yip et al., 2005; Buchwald et al., 2007; Yip et al., 2008). Garcia-Lodeiro et al. (Garcia-Lodeiro et al., 2011) even proposed a tentative phase diagram for the $\text{Na}_2\text{O}-\text{CaO}-\text{Al}_2\text{O}_3-\text{SiO}_2$ system at 25 °C, showing that the coexistence of geopolymer and C–S–H phases is highly related to the pH and that a further competition over time is expected.

The positive or negative effect of the presence of calcium has long been discussed. Some authors consider that the presence of calcium in high amounts may interfere with the polymerisation process and alter the microstructure (Provis and Deventer, 2009). While other studies agree on calcium being pivotal for the strength and durability of alkali activated materials through the formation of a cementitious Ca-Al-Si gel (Yip et al., 2005; Xu and Van Deventer, 2000; Phair and Van Deventer, 2002).

For those reasons, when using fly ash and more particularly calcium-rich fly ash it exists a wide range of potential binding phases with different properties.

2.4 Summary and conclusions

As a conclusion the use of alkali activated materials for soil stabilisation constitutes a promising research area. Clay soils at ambient temperature do not react much. That is why a reactive aluminosilicate has to be added to the system. This can be fly ash, metakaolin, slag or volcanic soils for instance following the local availability.

Many parameters influence the final characteristics of alkali activated materials. Each constituents and synthesis conditions must therefore be chosen carefully. A specific and adapted formulation was hence developed in this study to suit the particular purpose of soil stabilisation and following the general guidelines herein presented. Kaolin was for instance considered as unreactive. Moreover, the Al/Na ratio was not fixed to one because of the presence of calcium ions in high quantity from fly ash, and also playing a role of charge compensation as well as sodium. Consequently, the Si/Al ratio was slightly higher than what is generally proposed in the literature and mentioned here. A predominant part of the work was hence focused on developing a binder for soil stabilisation application with an emphasis on understanding its reactivity both in terms of physicochemical evolution and microstructure. That is why our system was generally studied considering the binder alone firstly and the binder mixed with kaolin afterwards.

Because of the complexity of the system chosen in this study comprising both calcium and sodium cations, various products can potentially be expected. The structure and chemistry of the new phases formed strongly influence the mechanical properties and durability of the final material. It is therefore of paramount importance to identify those phases in order to understand the mechanical behaviour.

In fact, the ability to innovate and to incorporate materials safely in a design is rooted in an understanding of how to manipulate materials properties and functionality through the control of materials structure and processing techniques (Askeland et al., 2011). A major key point of this study was therefore devoted at developing an understanding of this new material on various scale levels all interdependent of one-another.

2.5 References

- Aiello, R., Crea, F., Nastro, A., Subotić, B., Testa, F., 1991. Influence of cations on the physicochemical and structural properties of aluminosilicate gel precursors. Part 1. Chemical and thermal properties. *Zeolites* 11, 767–775.
- Askeland, D.R., Fulay, P.P., Wright, W.J., 2011. *The science and engineering of materials*, 6th ed. ed. Cengage Learning, Stamford, CT.
- Barbosa, V.F., MacKenzie, K.J., Thaumaturgo, C., 2000. Synthesis and characterisation of materials based on inorganic polymers of alumina and silica: sodium polysialate polymers. *Int. J. Inorg. Mater.* 2, 309–317.
- Buchwald, A., Hilbig, H., Kaps, C., 2007. Alkali-activated metakaolin-slag blends—performance and structure in dependence of their composition. *J. Mater. Sci.* 42, 3024–3032. <https://doi.org/10.1007/s10853-006-0525-6>
- Buchwald, A., Hohmann, M., Posern, K., Brendler, E., 2009. The suitability of thermally activated illite/smectite clay as raw material for geopolymer binders. *Appl. Clay Sci.* 46, 300–304. <https://doi.org/10.1016/j.clay.2009.08.026>
- Chen, X., Meawad, A., Struble, L.J., 2014. Method to Stop Geopolymer Reaction. *J. Am. Ceram. Soc.* 97, 3270–3275. <https://doi.org/10.1111/jace.13071>
- Criado, M., Fernández-Jiménez, A., Palomo, A., 2010. Alkali activation of fly ash. Part III: Effect of curing conditions on reaction and its graphical description. *Fuel* 89, 3185–3192. <https://doi.org/10.1016/j.fuel.2010.03.051>
- Criado, M., Fernández-Jiménez, A., Palomo, A., Sobrados, I., Sanz, J., 2008. Effect of the SiO₂/Na₂O ratio on the alkali activation of fly ash. Part II: ²⁹Si MAS-NMR Survey. *Microporous Mesoporous Mater.* 109, 525–534. <https://doi.org/10.1016/j.micromeso.2007.05.062>
- Cristelo, N., Glendinning, S., Fernandes, L., Pinto, A.T., 2012. Effect of calcium content on soil stabilisation with alkaline activation. *Constr. Build. Mater.* 29, 167–174. <https://doi.org/10.1016/j.conbuildmat.2011.10.049>
- Cristelo, N., Glendinning, S., Teixeira Pinto, A., 2011. Deep soft soil improvement by alkaline activation. *Proc. Inst. Civ. Eng. - Ground Improv.* 164, 73–82. <https://doi.org/10.1680/grim.900032>
- Davidovits, J., 2017. Why Alkali-Activated Materials are NOT Geopolymers? [WWW Document]. Geopolymer Inst. URL <https://www.geopolymer.org/faq/alkali-activated-materials-geopolymers/>

- Davidovits, J., 2011. Geopolymer chemistry and applications, 3. ed. ed. Inst. Géopolymère, Saint-Quentin.
- Davidovits, J., 2005. Geopolymer, Green Chemistry and Sustainable Development Solutions: Proceedings of the World Congress Geopolymer 2005. Geopolymer Institute.
- Davidovits, J., 2002. 30 years of successes and failures in geopolymer applications. Market trends and potential breakthroughs, in: Keynote Conference on Geopolymer Conference.
- Davidovits, J., 1994. Properties of geopolymer cements, in: Alkaline Cements and Concretes. Presented at the First International Conference on Alkaline Cements and Concretes, Scientific Research Institute on Binders and Materials, Kiev State Technical University, Kiev, Ukraine, pp. 131–149.
- Duxson, P., Fernández-Jiménez, A., Provis, J.L., Lukey, G.C., Palomo, A., van Deventer, J.S.J., 2007. Geopolymer technology: the current state of the art. *J. Mater. Sci.* 42, 2917–2933. <https://doi.org/10.1007/s10853-006-0637-z>
- Duxson, P., Provis, J.L., Lukey, G.C., Mallicoat, S.W., Kriven, W.M., van Deventer, J.S.J., 2005. Understanding the relationship between geopolymer composition, microstructure and mechanical properties. *Colloids Surf. Physicochem. Eng. Asp.* 269, 47–58. <https://doi.org/10.1016/j.colsurfa.2005.06.060>
- Fernández-Jiménez, A., Palomo, A., Sobrados, I., Sanz, J., 2006. The role played by the reactive alumina content in the alkaline activation of fly ashes. *Microporous Mesoporous Mater.* 91, 111–119. <https://doi.org/10.1016/j.micromeso.2005.11.015>
- Fletcher, R.A., MacKenzie, K.J.D., Nicholson, C.L., Shimada, S., 2005. The composition range of aluminosilicate geopolymers. *J. Eur. Ceram. Soc.* 25, 1471–1477. <https://doi.org/10.1016/j.jeurceramsoc.2004.06.001>
- Garcia-Lodeiro, I., Palomo, A., Fernández-Jiménez, A., Macphee, D.E., 2011. Compatibility studies between N-A-S-H and C-A-S-H gels. Study in the ternary diagram Na₂O–CaO–Al₂O₃–SiO₂–H₂O. *Cem. Concr. Res.* 41, 923–931. <https://doi.org/10.1016/j.cemconres.2011.05.006>
- Granizo, M.L., Alonso, S., Blanco-Varela, M.T., Palomo, A., 2002. Alkaline activation of metakaolin: effect of calcium hydroxide in the products of reaction. *J. Am. Ceram. Soc.* 85, 225–231.
- Granizo, M.L., Blanco-Varela, M.T., Martínez-Ramírez, S., 2007. Alkali activation of metakaolins: parameters affecting mechanical, structural and microstructural properties. *J. Mater. Sci.* 42, 2934–2943. <https://doi.org/10.1007/s10853-006-0565-y>
- Hardjito, D., Rangan, B.V., 2005. Development and properties of low-calcium fly ash-based geopolymer concrete. Faculty of Engineering. Curtin University of Technology, Perth, Australia.

Ivanova, I.I., Aiello, R., Nagy, J.B., Crea, F., Derouane, E.G., Dumont, N., Nastro, A., Subotic, B., Testa, F., 1994. Influence of cations on the physicochemical and structural properties of aluminosilicate gel precursors: II. Multinuclear magnetic resonance characterization. *Microporous Mater.* 3, 245–257.

Lea, F.M., Hewlett, P.C., 2004. *Lea's chemistry of cement and concrete*.

MacKenzie, K.J.D., Brew, D.R.M., Fletcher, R.A., Vagana, R., 2007. Formation of aluminosilicate geopolymers from 1:1 layer-lattice minerals pre-treated by various methods: a comparative study. *J. Mater. Sci.* 42, 4667–4674. <https://doi.org/10.1007/s10853-006-0173-x>

MacKenzie, K.J.D., Komphanchai, S., Vagana, R., 2008. Formation of inorganic polymers (geopolymers) from 2:1 layer lattice aluminosilicates. *J. Eur. Ceram. Soc.* 28, 177–181. <https://doi.org/10.1016/j.jeurceramsoc.2007.06.004>

MacKenzie, K.J.D., Okada, K., Temuujin, J., 2004. Nanoporous inorganic materials from mineral templates. *Curr. Appl. Phys.* 4, 167–170. <https://doi.org/10.1016/j.cap.2003.10.023>

McCormick, A.V., Bell, T., 1989. The Solution Chemistry of Zeolite Precursors. *Catal. Rev. Sci. Eng.* 31, 97.

Mitchell, J.K., Soga, K., 2005. *Fundamentals of soil behavior*, 3rd ed. ed. John Wiley & Sons, Hoboken, N.J.

Pacheco-Torgal, F., Labrincha, J.A., Leonelli, C., Palomo, A., Chindaprasirt, P., 2015. *Handbook of Alkali-activated Cements, Mortars and Concretes*, Woodhead Publishing series in Civil and Structural Engineering. Elsevier.

Phair, J.W., Van Deventer, J.S.J., 2002. Effect of the silicate activator pH on the microstructural characteristics of waste-based geopolymers. *Int. J. Miner. Process.* 66, 121–143.

Pimraksa, K., Chindaprasirt, P., Rungchet, A., Sagoe-Crentsil, K., Sato, T., 2011. Lightweight geopolymer made of highly porous siliceous materials with various Na₂O/Al₂O₃ and SiO₂/Al₂O₃ ratios. *Mater. Sci. Eng. A* 528, 6616–6623. <https://doi.org/10.1016/j.msea.2011.04.044>

Provis, J.L., Deventer, J.S.J. va., 2009. *Geopolymers Structure, processing, properties and industrial applications*, Woodhead Publishing in materials. Woodhead, Cambridge.

Provis, J.L., van Deventer, J.S.J. (Eds.), 2014. *Alkali Activated Materials*, RILEM State-of-the-Art Reports. Springer Netherlands, Dordrecht.

- Rios, S., Cristelo, N., Viana da Fonseca, A., Ferreira, C., 2016. Structural Performance of Alkali-Activated Soil Ash versus Soil Cement. *J. Mater. Civ. Eng.* 28, 4015125. [https://doi.org/10.1061/\(ASCE\)MT.1943-5533.0001398](https://doi.org/10.1061/(ASCE)MT.1943-5533.0001398)
- Rowles, M., O'Connor, B., 2003. Chemical optimisation of the compressive strength of aluminosilicate geopolymers synthesised by sodium silicate activation of metakaolinite. *J. Mater. Chem.* 13, 1161–1165. <https://doi.org/10.1039/b212629j>
- Sargent, P., Hughes, P.N., Rouainia, M., White, M.L., 2013. The use of alkali activated waste binders in enhancing the mechanical properties and durability of soft alluvial soils. *Eng. Geol.* 152, 96–108. <https://doi.org/10.1016/j.enggeo.2012.10.013>
- Shi, C., Li, Y., 1989. Investigation on some factors affecting the characteristics of alkali-phosphorus slag cement. *Cem. Concr. Res.* 19, 527–533.
- Silva, R.A., Oliveira, D.V., Miranda, T., Cristelo, N., Escobar, M.C., Soares, E., 2013. Rammed earth construction with granitic residual soils: The case study of northern Portugal. *Constr. Build. Mater.* 47, 181–191. <https://doi.org/10.1016/j.conbuildmat.2013.05.047>
- Singhi, B., Laskar, A.I., Ahmed, M.A., 2016. Investigation on Soil–Geopolymer with Slag, Fly Ash and Their Blending. *Arab. J. Sci. Eng.* 41, 393–400. <https://doi.org/10.1007/s13369-015-1677-y>
- Slaty, F., Khoury, H., Wastiels, J., Rahier, H., 2013. Characterization of alkali activated kaolinitic clay. *Appl. Clay Sci.* 75–76, 120–125. <https://doi.org/10.1016/j.clay.2013.02.005>
- Swaddle, T.W., 2001. Silicate complexes of aluminum (III) in aqueous systems. *Coord. Chem. Rev.* 219, 665–686.
- Tenn, N., Allou, F., Petit, C., Absi, J., Rossignol, S., 2015. Formulation of new materials based on geopolymer binders and different road aggregates. *Ceram. Int.* 41, 5812–5820. <https://doi.org/10.1016/j.ceramint.2015.01.010>
- van Jaarsveld, J.G.S., van Deventer, J.S.J., 1999. Effect of the Alkali Metal Activator on the Properties of Fly Ash-Based Geopolymers. *Ind. Eng. Chem. Res.* 38, 3932–3941. <https://doi.org/10.1021/ie980804b>
- V.D. Glukhovskiy, 1959. *Glukhovskiy_ref.docx*. Gosstroyizdat.
- Verdolotti, L., Iannace, S., Lavorgna, M., Lamanna, R., 2008. Geopolymerization reaction to consolidate incoherent pozzolanic soil. *J. Mater. Sci.* 43, 865–873. <https://doi.org/10.1007/s10853-007-2201-x>

- Wang, H., Li, H., Yan, F., 2005. Synthesis and mechanical properties of metakaolinite-based geopolymer. *Colloids Surf. Physicochem. Eng. Asp.* 268, 1–6. <https://doi.org/10.1016/j.colsurfa.2005.01.016>
- Wang, S.-D., Scrivener, K.L., Pratt, P.L., 1994. Factors affecting the strength of alkali-activated slag. *Cem. Concr. Res.* 24, 1033–1043.
- Wilkinson, A., Haque, A., Kodikara, J., 2010. Stabilisation of clayey soils with industrial by-products: part A. *Proc. Inst. Civ. Eng. - Ground Improv.* 163, 149–163. <https://doi.org/10.1680/grim.2010.163.3.149>
- Xu, H., van Deventer, J.S., 2003. The effect of alkali metals on the formation of geopolymeric gels from alkali-feldspars. *Colloids Surf. Physicochem. Eng. Asp.* 216, 27–44.
- Xu, H., Van Deventer, J.S.J., 2000. The Geopolymerisation of Alumino-Silicate Minerals. *Int. J. Miner. Process.* 59 247–266.
- Yip, C.K., Lukey, G.C., Provis, J.L., van Deventer, J.S.J., 2008. Effect of calcium silicate sources on geopolymerisation. *Cem. Concr. Res.* 38, 554–564. <https://doi.org/10.1016/j.cemconres.2007.11.001>
- Yip, C.K., Lukey, G.C., van Deventer, J.S.J., 2005. The coexistence of geopolymeric gel and calcium silicate hydrate at the early stage of alkaline activation. *Cem. Concr. Res.* 35, 1688–1697. <https://doi.org/10.1016/j.cemconres.2004.10.042>
- Yip, C.K., Van Deventer, J.S.J., 2003. Microanalysis of calcium silicate hydrate gel formed within a geopolymeric binder. *J. Mater. Sci.* 38, 3851–3860.
- Yousef, R.I., El-Eswed, B., Alshaaer, M., Khalili, F., Rahier, H., 2012. Degree of reactivity of two kaolinitic minerals in alkali solution using zeolitic tuff or silica sand filler. *Ceram. Int.* 38, 5061–5067. <https://doi.org/10.1016/j.ceramint.2012.03.008>
- Yusuf, M.O., Megat Johari, M.A., Ahmad, Z.A., Maslehuddin, M., 2014. Effects of H₂O/Na₂O molar ratio on the strength of alkaline activated ground blast furnace slag-ultrafine palm oil fuel ash based concrete. *Mater. Des.* 56, 158–164. <https://doi.org/10.1016/j.matdes.2013.09.078>
- Zhang, M., Guo, H., El-Korchi, T., Zhang, G., Tao, M., 2013. Experimental feasibility study of geopolymer as the next-generation soil stabilizer. *Constr. Build. Mater.* 47, 1468–1478. <https://doi.org/10.1016/j.conbuildmat.2013.06.017>

**Use of alkali activated fly ash binder for
kaolin clay soil stabilisation:
Physicochemical evolution**

Chapter 3 has already been published in *Construction and Building Materials*, Volume 201 on 20 March 2019 (Pages 539-552).

Samples were prepared at the University of Cassino and Southern Lazio. While all experiments were carried out at the Institute of Materials Jean Rouxel.

The Candidate performed the analysis, collected the data, conceived and designed the analysis and wrote the paper. Michael Paris from the Institute of Materials Jean Rouxel helped and supervised the performance of Nuclear Magnetic Resonance analysis. He also corrected the paper and helped refine the interpretation of NMR results and the discussion. Dimitri Deneele from the Institute of Materials Jean Rouxel helped and supervised the performance of Scanning Electron Microscopy. He also corrected the paper and helped refine the interpretation of results. Giacomo Russo from the University of Cassino and Southern Lazio and Alessandro Tarantino from the University of Strathclyde helped in correcting the paper.

3.1 Abstract

This study addresses the use of alkali activated fly ash-based binder to improve engineering characteristics of soft clay-rich soils as an alternative to common stabilisers such as lime and Ordinary Portland Cement. In particular, it investigates the physicochemical evolution of a calcium-rich fly ash from coal combustion binder activated by a sodium-based alkaline solution. The aim of this work is to explore the feasibility of this binder as a potential soil stabiliser. To this end, the phases that are dissolved following alkaline activation, the phases that are subsequently formed, and reactivity timescale are investigated to anticipate the short and the long-term performance of the binder. A second question addressed by this study is whether the presence of kaolin affects the reactivity of the binder. The reaction sequence has therefore been investigated by considering the binder alone and the binder mixed with kaolin.

A set of complementary techniques have been used including X-ray diffraction, Derivative thermogravimetric analysis, Fourier Transform Infrared spectroscopy, Scanning Electron Microscopy, ^{29}Si and ^{27}Al Nuclear Magnetic Resonance.

An insight into the reactivity evidenced that calcium-containing phases derived from fly ash represent the reactive phases and, hence, pozzolanic activity is the dominant process. New compounds are formed, thenardite Na_2SO_4 and an amorphous silicate consisting of chains combined with calcium probably incorporating three-dimensional four-fold aluminium environments. Concerning timescale, reactions essentially occur within 28 days. Results also showed that kaolin is unreactive whatever the proportion of added binder down to 20%.

From the chemical composition and molecular structure, it can be inferred that binding phases resulting from alkaline activation have higher long-term stability than phases generally encountered in lime treated kaolin. On the other hand, the newly-formed thenardite is a highly soluble salt and its stability to possible leaching should be investigated in the stabilised soil.

3.2 Introduction

Soft clay-rich soils are frequently encountered in construction sites. Their poor mechanical performance represents a critical issue in engineering projects. These soils cannot be directly used as earthfill materials and may cause excessive settlements of foundation structures. To improve their engineering characteristics chemical stabilisation involving the addition of a binder to the soil has been widely practiced. The commonly used stabilisers are Ordinary Portland Cement and lime whose stabilisation mechanisms have been widely reported (Pomakhina et al., 2012; Lemaire et al., 2013; Chemedda et al., 2015; Deneele et al., 2016; Vitale et al., 2016; Maubec et al., 2017; Vitale et al., 2017; Guidobaldi et al., 2017).

Nevertheless, a major issue with those conventional stabilisers is a very significant environmental penalty due to high carbon dioxide emissions and energy intensive processes. In the low carbon agenda, the development of novel technologies that are both cost- and carbon-efficient is of prime importance, particularly in the construction sector for which cement production contributes to at least 5–8% of global carbon dioxide emissions (Scrivener and Kirkpatrick, 2008). As an alternative, industrial by-products such as fly ash, rice husk ash, and silica fume have been successfully mixed as cementing additives to soft soils resulting in environmental and economic benefits (Rahman, A, 1986; Basha et al., 2003; Nalbantoğlu, 2004; Koliass et al., 2005; Parsons and Kneebone, 2005; Sharmaa et al., 2014; James and Pandian, 2016).

Another alternative gaining attention is the use of Alkali Activated Materials as a viable sustainable binder whose often-claimed advantage is a much lower CO₂ emission process compared to traditional Portland cement. Works on alkali activated binders for soil stabilisation are recent and aim to stabilise different types of soil from clayey soil (Wilkinson et al., 2010; Singhi et al., 2016), sandy clay (Cristelo et al., 2011), marl, marlstone (Cristelo et al., 2012), silty sand (Rios et al., 2016), road aggregates (Tenn et al., 2015) to mixed soil synthesised in laboratory (Sargent et al., 2013; Zhang et al., 2013). The overall work shows the potential of alkaline activation for soil improvement, and this for different designed applications i.e. in deep soft soil (Cristelo et al., 2011), at shallow depth (Zhang et al., 2013) or in rammed earth construction (Silva et al., 2013).

Alkali Activated Materials are defined as any binder system derived by the reaction of an alkali metal source (usually alkali hydroxide and alkali silicate solutions) with a solid aluminosilicate powder (commonly metakaolin, fly ash, blast furnace slag or natural pozzolan) (Buchwald et al., 2003; Shi et al., 2006). It gives a hardened material at room temperature with mechanical properties potentially suitable for Portland cement replacement.

The type of aluminosilicate material needed in the alkali activation process varies as well. In fact, most of the studies were conducted on the use of fly ash (Wilkinson et al., 2010; Cristelo et al., 2011; Cristelo et al., 2012; Sargent et al., 2013; Silva et al., 2013; Singhi et al., 2016; Rios et al., 2016). Nevertheless, Zhang et al. (2013) also examined the feasibility of metakaolin-based alkali activated binder treated soil (Zhang et al., 2013), and some other studies established on slag-based alkali activated binder treated soil are as well existing (Wilkinson et al., 2010; Sargent et al., 2013; Singhi et al., 2016).

As stabilisation using alkaline activated binders is a recent research area, studies about the understanding of the physicochemical reactivity of such systems have received little attention so far (Wilkinson et al., 2010). Yet, the molecular structure and the chemical composition of the alkali activated binders is essential to properly assess the resulting strength and durability of the final material.

This work focuses on the use of calcium-rich fly ash from coal combustion activated by sodium-based alkaline solution as a binder for clay kaolin stabilisation. Fly ash was selected in the context of resource-saving being an industrial waste. Kaolin was selected as a model soil to represent a wide class of clays encountered in engineering projects.

The study was designed in three stages. An initial stage consisted in the investigation of the reactivity of the alkali activated fly ash binder by itself, including (i) which phases are present and which phases are accessible during alkaline activation, (ii) which compounds are subsequently formed, and (iii) reactivity timescale. A second stage focused on the interaction of the fly ash-based binder with the kaolin clay to understand how the presence of kaolin modifies the reactivity of the system. Kaolinite is generally unreactive to alkali attack at ambient temperature. However, the addition of clay may affect chemical reactions as occurs in clay-cement mix (Snellings et al., 2012).

Finally, the physicochemical evolution occurring in the alkali activated fly ash is compared with one occurring in the same kaolin stabilised by i) lime or ii) a mix of lime and the same fly ash used in this experimental programme. This is aimed at assessing the potential benefit of fly ash-based binder compared to the more traditional lime.

3.3 Material and methods

3.3.1 Materials

A Polish fly ash derived from hard coal and coal slime combustion in fluidised bed boiler was used. Its chemical analysis is given in Table 1, and consists primarily of SiO_2 , Al_2O_3 and CaO . The fly ash contains, approximately, 52% of particles sized lower than $45\ \mu\text{m}$ and 41% lower than $10\ \mu\text{m}$.

Table 1: Chemical composition (wt. %) of raw fly ash and kaolin

	SiO ₂	Al ₂ O ₃	Fe ₂ O ₃	CaO	CaO _{free} ^a	MgO	SO ₃	Na ₂ O	K ₂ O	H ₂ O	L.o.I.
Fly ash	39.4	19.8	7.4	18.6	5.2	1.8	4.1	2.0	1.8	0.0	1.7 ^b
Kaolin	49.2	34.5	1.2	0.0	0.0	0.2	0.0	0.1	1.7	13.1	12.0 ^c

^a Free calcium oxide content

^b L.o.I = Loss on ignition 900 °C

^c L.o.I = Loss on ignition 1000 °C

Speswhite kaolin provided by Imerys Minerals UK, and whose chemical composition is given in Table 1 was used. It is mainly constituted of kaolinite (95%) and secondarily of muscovite (4%) (Chemeda, 2015). The kaolin contains, approximately, 100 % of particles sized lower than 10 µm and 80 % lower than 2 µm.

A unique alkaline solution was used: a sodium silicate with a mass ratio SiO₂/Na₂O of 1.7 and a dry mass percentage of 44%; supplied by Woellner Group and named GEOSIL 34417.

3.3.2 Sample preparation

Sample preparation consisted in (i) mix of liquid sources i.e. silicate and water (ii) mix of aluminosilicate powders i.e. fly ash and kaolin in the case of soil-source sample (iii) mix of (i) and (ii) previously prepared.

Three types of mixes were studied and named F100, KF50 and KF20 (see Table 2). F100 is the fly ash-based alkali activated binder. It corresponds to a solid phase made of fly ash only, whereas KF50 and KF20 are the alkali activated binder treated soils. KF50 corresponding to a solid phase made of 50% of fly ash and 50% of kaolin in mass, and KF20 corresponding to a solid phase made of 20% of fly ash and 80% of kaolin.

To ensure a good workability, the amount of added water with respect to the solid mass (e.g. mass of kaolin and fly ash) was fixed to 50% for all the samples. Additionally, the mass ratio of alkaline solution to fly ash was fixed to 50% for all the samples, giving the initial molar ratios (considering that kaolin is unreactive): Si/Al = 2.0, Si/Na = 3.5 and Al/Na = 1.8. The Al/Na ratio was not fixed to one because of the presence of calcium ions in high quantity in our system playing a role of charge compensation as well as sodium.

Table 2: Samples composition wt. %

Sample	Fly ash	Kaolin	Water	Alkaline solution
F100	50	0	25	25
KF50	28.6	28.6	28.6	14.3
KF20	12.5	50	31.3	6.3

The paste obtained was poured in closed plastic molds and cured at room temperature (20 °C). Samples were finally demoulded and freeze-dried at curing times of 1, 3, 7 or 28 days.

3.3.3 Methods

A variety of characterisation techniques were complementary used to probe the mineralogical, structural and microstructural sample characteristics.

X-ray diffractograms of powdered samples were obtained with a Bruker D8 Advance diffractometer, using CuK α radiation generated at 40 mA and 40kV. Specimens were step-scanned from 2 to 60° 2 θ at 0.017° 2 θ steps integrated at the rate of 1s/step.

Derivative thermogravimetric curves were obtained on a Netzsch STA 449F3 Jupiter thermal analyser. The samples were heated from 20–1000 °C at a rate of 10 °C/min under argon atmosphere.

FTIR spectra were obtained on an FTIR Bruker Vertex 70 spectrometer. Specimens were prepared by mixing 30 mg of sample in 270 mg of KBr. Spectral analysis was performed over the range 4000–400 cm⁻¹ at a resolution of 4 cm⁻¹.

Solid-state ²⁹Si NMR spectroscopy was performed using a Bruker Avance III 300 MHz (7 T) spectrometer and 7 mm MAS probe. ²⁹Si MAS spectra were acquired with a single $\pi/2$ pulse excitation of 5.5 μ s and ¹H decoupling. The repetition times were 2 s, 120 s and 30 s for the raw fly ash, the raw kaolin and all the activated samples, respectively. For all ²⁹Si spectra, MAS spinning rate was set to 5 kHz. Solid-state ²⁷Al NMR spectroscopy was performed using a Bruker Avance III 500 MHz (11.7 T) spectrometer and 2.5 mm MAS probe. ²⁷Al MAS spectra were acquired with a single pulse excitation of $\pi/12$ pulse of 3.3 μ s and ¹H decoupling. Repetition time was set to 1 s and MAS spinning rate to 30 kHz. Spectra were referenced against TMS (tetramethylsilane) for ²⁹Si and an Al(NO₃)₃ aqueous solution for ²⁷Al. Lastly, attention should be drawn to the fact that iron initially present in

the fly ash renders the interpretation more complex, notably spectra from different mixes cannot be quantitatively compared.

Finally, samples were studied by SEM from polished section. Freeze-dried samples were impregnated under a vacuum with an acrylic resin (LR White). The polymerisation of the resin was performed in an oven at 60 °C over 48 h. The samples were then polished with diamond powder and coated with carbon before the observation. The observations were done with a HITACHI SU5000 scanning electron microscope equipped with an energy-dispersive X-ray analyser (Quantax microanalyser system composed of X-Flash® SDD detector and the Esprit software). The microscope was operated at an accelerating voltage of 20 kV and working distances of 10 mm.

3.4 Results and discussion

The first section of results presents the physicochemical evolution of the binder alone without the addition of kaolin. The second part focuses on the description of the soil source material mixed with binder. To end with, the system investigated in this study is compared with lime-based systems already described in the literature.

3.4.1 Alkali activated fly ash binder

3.4.1.1 X-ray diffraction (XRD)

Results obtained by XRD show that the original fly ash is constituted of a vitreous phase (hump between $17^{\circ}2\theta$ and $38^{\circ}2\theta$), and crystalline phases which include calcium-containing minerals: anhydrite CaSO_4 , calcite CaCO_3 and portlandite $\text{Ca}(\text{OH})_2$, and other minerals: quartz SiO_2 , feldspar $(\text{K},\text{Na},\text{Ca})(\text{Si},\text{Al})_4\text{O}_8$, hematite Fe_2O_3 and muscovite $(\text{Si}_3\text{Al})\text{O}_{10}(\text{Al}_2)(\text{OH})_2\text{K}$ (Figure 9).

Figure 9 also shows XRD patterns of the alkali activated fly ash as a function of curing time. Regarding the crystalline phases, anhydrite CaSO_4 and portlandite $\text{Ca}(\text{OH})_2$ are consumed as a function of time. In addition, thenardite Na_2SO_4 starts forming at 3 days. Its formation can be explained by the release of sulphate anions from anhydrite dissolution, and its subsequent combination with sodium issued from the alkaline solution.

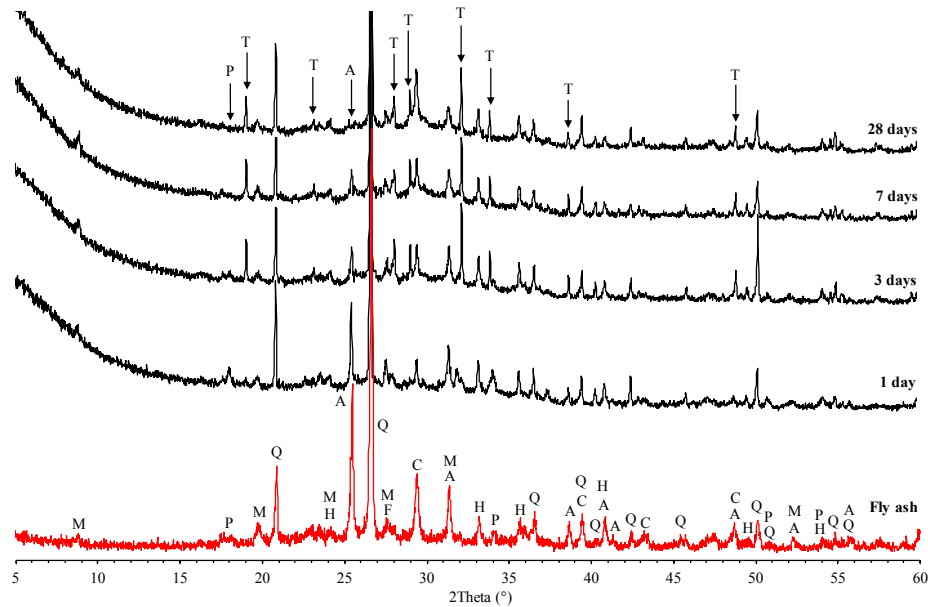


Figure 9: XRD of raw fly ash and fly ash-based alkali activated material F100 as a function of curing time; A=anhydrite; C=calcite; F=feldspar; H=hematite; M=muscovite; P=portlandite; Q=quartz; T=thenardite

3.4.1.2 Derivative thermogravimetric analysis (DTG)

Figure 10 shows derivative thermogravimetric analyses of the original fly ash, and the fly ash-based alkali activated binder as a function of time. The DTG peaks of the original fly ash detected at 385, 605 and 965 °C indicate the decomposition of portlandite $\text{Ca}(\text{OH})_2$, calcium carbonate CaCO_3 and anhydrite CaSO_4 respectively. The relatively low decomposition temperature of anhydrite is ascribed to the fact that anhydrite is found interlinked with other calcium-rich phases by SEM (as demonstrated later in section 3.4.1.4).

Regarding the alkali activated fly ash, and complementary to XRD, thermogravimetric analyses confirm the consumption of portlandite $\text{Ca}(\text{OH})_2$ over time. DTG curves also show the dissolution of calcium carbonate CaCO_3 with time. Finally, above 780 °C, the observed mass losses of the activated samples reveal the decomposition of sulphate minerals: either anhydrite CaSO_4 , or thenardite Na_2SO_4 being formed from 3 days as detected earlier by XRD (see 3.4.1.1).

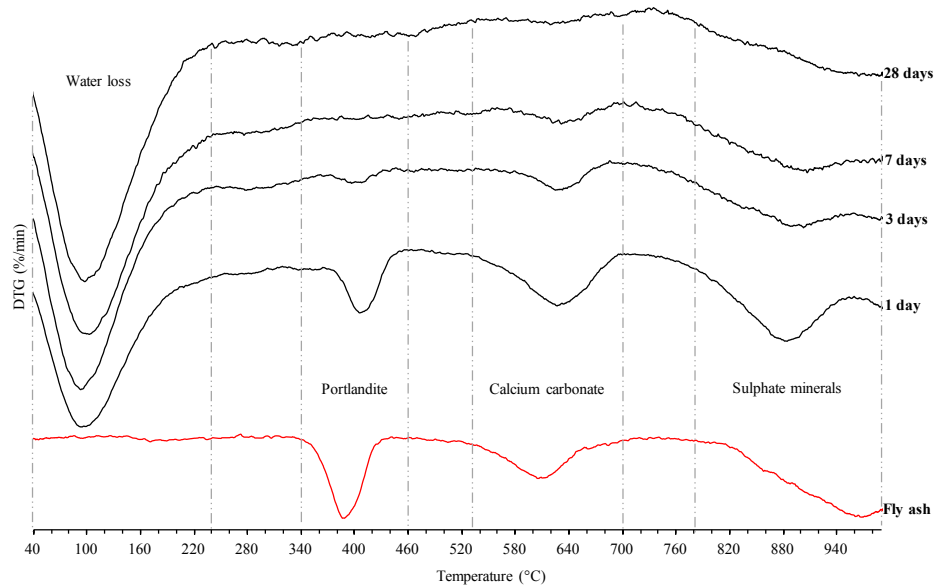


Figure 10: DTG curves of raw fly ash and fly ash-based alkali activated material F100 as a function of curing time

3.4.1.3 Fourier Transform Infrared spectroscopy (FTIR)

Figure 11 shows FTIR spectra of the original fly ash, and the fly ash-based alkali activated binder as a function of time in the range of CO_3^{2-} stretching vibrations.

Different features of the CO_3^{2-} band is observed over time: at 1 day a single band around 1453 cm^{-1} is seen, while at 28 days a doublet positioned at 1426 and 1483 cm^{-1} is observed. Those modifications validate the dissolution of calcium carbonate CaCO_3 from fly ash formerly seen by DTG, and suggest the subsequent combination of released carbonate ions CO_3^{2-} with either calcium or sodium cations present in the medium to form another type of carbonate.

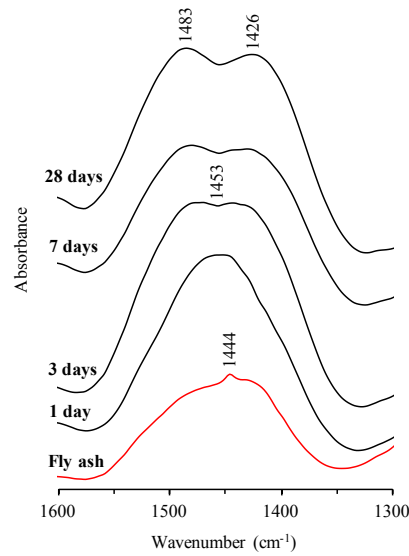


Figure 11: FTIR of raw fly ash and fly ash-based alkali activated material F100 as a function of curing time in the CO_3^{2-} stretching vibrations range

Finally, Figure 12 shows FTIR spectra in the area of sulphate minerals. It confirms the dissolution of calcium sulphate (anhydrite, CaSO_4) along with the subsequent formation of sodium sulphate (thenardite, Na_2SO_4) as previously seen by XRD (see 3.4.1.1).

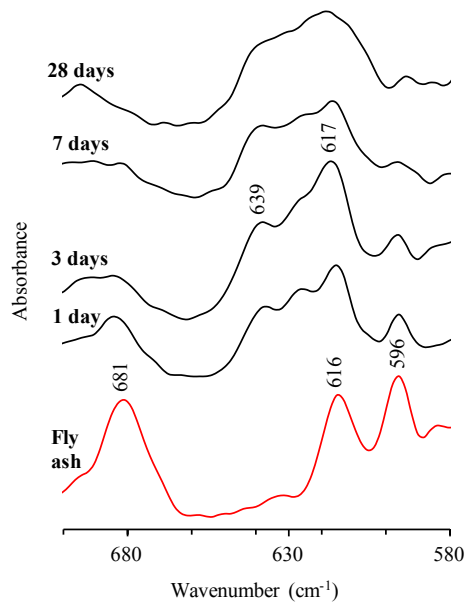


Figure 12: FTIR of raw fly ash and fly ash-based alkali activated material F100 as a function of curing time in the SO_4^{2-} stretching vibrations range; 681, 616 and 596 cm^{-1} = anhydrite CaSO_4 ; 639 and 617 cm^{-1} = thenardite Na_2SO_4

3.4.1.4 Scanning Electron Microscopy (SEM)

Calcium-rich phases

Figure 13 shows SEM observations of the alkali activated fly ash at 1 day. More specifically, it focuses on calcium-rich phases previously detected as reactive phases being dissolved following the alkali attack by XRD, TGA and FTIR.

Calcium-rich phases are initially present in fly ash as nodules of large size from 100 to 250 μm . Besides, it is seen that chemical elements such as calcium, sulphur and silicon are not homogeneously spread within nodules suggesting a varying mineralogy. For instance, in area 2, despite a high content of sulphur indicating a prevalence of anhydrite (CaSO_4), the detected percentage of SO_3 with respect to CaO remains too low to be owed to the presence of anhydrite phases only. It is therefore concluded that the various calcium-containing phases such as anhydrite CaSO_4 , calcite CaCO_3 and portlandite $\text{Ca}(\text{OH})_2$ (previously detected by XRD and DTG in section 3.4.1.1 and 3.4.1.2) are interlaced within those nodule structures which represent reactive structures under alkaline attack.

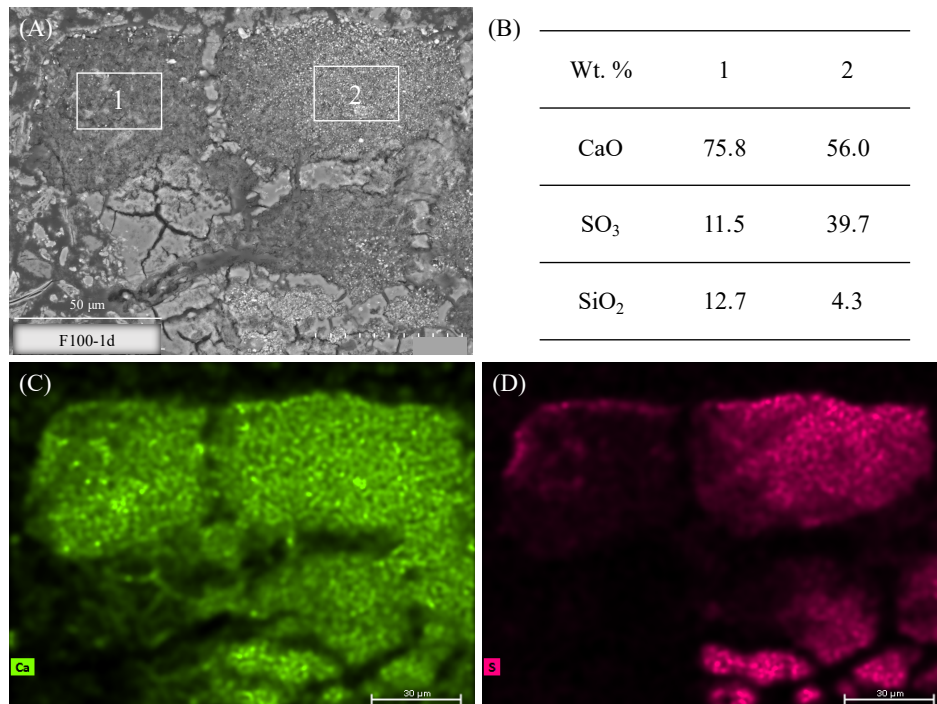


Figure 13: SEM observations of a calcium-rich nodule from the alkali activated fly ash at 1 day: (A) SEM micrograph, (B) chemical composition (wt. %) of areas 1 and 2, (C) and (D) chemical mappings of calcium and sulphur respectively

Overall sample

Figure 14 additionally shows microstructural observations of the alkali activated fly ash binder. At 1 day (Figure 14A), a porous material along with distinct unreacted fly ash particles is seen. In contrast, at 28 days (Figure 14B), a more closed material (with less pores) is observed evidencing the formation of new compounds. Moreover, at 28 days, several unreacted fly ash particles are still observed especially from the vitreous phase i.e. spherical and vesicular particles (see Figure 14B, C and D).

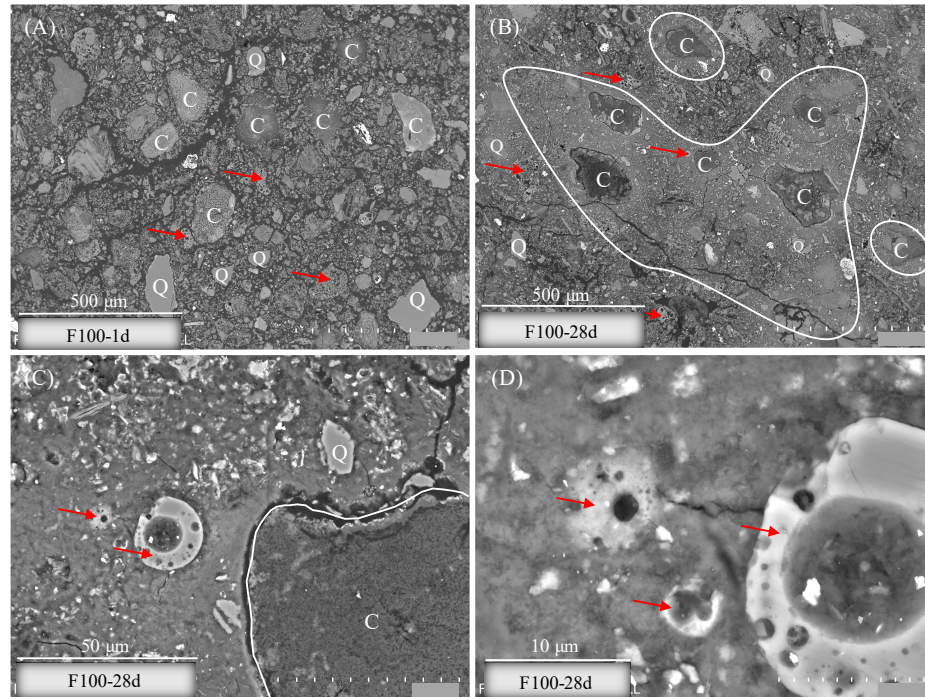


Figure 14: SEM micrographs of the alkali activated fly ash binder F100 (A) at 1 day and (B), (C) and (D) at 28 days; C=calcium nodules; Q=quartz; arrows=glass

Additional chemical analyses revealed that changes in microstructure are more significant around calcium-rich particles which were previously detected as the main reactive part of the raw fly ash. As a matter of fact, SEM micrographs show zones of higher density appearing brighter around calcium-rich nodules (see encircled area in Figure 14B).

Table 3 gives an average chemical composition of the denser reactive areas. Notably, it indicates a ratio of sodium to sulphur around 2 matching with that of precipitated thenardite whose formula is Na_2SO_4 , and implying that most of the sodium from the alkaline solution is taken up to form thenardite.

Furthermore, Table 3 indicates that the massive reactive area is primarily composed of silicon and calcium. Supposing that the new compounds are mainly located in those

denser areas, these results suggest that apart from thernardite the new compounds are enriched in silicon and calcium.

Table 3: Average elemental composition (wt. %) of F100 and KF50 denser areas at 28 days

	Si	Ca	Al	Na	S	K	Fe	Mg	O
F100-28d	22.1	19.2	7.0	3.7	1.7	1.2	0.8	0.5	43.8
KF50-28d	24.1	14.5	8.8	3.1	1.6	1.6	0.7	0.3	45.3

3.4.1.5 Nuclear Magnetic Resonance (NMR)

Nuclear Magnetic Resonance was finally used to follow amorphous phases and precise the structure of the new compounds formed in our investigated system.

Figure 15 shows ^{27}Al MAS-NMR spectrum of the original fly ash as well as the spectrum belonging to the alkali activated fly ash at 28 days. ^{27}Al NMR spectrum of the original fly ash displays two resonances whose dissymmetrical shapes are due to not well organised environments. More specifically, the main resonance whose maximum is detected at 55 ppm corresponds to Al(IV) of the vitreous phase. While the resonance located at 3 ppm corresponds to Al(VI) of the vitreous phase.

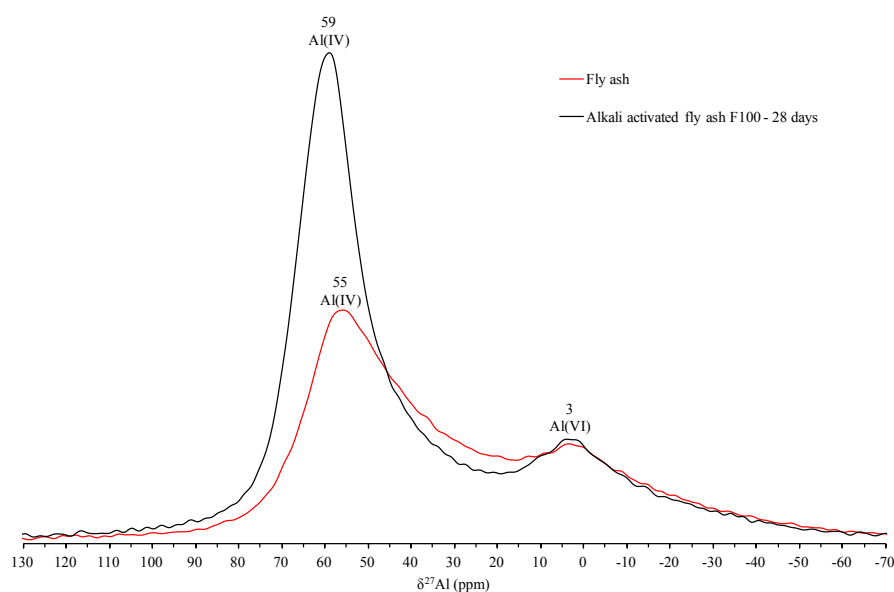


Figure 15: ^{27}Al MAS-NMR spectra of the raw fly ash and alkali activated fly ash at 28 days

Comparatively, the fly ash-based alkali activated material spectrum at 28 days exhibits a main resonance sharper and a maximum shifted to 59 ppm corresponding to four-fold

coordination of aluminium namely $q^4(4Si)$. Those modifications in the spectrum compared to the original fly ash indicate that part of the aluminium released from fly ash leads to the formation a new aluminium bearing phase whose aluminium is tetrahedrally coordinated. Lastly, the resonance owed to octahedral aluminium at 3 ppm is still present which means that fly ash is not totally dissolved after 28 days.

Figure 16 shows ^{29}Si MAS-NMR spectra of the original fly ash as well as the alkali activated fly ash at 28 days. ^{29}Si NMR spectrum of the original fly ash shows a broad resonance between -85 and -105 ppm attributed to the presence of a wide range of Q^3 and Q^4 silicon local environments from the vitreous phase.

In contrast, the alkali activated fly ash spectrum at 28 days displays a clear additional resonance centred at -85 ppm. This new position can be attributed to both the formation of $Q^4(4Al)$ or else Q^2 -type silicon environments. Nevertheless, regarding the high value of the Si/Al ratio around 3.2 in the denser area comprising the new products, and measured by SEM (see Table 3) it is unlikely that $Q^4(4Al)$ environments are present. The new resonance at -85 ppm consequently indicates the formation of Q^2 -type silicon environments in chain structure. Considering that the spectrum does not show any resonance corresponding to Q^1 silicon environments the length of those formed chains is high. It is also worth noting that Q^2 Si environments in chain possess a charge deficit of 2- which must be compensated. However, sodium cations are not available as they are associated with sulphur to form thenardite Na_2SO_4 (see sections 3.4.1.1 and 3.4.1.3). Consequently, only calcium cations released from calcium reactive phases of fly ash can compensate this charge deficit. Those silicon chain structures are therefore combined with dissolved calcium which matches with the chemical composition of the denser reactive area primarily made of silicon and calcium (see Table 3). The significant broadening of the resonance at -85 ppm also indicates that those chains are not well organised as C-S-H structures generally observed in Portland cement (Cong and Kirkpatrick, 1996).

Finally, the broadest part of the activated fly ash spectrum at 28 days from -90 ppm to -100 ppm indicates the presence of Q^3 and Q^4 environments mainly issued from the remaining vitreous phase of fly ash, and in accordance with the previous observations of unreacted fly ash particles at 28 days by SEM (see 3.4.1.4).

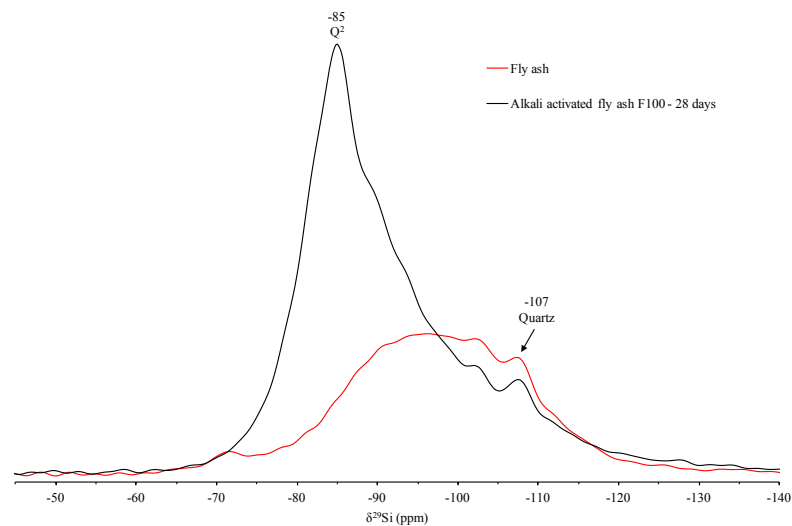


Figure 16: ^{29}Si MAS-NMR spectra of the raw fly ash and alkali activated fly ash at 28 days

In summary, both ^{29}Si and ^{27}Al MAS-NMR spectroscopy indicates the formation of new signals following alkaline activation. It is of interest to understand whether the new aluminium-containing phase seen in ^{27}Al NMR correlates with the silicate chain structure observed in ^{29}Si NMR. As a comparison, aluminium in linear structure such as C–S–H is either found (i) as Q^2 environments corresponding to aluminium substituting for silicon atoms, and located around 68–74 ppm in ^{27}Al NMR or else (ii) as Q^3 environments corresponding to crosslinking through alumina bridging tetrahedra positioned around 63–68 ppm in ^{27}Al NMR (Andersen et al., 2003; Sun et al., 2006; Pardal et al., 2012). However, as mentioned above, the new aluminium resonance observed in our investigation at 59 ppm would rather correspond to $\text{q}^4(4\text{Si})$ environment. Consequently, if aluminium is incorporated into the silicate chain structure, it would be in a three-dimensional environment which has not been described in literature yet.

3.4.1.6 pH evolution

Figure 17 shows the pH evolution of the fly ash-based alkali activated binder as a function of time. It shows an increase of pH until 3 days due to the dissolution of calcium-rich phases anhydrite CaSO_4 , portlandite $\text{Ca}(\text{OH})_2$ and calcium carbonate CaCO_3 (see sections 3.4.1.1 and 3.4.1.2) releasing in the medium its constitutive elements whose anions SO_4^{2-} , OH^- and CO_3^{2-} . Later on, those anions responsible of the pH variation are taken up to precipitate new phases: thenardite Na_2SO_4 (see 3.4.1.1) and calcium-silicate chains (see 3.4.1.5) explaining the pH decrease from 3 to 28 days. Figure 17 therefore shows that the precipitation of news phases is already predominant from 3 days.

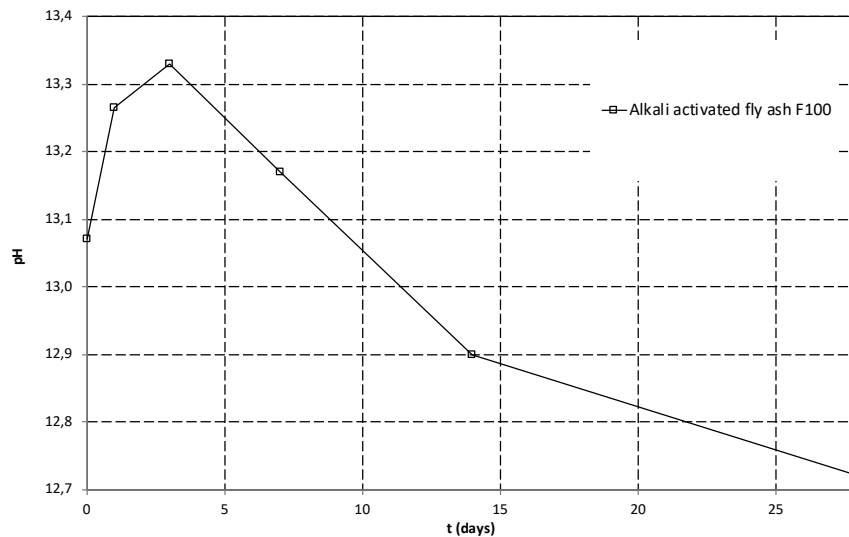


Figure 17 pH curves of the fly ash-based alkali activated material F100 as a function of curing time

To conclude, results concerning the alkali activated fly ash binder showed that calcium-rich phases constitute the reactive part of the raw fly ash, while its vitreous phase remains mainly unreactive. The new compounds formed are mainly located around calcium-rich reactive particles and present a complex chemistry and structure which differ from cementitious compounds generally encountered in cement or lime-based system.

3.4.2 Interaction between the alkali activated fly ash binder and kaolin

The following section aims at understanding the interaction between kaolin and the alkali activated fly ash binder previously described. More specifically, it aims at answering the following question: does the presence of kaolin modify the reaction sequence?

Two stabilised soils were studied i.e. KF50 for which the solid phase is made in mass of 50% of fly ash and 50% of kaolin, and KF20 made of 20% of fly ash and 80% of kaolin. Observations made for these two mixes turned out to be similar for all the techniques used.

Firstly, Figure 18 shows the infrared spectrum of the original kaolin as well as the spectra belonging to the alkali activated binder treated soils KF50 and KF20 as a function of time.

The four bands observed in the 3695–3620 cm^{-1} range are typical of the presence of kaolinite, and arise from the vibration of its internal OH groups. Notably, disorder in kaolinite is mainly detectable in this OH-stretching region by FTIR (Wilson, 1994). Those bands being still observed over time in the alkali activated binder treated soils suggest that kaolinite does not react under alkaline conditions.

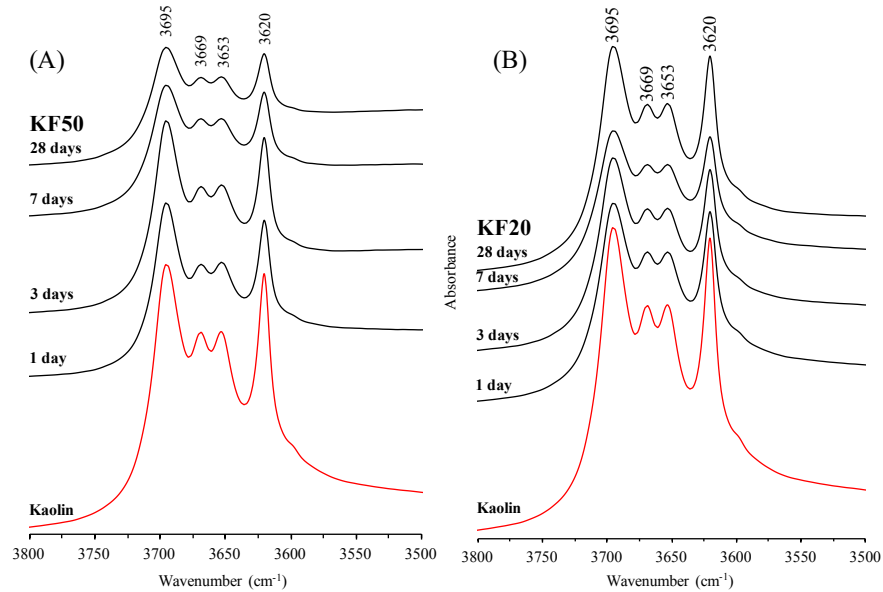


Figure 18: FTIR of the raw kaolin and alkali activated kaolin (A) KF50 and (B) KF20 as a function of curing time in the OH stretching vibrations range

The smaller heights seen at 7 and 28 days for KF50 are only due to higher sample densities at higher curing times after the formation of new compounds, leading to smaller probed distance and therefore lesser absorbance.

Figure 19 and Figure 20 shows XRD patterns of the activated soils KF50 and KF20 respectively and as a function of curing time. Similarly to the alkali activated fly ash binder (see 3.4.1.1), it indicates the dissolution of anhydrite CaSO_4 along with the formation of thenardite Na_2SO_4 .

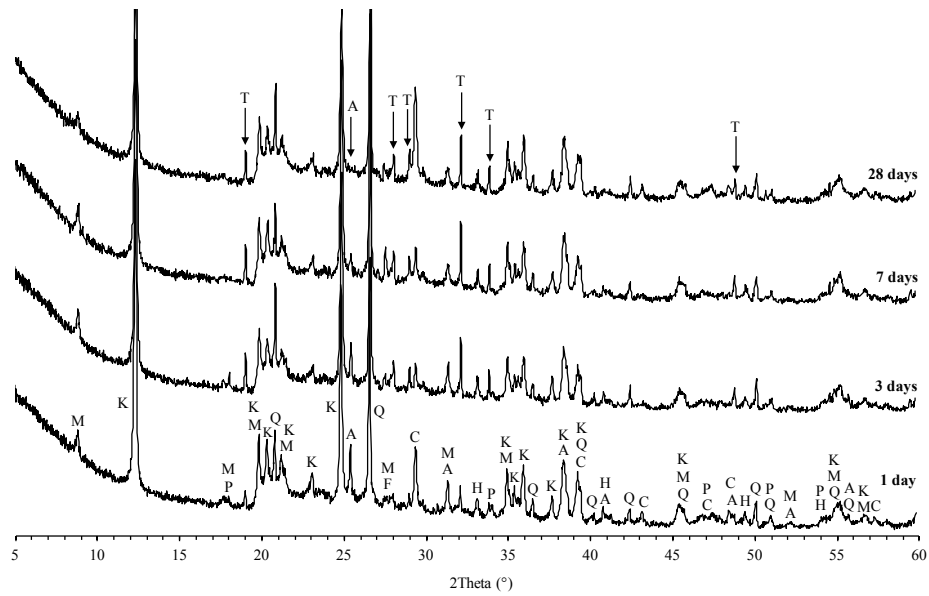


Figure 19: XRD of the alkali activated kaolin KF50 as a function of curing time; A=anhydrite; C=calcite; F=feldspar; H=hematite; K=kaolinite; M=muscovite; P=portlandite; Q=quartz; T=thenardite

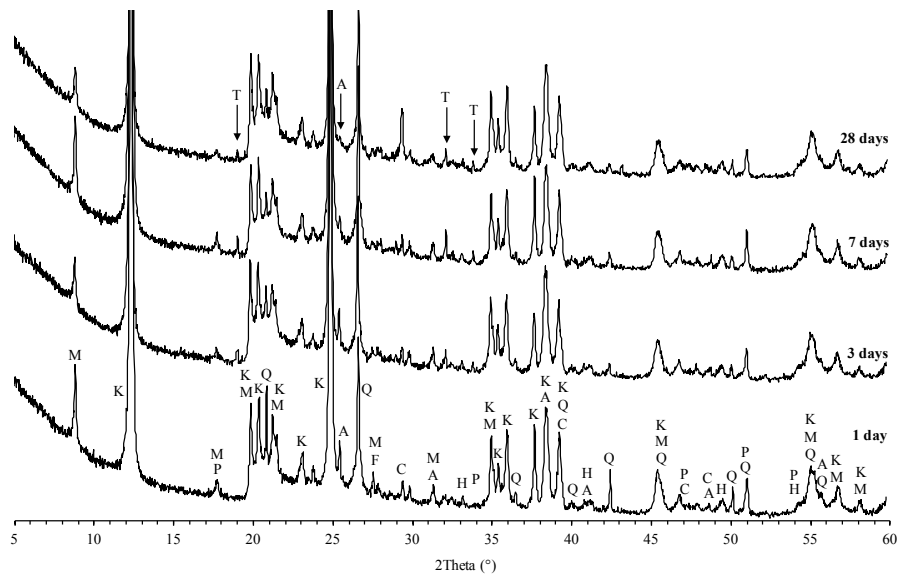


Figure 20: XRD of the alkali activated kaolin KF20 as a function of curing time; A=anhydrite; C=calcite; F=feldspar; H=hematite; K=kaolinite; M=muscovite; P=portlandite; Q=quartz; T=thenardite

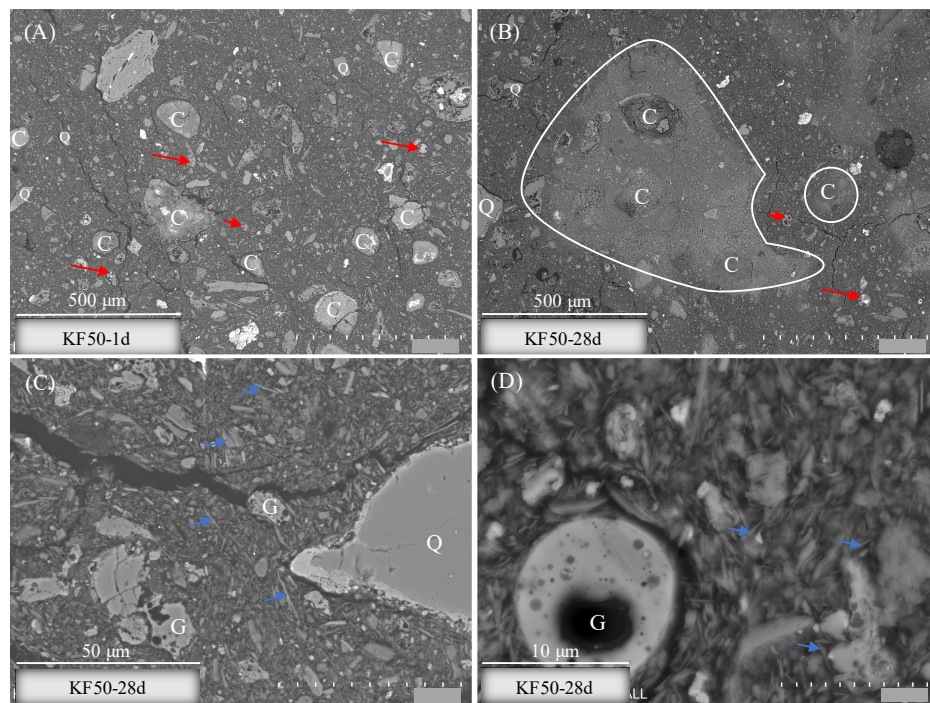


Figure 21 SEM micrographs of the alkali activated kaolin KF50 (A) at 1 day and (B), (C) and (D) at 28 days; C=calcium nodules; Q=quartz; red arrows=glass; blue arrows=kaolinite platelets

Figure 21A, B, C and D shows microstructural observations of the alkali activated kaolin KF50. At 1 day, and in contrast with the alkali activated fly ash (Figure 14A), KF50 presents a relatively low porosity due to the presence of small-sized kaolinite platelets filling the pores (Figure 21A). At 28 days, and in a similar way to the activated fly ash (Figure 14B), KF50 presents a more compact microstructure around calcium-rich phases (see encircled area in Figure 21B).

Furthermore, by comparing the alkali activated fly ash binder (Figure 14C and D) with the activated soil KF50 (Figure 21C and D), kaolinite platelets are distinctly observed (see blue arrows as an example of platelet observation), and homogeneously spread across the whole sample. In fact, kaolinite platelets were observed not merely in the matrix but also in the most reactive massive areas supporting that kaolinite does not react even in the reactive areas but rather acts as a filler.

Table 3 gives an average chemical composition of KF50 massive areas. It shows similar tendencies than for the alkali activated fly ash binder F100. Only slightly higher contents of silicon and aluminium are measured for KF50 due to the presence of kaolinite.

Figure 22 shows ^{27}Al MAS-NMR spectra of the alkali activated fly ash binder F100 studied in the first section, and the alkali activated binder treated soil KF50 at 1 and 28 days. By

comparison with the binder F100, ^{27}Al NMR spectroscopy of KF50 displays two additional resonances due to the presence of kaolin i.e. a main resonance at 4 ppm due to Al(VI) of the octahedral layer of kaolinite, and a resonance at 70 ppm owed to Al(IV) and corresponding to substitution of Al for Si in the tetrahedral layer of kaolinite and muscovite.

At 1 day, KF50 presents a resonance whose maximum is located at 55 ppm and owed to the vitreous phase of fly ash, while at 28 days a shift of this resonance to 58 ppm indicates the formation of tetrahedral aluminium in $q^4(4\text{Si})$ environments (as previously described for the alkali activated fly ash in section 3.4.1.5).

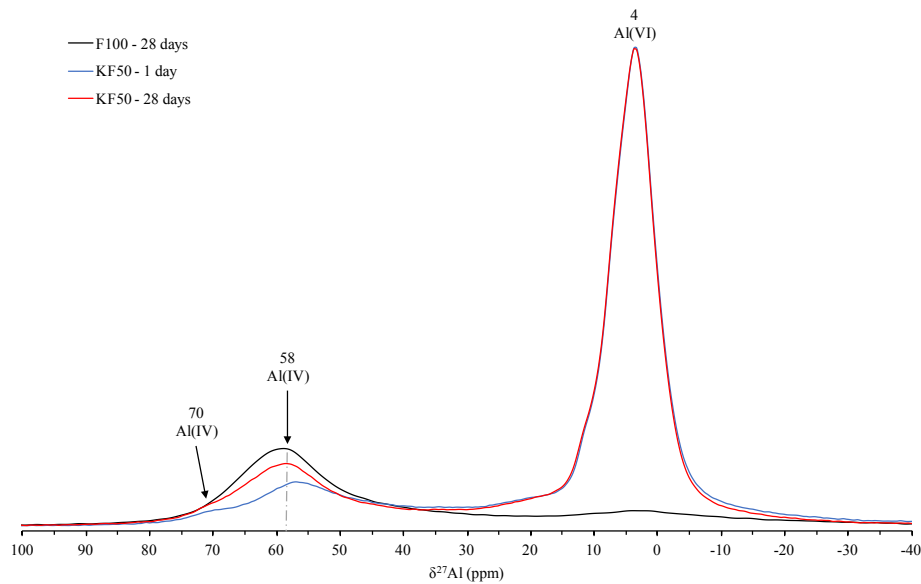


Figure 22: ^{27}Al MAS-NMR spectra of the alkali activated fly ash F100 at 28 days and alkali activated kaolin KF50 at 1 and 28 days

Figure 23 shows ^{27}Al MAS-NMR of the alkali activated binder treated soil KF20 at 1 and 28 days. It presents similar characteristics than KF50 as described above.

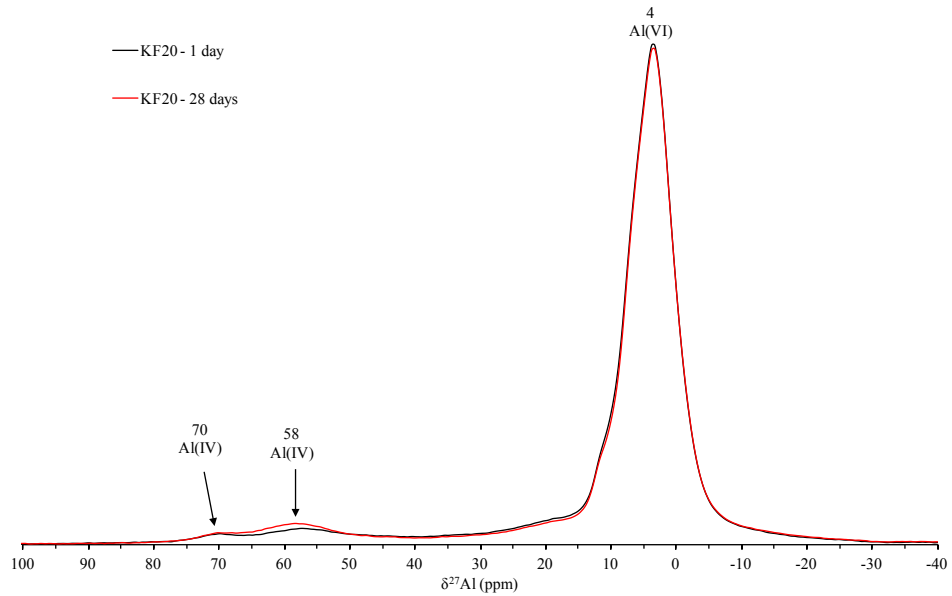


Figure 23: ^{27}Al MAS-NMR of the alkali activated kaolin KF20 at 1 and 28 days

Figure 24 shows ^{29}Si MAS-NMR spectra of the alkali activated fly ash binder F100 studied in the first section, and the alkali activated binder treated soil KF50 at 1 and 28 days. ^{29}Si NMR spectroscopy of KF50 samples show an additional thin resonance at -91 ppm corresponding to the silicon of the tetrahedral layer of kaolinite. This resonance does not undergo any modification over time confirming the non-reactivity of kaolinite.

Furthermore, from 1 to 28 days KF50 shows the clear appearance of a resonance at -85 ppm due to the formation of silicon chains combined with dissolved calcium, and as previously described for the alkali activated fly ash binder (see 3.4.1.5).

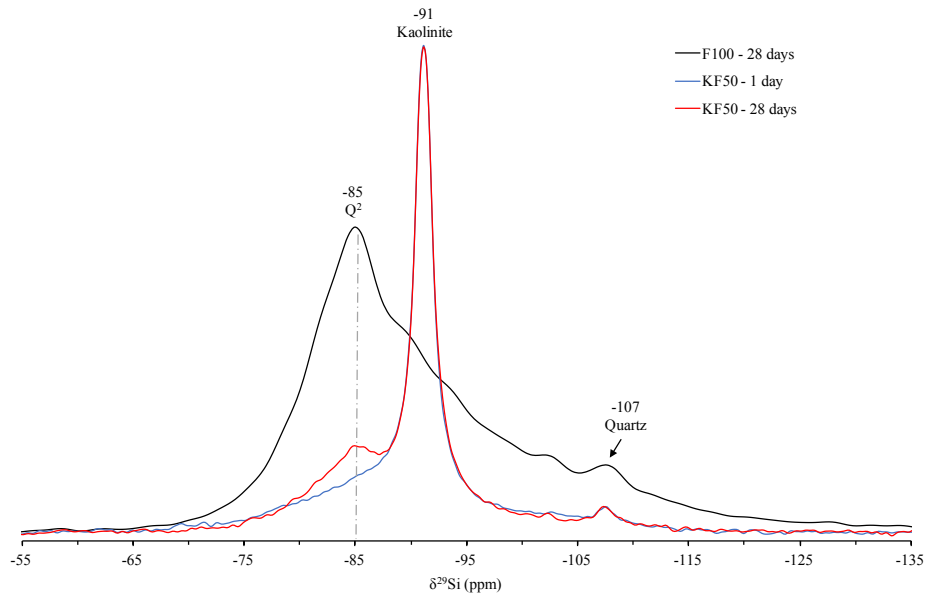


Figure 24: ^{29}Si MAS-NMR spectra of the alkali activated fly ash F100 at 28 days and alkali activated kaolin KF50 at 1 and 28 days

Figure 25 shows ^{29}Si MAS-NMR of the alkali activated binder treated soil KF20 at 1 and 28 days. It presents similar characteristics than KF50 as described above but in a lesser extent due to the lesser amount of reactive fly ash in this mix.

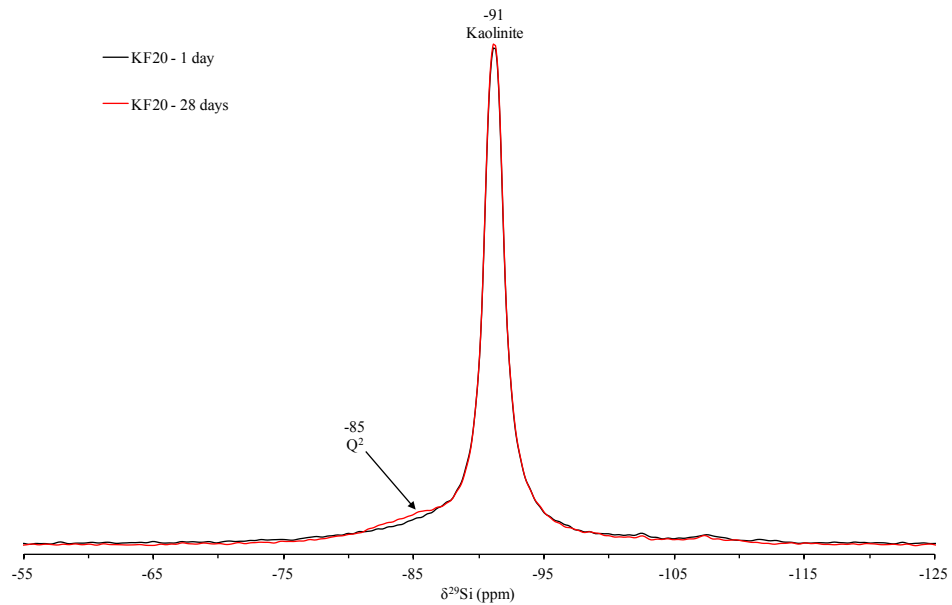


Figure 25: ^{29}Si MAS-NMR of the alkali activated kaolin KF20 at 1 and 28 days

Figure 26 shows the pH evolution of the treated soils KF50 and KF20 as a function of time. Similarly to the binder it shows an increase of pH at short curing time and until 3 days owed to the dissolution of calcium-rich phases. Whereas from 3 to 28 days the decrease of pH is associated with the precipitation of new phases.

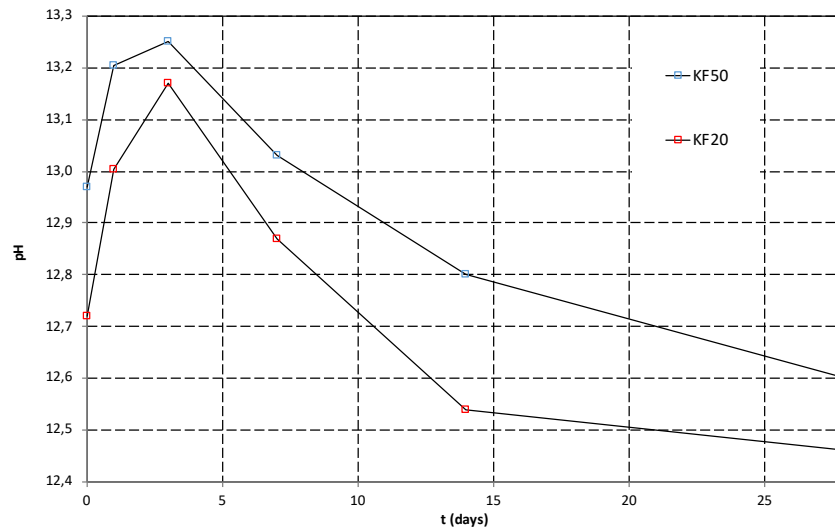


Figure 26 Comparison of the pH curves as a function of curing time for the treated soils KF50 and KF20

The pH values of the treated soils are slightly lower than the binder as the quantity of alkaline solution is lower. In a similar way the pH of KF20 is lower than KF50 as it contains less alkaline solution.

To conclude, results of this second section showed that kaolin is unreactive during alkaline attack. Besides, a similar reaction sequence than for the alkali activated fly ash binder occurs.

3.4.3 Comparison with lime treated kaolin

This last section focuses on a comparison with previous studies which reported the physicochemical evolution of the same kaolin treated either by a common stabiliser: lime (Vitale et al., 2017), but also treated by a mix of lime and the fly ash used here (Knapik, 2016).

Table 4 gives a summary of the reaction sequences for each system highlighting strong differences. This section consequently aims at providing a better understanding of the consequences of those variable reaction sequences on the final material in terms of performance and durability.

Table 4: Compared reactivity sequences of kaolin treated either by lime, or a mix of lime and fly ash or an alkali activated fly ash

		Kaolin + Lime (Vitale et al., 2017)	Kaolin + Lime + Fly ash (Knapik, 2016)	Kaolin + Alkali activated fly ash
1. Phases dissolved		Kaolin, lime	Kaolin, lime, fly ash	Fly ash
2. Reactivity timescale		Slow	Fast	Fast
3. Phases formed	Aluminate	Calcium Aluminate Hydrate C–A–H Monocarboaluminate hydrate C ₄ –A–C–H ₁₁	Calcium Aluminate Hydrate C– A–H Calcium Aluminium Oxide Carbonate Hydrate C–A–O–C–H Calcium Aluminium Oxide Hydrate C–A–O–H Ettringite Ca ₆ Al ₂ (SO ₄) ₃ (OH) ₁₂ .26H ₂ O	Amorphous silicate consisting of chains combined with calcium - and probably incorporating the observed q ⁴ (4Si) aluminium environments
	Silicate	None	Calcium Silicate Hydrate C–S–H	
	Sulphate	None	Ettringite Ca ₆ Al ₂ (SO ₄) ₃ (OH) ₁₂ .26H ₂ O	Thenardite Na ₂ SO ₄

3.4.3.1 Reactivity of initial phases

Firstly, and regarding the reactivity of the phases initially present, it was found that kaolin is inert in our alkali activated samples which contrasts with the two other lime-based systems for which kaolinite is dissolved. The limited reactivity of kaolinite in the alkali activated binder treated soils herein studied is due to the presence of other more reactive phases. Besides, its limited reactivity is beneficial for the system as no side effects will occur.

For the three systems, calcium-containing phases constitute the main reactive part of the mixes playing a pivotal role in the reaction development scheme. In fact, their dissolution leads to the release of dissolved calcium into the medium and hence pozzolanic activity i.e. formation of new calcium cementitious compounds responsible of the strength

improvement. In the case of our alkali activated binder treated soils however, it is not lime CaO that constitutes a supply of calcium but calcium-containing minerals from fly ash CaSO₄, CaCO₃ or Ca(OH)₂. For all calcium-source types the supply of Ca²⁺ cations remains identical. What changes is the anion simultaneously released from their dissolution: when fly ash is present the dissolution of its calcium-containing minerals is accompanied by the release of various anions such as OH⁻, SO₄²⁻ and CO₃²⁻ influencing the reaction sequence, and with potential negative effects for the durability as seen later.

Finally, concerning the vitreous phase of fly ash, although amorphous and hence metastable it showed few reactivity leading to a preferential pozzolanic activity as seen in Portland cement, rather than polymerisation reactions associated with the formation of an aluminosilicate three-dimensional network characteristic of low-calcium alkali activated materials and geopolymers.

3.4.3.2 Reactivity timescale

Reactions in presence of fly ash are fast with new compounds already observed at 28 days for both systems made of kaolin, lime and fly ash (Knapik, 2016) but also kaolin and alkali activated fly ash. Whereas, longer reactivity timescale occurs for lime treated kaolin: new cementitious compounds being previewed from 60 days and clearly detected only after 270 days (Vitale et al., 2017).

For a system made of lime and kaolin its pozzolanic activity depends on the dissolution of kaolinite which constitutes the only source of aluminium and silicon. Considering that kaolinite possesses a stable crystalline mineral structure hard to dissolve it explains the slow reactivity of that system. By contrast, fly ash contains reactive phases i.e. calcium-rich phases primarily and to a small extent its vitreous phase (for the fly ash used here) thermodynamically less stable than kaolinite and therefore easier to dissolve. That is why reaction sequences are faster for both fly ash systems. It is even faster for our alkali activated binder treated soils as the alkaline solution brings a mixture of ions readily available. Those fastest reaction times would constitute an advantage in the case where the quickly formed products are as well stable binding phases which will be discussed in the following section.

3.4.3.3 Stability and structure of the compounds formed

In the case of formerly studied systems made of kaolin and lime as well as kaolin, lime and fly ash, a preferential release of aluminium over silicon from kaolinite and/or fly ash

dissolution occurs conducting to the formation of aluminium compounds primarily. In fact, for a lime treated kaolin Calcium Aluminate Hydrate C–A–H and monocarboaluminate hydrate C₄–A–C–H₁₁ are formed (Vitale et al., 2017). In the case of a kaolin treated by a mix of lime and fly ash Calcium Aluminate Hydrate C–A–H but also Calcium Aluminium Oxide Carbonate Hydrate C–A–O–C–H, Calcium Aluminium Oxide Hydrate C–A–O–H and ettringite Ca₆Al₂(SO₄)₃(OH)₁₂.26H₂O are formed (Knapik, 2016). Whereas, in our alkali activated binder treated soils investigated here, aluminium dissolved from the vitreous phase of fly ash was found in a three-dimensional four-fold environment (q⁴(4Si)) which strongly contrasts with the six-fold environments found in the Calcium Aluminate Hydrates.

Regarding the formation of silicate compounds, none are formed in a system made of kaolin and lime (Vitale et al., 2017) because the dissolution of kaolinite is slow and starts by the release of its aluminium. Hence, no silicon is made available. Kaolinite being the only source of silicon in that system the limited dissolution of silicon implies the non-formation of silicon compounds. By contrast in a kaolin, lime and fly ash system, the dissolution of silicon from the vitreous phase of fly ash leads to the formation of Calcium Silicate Hydrate C–S–H (Knapik, 2016). Finally, in the alkali activated binder treated soils herein studied, the supply of silicon from the alkaline solution primarily and also from the vitreous phase of fly ash leads to the formation of silicon chains combined with calcium, but whose NMR signature greatly differs from C–S–H commonly observed as described above (see section 3.4.1.5). It is also likely that aluminium found in three-dimensional four-fold environment (q⁴(4Si)) is incorporated into those silicon chains.

Calcium Silicate Hydrate C–S–H is the principal binding phase of Portland cement and concrete primarily responsible for its strength (Tajuelo Rodriguez et al., 2017). In addition, its structure is more stable than Calcium Aluminate Hydrates (Provis and Deventer, 2009). Their presence is consequently beneficial for the performances. The fact that in our alkali activated samples, a diverse structure compared to usual C–S–H is observed cannot easily be assessed in term of strength and durability at the present moment. Indeed, regarding the lack of crystallinity of our silicon chains formed, experience proved that the crystallinity of the binding agent alone constitutes a poor indication of mechanical performances over the timescales relevant to the majority of concrete structures (Provis and Deventer, 2009). A further investigation of the performances would help apprehending a potential beneficial effect of this uncommon silicon chains structure over time.

Finally, for both fly ash systems, sulphate minerals are formed: either ettringite $\text{Ca}_6\text{Al}_2(\text{SO}_4)_3(\text{OH})_{12}\cdot 26\text{H}_2\text{O}$ for a system made of kaolin, lime and fly ash (Knapik, 2016), or thenardite Na_2SO_4 in our alkali activated binder treated soils.

Their formation is due to the dissolution of anhydrite CaSO_4 initially present in the fly ash, and releasing sulphate anions SO_4^{2-} that are subsequently recombining with available cations. For the case of a kaolin, lime and fly ash system the formation of ettringite is taking up aluminium and calcium hence slowing down both the simultaneous formation of aluminate and silicate hydrates. Whereas, in our alkali activated system, sodium cations readily available from the alkaline solution combine with sulphate anions. Therefore, the formation of sulphate minerals does not affect the parallel development of the pozzolanic activity i.e. the formation of silicate chains. Finally, a key point to consider for durability aspects is the high solubility of sulphate minerals which are few stable salts in water. In fact, a previous study in which leaching tests were performed on an alkali activated sulphate-bearing kaolin showed that the uptake of sulphate anions by the gel is low, namely less than 40% (Occhipinti et al., 2017). The study of the effect of leaching is consequently necessary to verify a further impact of the presence of thenardite on the long-term performances.

3.5 Conclusions

Here, the development of a novel binder that is an alkali activated calcium-rich fly ash for clay soil stabilisation was explored. The study of its reactivity showed that (i) the overall calcium-bearing minerals from fly ash constitute the reactive phases while its vitreous phase remains mainly unreactive, (ii) new compounds are formed, thenardite Na_2SO_4 and an amorphous silicate consisting of chains combined with calcium and probably incorporating the observed $q^4(4\text{Si})$ aluminium environments (iii) reactions happen within 1 to 28 days.

The interaction between the binder developed and the model soil chosen i.e. kaolin, showed that kaolin is unreactive. Its presence whatever the proportion does not modify the physicochemical evolution of the system that is neither the dissolved phases, formed compounds, nor reactivity timescale. The inert kaolinite platelets were in addition found homogeneously embedded in the matrix acting as a filler.

When compared to lime treated kaolin, although pozzolanic activity remains the dominant process reaction sequences are strongly different. In the case of alkali activated binder treated soils the formation of calcium-silicon chains phases more stable than calcium aluminium hydrates encountered in lime-based systems is beneficial for long-term stability purpose. Those observed silicon chains however show an uncommon structure whose effect on the performances will be checked later. Finally, the formation of thenardite a highly soluble salt in water raises interest about the durability of the material which could be further investigated.

3.6 References

- Andersen, M.D., Jakobsen, H.J., Skibsted, J., 2003. Incorporation of Aluminum in the Calcium Silicate Hydrate (C–S–H) of Hydrated Portland Cements: A High-Field ^{27}Al and ^{29}Si MAS NMR Investigation. *Inorg. Chem.* 42, 2280–2287. <https://doi.org/10.1021/ic020607b>
- Basha, E.A., Hashim, R., Muntohar, A., 2003. Effect of the cement-rice husk ash on the plasticity and compaction of soil. *Electron. J. Geotech. Eng.* 8.
- Buchwald, A., Kaps, C., Hohmann, M., 2003. Alkali-activated binders and pozzolan cement binders—complete binder reaction or two sides of the same story, in: *Proceedings of the 11th International Conference on the Chemistry of Cement*. Portland Cement Association Durban, South Africa, pp. 1238–1246.
- Chemed Y, 2015. Effect of hydrated lime on kaolinite surface properties and its rheological behaviour. Université de Nantes.
- Chemed, Y.C., Deneele, D., Christidis, G.E., Ouvrard, G., 2015. Influence of hydrated lime on the surface properties and interaction of kaolinite particles. *Appl. Clay Sci.* 107, 1–13. <https://doi.org/10.1016/j.clay.2015.01.019>
- Cong, X., Kirkpatrick, R.J., 1996. ^{29}Si MAS NMR study of the structure of calcium silicate hydrate. *Adv. Cem. Based Mater.* 3, 144–156.
- Cristelo, N., Glendinning, S., Fernandes, L., Pinto, A.T., 2012. Effect of calcium content on soil stabilisation with alkaline activation. *Constr. Build. Mater.* 29, 167–174. <https://doi.org/10.1016/j.conbuildmat.2011.10.049>
- Cristelo, N., Glendinning, S., Teixeira Pinto, A., 2011. Deep soft soil improvement by alkaline activation. *Proc. Inst. Civ. Eng. - Ground Improv.* 164, 73–82. <https://doi.org/10.1680/grim.900032>
- Deneele, D., Le Runigo, B., Cui, Y.-J., Cuisinier, O., Ferber, V., 2016. Experimental assessment regarding leaching of lime-treated silt. *Constr. Build. Mater.* 112, 1032–1040. <https://doi.org/10.1016/j.conbuildmat.2016.03.015>
- Guidobaldi, G., Cambi, C., Cecconi, M., Deneele, D., Paris, M., Russo, G., Vitale, E., 2017. Multi-scale analysis of the mechanical improvement induced by lime addition on a pyroclastic soil. *Eng. Geol.* 221, 193–201. <https://doi.org/10.1016/j.enggeo.2017.03.012>
- James, J., Pandian, P.K., 2016. Industrial Wastes as Auxiliary Additives to Cement/Lime Stabilization of Soils. *Adv. Civ. Eng.* 2016, 1–17. <https://doi.org/10.1155/2016/1267391>

- Knapik, K., 2016. Experimental and numerical analyses of fly ash from fluidized bed combustion applications for selected ground improvement. The Silesian University of Technology.
- Kolias, S., Kasselouri-Rigopoulou, V., Karahalios, A., 2005. Stabilisation of clayey soils with high calcium fly ash and cement. *Cem. Concr. Compos.* 27, 301–313. <https://doi.org/10.1016/j.cemconcomp.2004.02.019>
- Lemaire, K., Deneele, D., Bonnet, S., Legret, M., 2013. Effects of lime and cement treatment on the physicochemical, microstructural and mechanical characteristics of a plastic silt. *Eng. Geol.* 166, 255–261. <https://doi.org/10.1016/j.enggeo.2013.09.012>
- Maubec, N., Deneele, D., Ouvrard, G., 2017. Influence of the clay type on the strength evolution of lime treated material. *Appl. Clay Sci.* 137, 107–114. <https://doi.org/10.1016/j.clay.2016.11.033>
- Nalbantoğlu, Z., 2004. Effectiveness of Class C fly ash as an expansive soil stabilizer. *Constr. Build. Mater.* 18, 377–381. <https://doi.org/10.1016/j.conbuildmat.2004.03.011>
- Occhipinti, R., Tarantino, S.C., Riccardi, M.P., Sturini, M., Speltini, A., Maraschi, F., Elmaleh, A., Zema, M., 2017. Alkali activation of sulfate-bearing kaolin. Presented at the 16th International Clay Conference, Granada, Spain.
- Pardal, X., Brunet, F., Charpentier, T., Pochard, I., Nonat, A., 2012. 27 Al and 29 Si Solid-State NMR Characterization of Calcium-Aluminosilicate-Hydrate. *Inorg. Chem.* 51, 1827–1836. <https://doi.org/10.1021/ic202124x>
- Parsons, R.L., Kneebone, E., 2005. Field performance of fly ash stabilised subgrades. *Ground Improv.* 9, 33–38. <https://doi.org/10.1680/grim.9.1.33.58543>
- Pomakhina, E., Deneele, D., Gaillot, A.-C., Paris, M., Ouvrard, G., 2012. 29Si solid state NMR investigation of pozzolanic reaction occurring in lime-treated Ca-bentonite. *Cem. Concr. Res.* 42, 626–632. <https://doi.org/10.1016/j.cemconres.2012.01.008>
- Provis, J.L., Deventer, J.S.J. va., 2009. *Geopolymers Structure, processing, properties and industrial applications*, Woodhead Publishing in materials. Woodhead, Cambridge.
- Rahman, A., 1986. The Potentials of Some Stabilizers for the Use of Lateritic Soil in Construction. *Build. Environ.* 21, 57–61.
- Rios, S., Cristelo, N., Viana da Fonseca, A., Ferreira, C., 2016. Structural Performance of Alkali-Activated Soil Ash versus Soil Cement. *J. Mater. Civ. Eng.* 28, 4015125. [https://doi.org/10.1061/\(ASCE\)MT.1943-5533.0001398](https://doi.org/10.1061/(ASCE)MT.1943-5533.0001398)
- Sargent, P., Hughes, P.N., Rouainia, M., White, M.L., 2013. The use of alkali activated waste binders in enhancing the mechanical properties and durability of soft alluvial soils. *Eng. Geol.* 152, 96–108. <https://doi.org/10.1016/j.enggeo.2012.10.013>

- Scrivener, K.L., Kirkpatrick, R.J., 2008. Innovation in use and research on cementitious material. *Cem. Concr. Res.* 38, 128–136. <https://doi.org/10.1016/j.cemconres.2007.09.025>
- Sharma, U., Khatrib, A., Kanoungoc, A., 2014. Use of Micro-silica as Additive to Concrete-state of Art. *Int. J. Civ. Eng. Res.* 5, 9–12.
- Shi, C., Krivenko, P.V., Roy, D.M., 2006. Alkali-activated cements and concretes. Taylor & Francis, London ; New York.
- Silva, R.A., Oliveira, D.V., Miranda, T., Cristelo, N., Escobar, M.C., Soares, E., 2013. Rammed earth construction with granitic residual soils: The case study of northern Portugal. *Constr. Build. Mater.* 47, 181–191. <https://doi.org/10.1016/j.conbuildmat.2013.05.047>
- Singhi, B., Laskar, A.I., Ahmed, M.A., 2016. Investigation on Soil–Geopolymer with Slag, Fly Ash and Their Blending. *Arab. J. Sci. Eng.* 41, 393–400. <https://doi.org/10.1007/s13369-015-1677-y>
- Snellings, R., Mertens, G., Elsen, J., 2012. Supplementary Cementitious Materials. *Rev. Mineral. Geochem.* 74, 211–278. <https://doi.org/10.2138/rmg.2012.74.6>
- Sun, G.K., Young, J.F., Kirkpatrick, R.J., 2006. The role of Al in C–S–H: NMR, XRD, and compositional results for precipitated samples. *Cem. Concr. Res.* 36, 18–29. <https://doi.org/10.1016/j.cemconres.2005.03.002>
- Tajuelo Rodriguez, E., Garbev, K., Merz, D., Black, L., Richardson, I.G., 2017. Thermal stability of C-S-H phases and applicability of Richardson and Groves’ and Richardson C-(A)-S-H(I) models to synthetic C-S-H. *Cem. Concr. Res.* 93, 45–56. <https://doi.org/10.1016/j.cemconres.2016.12.005>
- Tenn, N., Allou, F., Petit, C., Absi, J., Rossignol, S., 2015. Formulation of new materials based on geopolymer binders and different road aggregates. *Ceram. Int.* 41, 5812–5820. <https://doi.org/10.1016/j.ceramint.2015.01.010>
- Vitale, E., Deneele, D., Paris, M., Russo, G., 2017. Multi-scale analysis and time evolution of pozzolanic activity of lime treated clays. *Appl. Clay Sci.* 141, 36–45. <https://doi.org/10.1016/j.clay.2017.02.013>
- Vitale, E., Deneele, D., Russo, G., Ouvrard, G., 2016. Short-term effects on physical properties of lime treated kaolin. *Appl. Clay Sci.* 132–133, 223–231. <https://doi.org/10.1016/j.clay.2016.04.025>
- Wilkinson, A., Haque, A., Kodikara, J., 2010. Stabilisation of clayey soils with industrial by-products: part A. *Proc. Inst. Civ. Eng. - Ground Improv.* 163, 149–163. <https://doi.org/10.1680/grim.2010.163.3.149>

Wilson, M.J., 1994. Clay mineralogy: spectroscopic and chemical determinative methods, Springer Science + Business Media.

Zhang, M., Guo, H., El-Korchi, T., Zhang, G., Tao, M., 2013. Experimental feasibility study of geopolymer as the next-generation soil stabilizer. *Constr. Build. Mater.* 47, 1468–1478. <https://doi.org/10.1016/j.conbuildmat.2013.06.017>

**Use of alkali activated fly ash binder for
kaolin clay soil stabilisation:
Microstructural evolution**

Chapter 4 is in preparation for submission.

Samples were prepared at the University of Cassino and Southern Lazio. All experiments were carried out at the Institute of Materials Jean Rouxel except for Mercury Intrusion Porosimetry analyses that were performed at the University of Cassino.

The Candidate performed the analysis except for Mercury Intrusion Porosimetry, collected the data, conceived and designed the analysis and wrote the paper. Dimitri Deneele from the Institute of Materials Jean Rouxel helped and supervised the performance of Scanning Electron Microscopy. He also corrected the paper and helped refine the interpretation of results. Giacomo Russo from the University of Cassino and Southern Lazio helped for the analysis and interpretation of MIP data. He also corrected the paper. Sebastiana Dal Vecchio from the University of Cassino performed Mercury Intrusion Porosimetry experiments.

4.1 Abstract

This work focusses on the use of alkali activated fly ash-based binder to enhance engineering characteristics of soft clay-rich soils and as a substitute to standard stabilisers that are lime and Ordinary Portland Cement. Especially, it examines the microstructural evolution of a calcium-rich fly ash from coal combustion-based binder activated by a sodium-based alkaline solution. To this end, the processes generating the microstructure and the evolution of the pore network over time are investigated. A second point addressed by this study is how the presence of small sized kaolin soil affects the microstructural features of the binder. The microstructure has therefore been investigated by considering the binder alone and the binder mixed with kaolin.

The combination of completing techniques has been used including Optical microscopy, Scanning Electron Microscopy and Mercury Intrusion Porosimetry in order to gain an overview of the complex pore structure.

Microstructural changes occur around calcium-containing phases derived from fly ash which are the reactive phases of the system. Namely, the dissolution of calcium-rich grains leads to the formation of new compounds that first cover the grain surfaces and then further grow into the available space. Furthermore, the evolution of the pore network over time is characterized by a progressive filling of capillary pores by new compounds while small nanometric pores are being formed and associated with the newly formed silicate-calcium chains. Similar tendencies are observed when the binder is mixed with the soil although the general porosity is lesser due to the filling of pores by small-sized kaolinite platelets.

4.2 Introduction

The presence of soft clay-rich soils commonly found on construction sites is problematic because of their poor mechanical performances. That is why Ordinary Portland Cement or lime are generally used as soil stabilisers to enhance those performances. Nevertheless, those conventional stabilisers are associated with high carbon dioxide emissions and energy intensive processes significantly increasing the worldwide carbon footprint (Scrivener and Kirkpatrick, 2008).

As an alternative the use of Alkali Activated Material as a soil stabiliser is gaining more and more attention over the past ten years. Alkali Activated Materials could constitute a viable sustainable soil binder because of their much lower CO₂ emission process compared to traditional Portland cement. Furthermore, recent studies have shown a positive potential and feasibility results of using alkali activated binders for soil improvement, and this not only for different types of soil i.e. clayey soil (Wilkinson et al., 2010; Singhi et al., 2016), sandy clay (Cristelo et al., 2011), marl, marlstone (Cristelo et al., 2012), silty sand (Rios et al., 2016) or else road aggregates (Tenn et al., 2015); but also for different applications i.e. in deep soft soil (Cristelo et al., 2011), at shallow depth (Zhang et al., 2013) or in rammed earth construction (Silva et al., 2013).

Works on alkali activated binder treated soils are recent and constitute a novel domain of application. Our study particularly focuses on the use of a calcium-rich fly ash from coal combustion activated by sodium-based alkaline solution as a binder for clay kaolin stabilisation. Kaolin was selected as a model soil that represent a wide class of clays encountered in engineering projects and for maintaining the system simple. Kaolinite being not very reactive to alkaline activation at ambient temperature, a more reactive aluminosilicate source is required for chemical reactions to occur. For that purpose, a calcium-rich fly ash was selected in the context of resource-saving being an industrial waste. The main aim is to assess the feasibility of using this novel binder for soil treatment.

When addressing the feasibility of using a class of material for a novel application, there are several important parameters to consider such as the composition, microstructure and processing which all ultimately affect the performance-to-cost ratio of a material (Askeland et al., 2011). A detailed understanding of both the composition but also the structure of the binder across length scales is therefore required in order to control materials properties through its processing.

Two main length scales of investigation can be distinguished with relevant importance. A first one is the particle scale and corresponds to the identification of the different phases constituting particles in terms of chemical composition and crystal structure. Important properties of particles depend on the arrangements of atoms and types of bonding within each phase (Clemens et al., 2008). A second scale of observation is at the level of group

of particles, or microstructure. Microstructural investigations for alkali activated materials are of prime importance as their physical properties depend largely on their pore network characteristics and microstructure (Lawrence and Jiang, 2017; Nath et al., 2016). This is associated with the fact that the microstructure controls the transport properties of the binder and the stability of the matrix when exposed to aggressive agents (van Deventer et al., 2015).

In the previous chapter the physicochemical evolution of similar systems than those herein studied was carried out i.e. identification and evolution of the constitutive phases until 28 days of curing time at an atomic level. It showed that the soil i.e. kaolin was not very reactive. Whereas, fly ash was partly reactive. Some of its phases such as the vitreous phase and quartz were mainly unreactive, while calcium-containing phases represented the reactive phases. The new compounds formed were an amorphous silicate consisting of chains combined with calcium probably incorporating three-dimensional four-fold aluminium environments and thenardite Na_2SO_4 .

The present work therefore constitutes a complementary study and focusses on the next level that is the microstructural description. It particularly aims at providing a first step towards an understanding of the microstructural evolution taking into account the knowledge gained about the physicochemical evolution of the system.

The study was designed in three stages. An initial stage consisted in the identification of the phases present in the reactive aluminosilicate source i.e. the original calcium-rich fly ash and description of their structure, shape and size distribution. The different constituents of fly ash being inhomogeneously reactive (Provis and Deventer, 2009), it was important to identify the reactive phases around which microstructural changes were predominant. A second stage focussed on the investigation of the microstructural evolution of the alkali activated fly ash binder during the first 28 days of curing, including (i) a description of the dispersion and arrangement of phases, (ii) an understanding of which processes generate the microstructure over time and (iii) a pore network characterisation. Fly ash being a highly inhomogeneous material (Provis and Deventer, 2009), a key point was to determine the homogeneity of processes across the sample at a microscopic level. Besides, a particular emphasis was put at understanding microstructural changes and processes around calcium particles which are the main reactive phases. A third stage focussed on the interaction of the fly ash-based binder with the kaolin clay to understand how the presence of kaolin modifies the microstructural features of the system. As previously stated, kaolinite is unreactive during the alkaline activation. However, because of its small size kaolinite acts as a filler of the porosity as seen in the previous chapter and undoubtedly plays a role on the microstructural evolution.

4.3 Material and methods

4.3.1 Materials

A Polish fly ash derived from hard coal and coal slime combustion in fluidised bed boiler was used. Its chemical analysis is given in Table 1. The fly ash contains, approximately, 52% of particles sized lower than 45 μm and 41% lower than 10 μm .

Speswhite kaolin provided by Imerys Minerals UK, and whose chemical composition is given in Table 1 was used. It is mainly constituted of kaolinite (95%) and secondarily of muscovite (4%) (Chemeda, 2015). The kaolin contains, approximately, 100 % of particles sized lower than 10 μm and 80 % lower than 2 μm .

A unique alkaline solution was used: a sodium silicate with a mass ratio $\text{SiO}_2/\text{Na}_2\text{O}$ of 1.7 and a dry mass percentage of 44%; supplied by Woellner Group and named GEOSIL 34417.

4.3.2 Sample preparation

Sample preparation consisted in (i) mix of liquid sources i.e. silicate and water (ii) mix of aluminosilicate powders i.e. fly ash and kaolin in the case of soil-source sample (iii) mix of (i) and (ii) previously prepared.

Two types of mixes were studied and named F100 and KF50. F100 is the fly ash-based alkali activated binder. It corresponds to a solid phase made of fly ash only, whereas KF50 is the alkali activated binder treated soils and corresponds to a solid phase made of 50% of fly ash and 50% of kaolin in mass.

To ensure a good workability, the amount of added water with respect to the solid mass (e.g. mass of kaolin and fly ash) was fixed to 50% for all the samples. Additionally, the mass ratio of alkaline solution to fly ash was fixed to 50% for all the samples, giving the initial molar ratios (considering that kaolin is unreactive): $\text{Si}/\text{Al} = 2.0$, $\text{Si}/\text{Na} = 3.5$ and $\text{Al}/\text{Na} = 1.8$. The Al/Na ratio was not fixed to one because of the presence of calcium ions in high quantity in our system playing a role of charge compensation as well as sodium.

The paste obtained was poured in closed plastic molds and cured at room temperature (20 °C). Samples were finally demoulded and freeze-dried at curing times of 24 hours, 3, 7 or 28 days.

4.3.3 Methods

Samples were studied by Optical and Scanning Electron Microscope from polished section. Freeze-dried samples were impregnated under a vacuum with an acrylic resin (LR White). The polymerisation of the resin was performed in an oven at 60 °C over 48 h. The samples were then polished with diamond powder. The observations from Optical Microscopy were done with a Nikon LV100 polarizing optical microscope combined with a ccd Nikon DS-2Mv camera and the NIS Element BS software. Whereas the observations from Scanning Electron Microscope were done with a HITACHI SU5000 scanning electron microscope equipped with an energy-dispersive X-ray analyser (Quantax microanalyser system composed of X-Flash® SDD detector and the Esprit software). The polished samples were coated with carbon before the observation. The microscope was operated at an accelerating voltage of 20 kV and working distances of 10 mm.

MIP tests were performed by a double chamber Micromeritics Autopore III apparatus. In the filling apparatus (dilatometer) samples were outgassed under vacuum and then filled by mercury allowing increase of absolute pressure up to ambient one. Using the same unit the intrusion pressure was then raised up to approximately 200 kPa by means of compressed air. The detected entrance pore diameters range between 134 µm and 7.3 µm (approximately 0.01 MPa - 0.2 MPa for a mercury contact angle of 139°). After depressurisation to ambient pressure, samples were transferred to high-pressure unit, where mercury pressure was increased up to 205 MPa following a previously set intrusion program. The smallest detected entrance pore diameter was about 7 nm. Corrections to pore-size distribution due to compressibility of intrusion system were applied performing a blank test.

4.4 Results and discussion

The first section of results presents the general characteristics of the raw fly ash which constitutes the reactive aluminosilicate source of the mixes. The second part examines the microstructural evolution of the binder. Finally, the third part focusses on the description of system made by kaolin and the alkali activated binder.

4.4.1 Raw fly ash

The fly ash used here contains various components. Its composition consisting of (i) a vitreous phase and (ii) various crystalline phases i.e. calcium-containing minerals: anhydrite CaSO_4 , calcite CaCO_3 and portlandite $\text{Ca}(\text{OH})_2$, and other minerals: quartz SiO_2 , feldspar $(\text{K,Na,Ca})(\text{Si,Al})_4\text{O}_8$, hematite Fe_2O_3 and muscovite $(\text{Si}_3\text{Al})\text{O}_{10}(\text{Al}_2)(\text{OH})_2\text{K}$ (see Chapter 3 section 3.4.1.1).

Its particle size distribution reflects this diversity with 52 % of particles lower than 45 μm , 41 % of particles lower than 10 μm and 12 % of particles lower than 2 μm .

Figure 27 confirms this great variety also detectable by Scanning Electron Microscopy. In fact, the fly ash presents an extremely heterogeneous microstructure with particles of different shapes and ranging from 1 μm to more than 200 μm . The vitreous phase is itself heterogeneous and made of (i) some spherical particles (see G Figure 27B), (ii) bigger unshaped particles (see G Figure 27C) and (iii) aggregates of small particles primarily (see G Figure 27D).

Some crystallised angular shaped minerals can also be distinguished and correspond to quartz (see Q Figure 27A&D) or feldspar (see F Figure 27B).

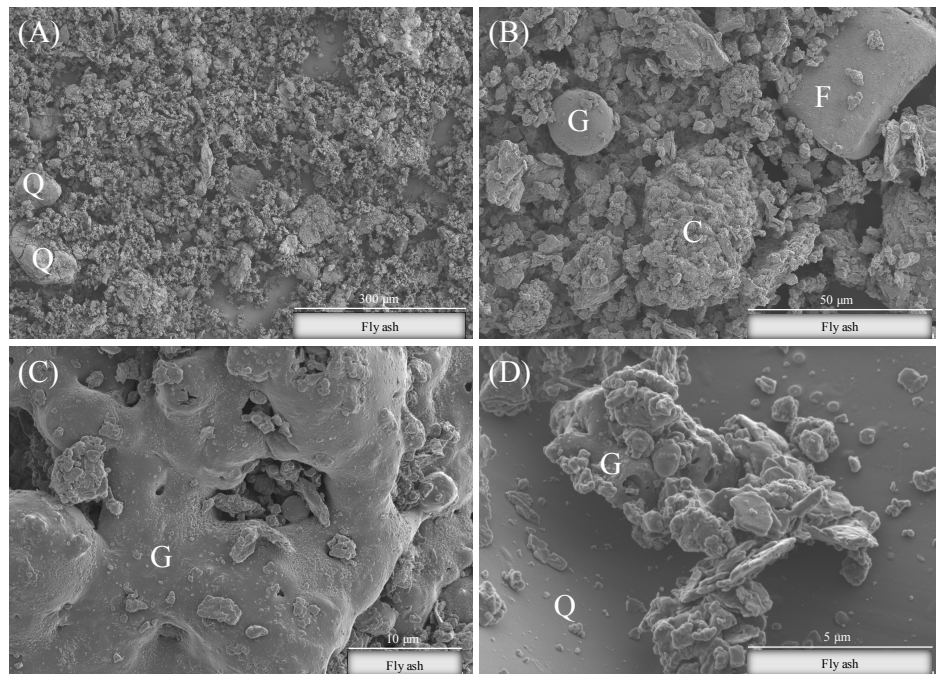


Figure 27: SEM micrographs of the raw fly ash; C=calcium-rich particle; F=feldspar; G=glass; Q=quartz

Finally, regarding calcium-rich phases, previous investigations (see Chapter 3 section 3.4.1.4) showed that calcium-containing minerals i.e. anhydrite CaSO_4 , calcite CaCO_3 and portlandite $\text{Ca}(\text{OH})_2$ are interlaced together. Especially, they are interlinked within a nodule shape structure generally of 50 to 200 μm size as seen on Figure 27B (particle labelled C).

4.4.2 Alkali activated fly ash binder

4.4.2.1 Optical Microscopy

Figure 28 shows the microstructural evolution of the alkali activated fly ash binder over time by optical microscopy. Observations were carried out until 28 days as chemical reactions are fully developed at that curing time as observed in the previous chapter.

After 24 hours of curing, dispersed dark spots of around 50 μm to 200 μm size are seen across the overall sample (see particles labelled C on Figure 28A&B), and correspond to reactive calcium-rich nodules by analogy with the previous observations of the raw fly ash constituents (section 4.4.1). They represent approximately 15 % of the mixture. Whereas the brown matrix includes the vitreous phase and calcium-free minerals from fly ash.

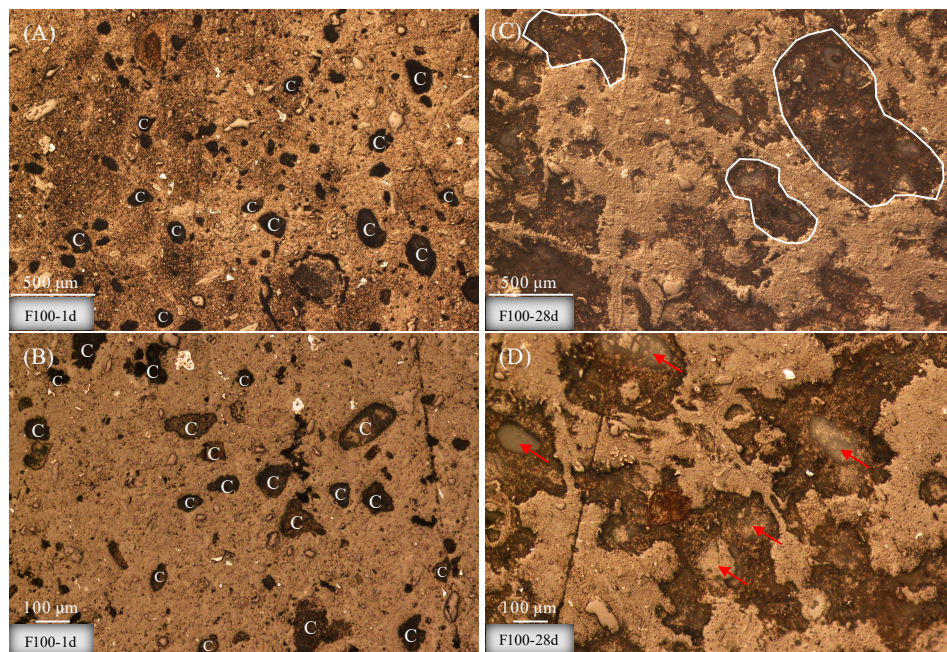


Figure 28: Optical microscopy images of the alkali activated fly ash binder F100 (A) and (B) after 24 hours, (C) and (D) at 28 days; C=calcium-rich particle

By comparison, at 28 days, no dark spots are visible but instead large dark zones whose edges are less well defined (see encircled areas on Figure 28C), and correspond to new products formed. Figure 28D shows a closer observation of those large dark reactive areas. The initial nodule shapes can still be distinguished at 28 days but instead of a dark spot as observed at 24 hours it is a hollowed greyish structure that is seen as shown by the red arrow (Figure 28D). This structure is associated with dissolution features over time of the calcium-rich phase, and in accordance with the previous results about the physicochemical evolution which indicate that calcium-containing phases are the main reactive phases. New compounds corresponding to dark areas are therefore formed around the hollowed dissolved calcium nodules. Those new compounds have been identified in the previous chapter as thenardite Na_2SO_4 , and an amorphous silicate consisting of chains combined with calcium probably incorporating three-dimensional four-fold aluminium environments.

As a consequence of those observations, the spreading of the darker areas at 28 days gives an idea of the extent of the reaction and widening of the new compounds formation across samples. In this system, half of the sample encompasses the new compounds and is hence reactive whereas the initial calcium nodules represented only 15 % of the sample. Besides, those new compounds seem homogeneously spread across the sample which likely could give a homogeneously reinforced material at the macroscopic scale.

Results from optical microscopy therefore match with the observed physicochemical evolution i.e. principal changes occur around calcium-rich reactive particles. That is why the next session focusses on the in-situ microstructural transformation of calcium-rich phases induced by the alkaline solution.

4.4.2.2 Scanning Electron Microscopy (SEM)

Figure 29 shows microstructural observations from a polished section and combined chemical mappings of the alkali activated fly ash binder after 24 hours of curing. Chemical mappings on Figure 29B&C indicate the presence of a calcium-rich nodule labelled 1 on Figure 29A and predominantly made of calcium and sulphur. Additionally, those calcium-rich particles display a granular aspect on their surface.

Surrounding this calcium-rich particle, the area labelled 2 on Figure 29A corresponds to a porous zone distinguishable by the presence of very dense black areas characteristic of

the filling resin of very low atomic mass. Chemical mappings of that porous zone show an enrichment in silicon and sodium (Figure 29D&E) indicating the presence of the sodium-silicate Na_2SiO_3 alkaline solution at that short curing time. Additionally, filament like structures are observed within that area (see red arrow on Figure 29A), and considered as the beginning of the secondary phases formation i.e. the amorphous silicate consisting of chains combined with calcium and potentially aluminium. In fact, a former study about cementitious microstructures has shown the formation of similar arrangements associated with Calcium Silicate Hydrates whose structure strongly resembles the one of our newly formed chains (Scrivener, 2004). Moreover, it appears that those filament structures are stacked around particles corresponding to the initiation of the reaction process after 24 hours of curing.

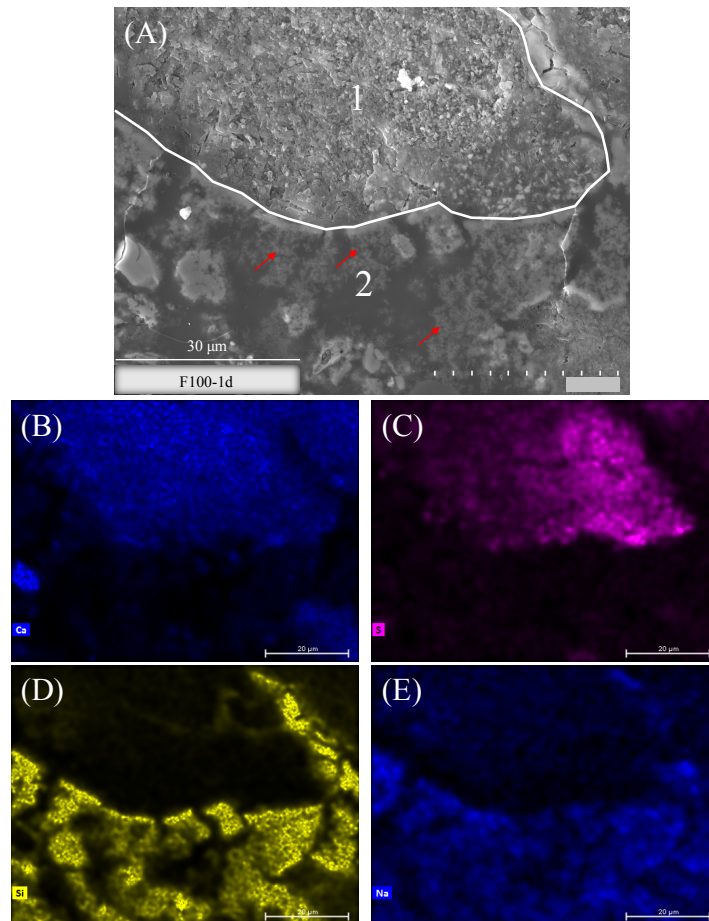


Figure 29: SEM observations of the alkali activated fly ash binder F100 after 24 hours of curing: (A) SEM micrograph, and chemical mappings of: (B) calcium, (C) sulphur, (D) silicon and (E) sodium

Figure 30 also shows microstructural observations of the alkali activated fly ash binder after 24 hours of curing, and particularly illustrates the microstructural difference between a calcium-rich particle and a particle from the vitreous phase both originally present in

the fly ash. They can both be distinguished by SEM by their chemical composition and microstructural features.

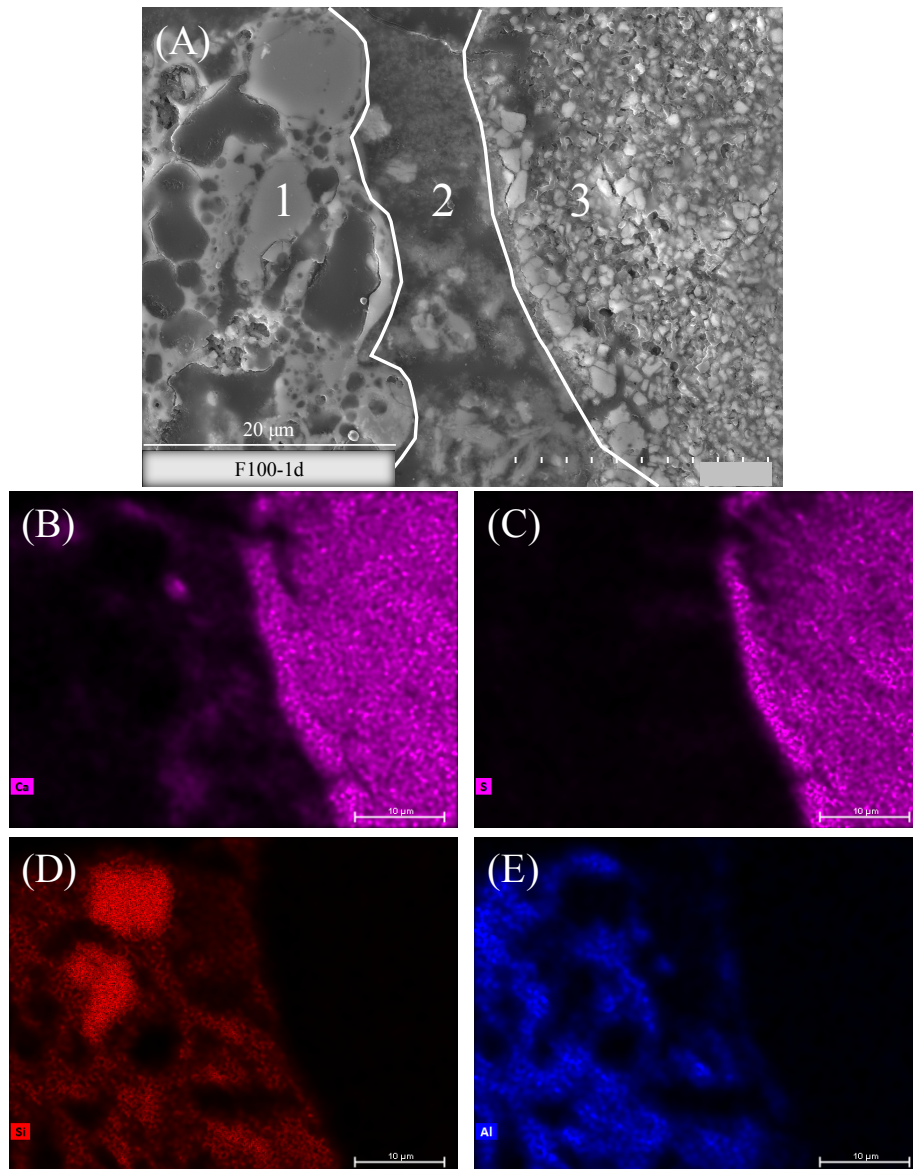


Figure 30: SEM observations of the alkali activated fly ash binder F100 after 24 hours of curing: (A) SEM micrograph, and chemical mappings of: (B) calcium, (C) sulphur, (D) silicon and (E) aluminium

Regarding calcium-rich particles, they present a nodule shape with a granular surface (see 3 on Figure 30A) as previously observed (Figure 29A). Whereas particles from the vitreous phase display a vesicular structure (see 1 on Figure 30A) and can be distinguished using chemical mappings by their enrichment in silicon and aluminium (Figure 30D&E).

In between those two particles, a porous area labelled 2 on Figure 30A and with filament like structures can once again be observed and evidences the initiation of the reaction processes. Consequently, from Figure 29 as from Figure 30 it is noticeable that the alkali activated binder after 24 hours of curing presents a high porosity created by the fly ash grains of various sizes and that is filled by water, alkaline solution, and the new product starting to be formed.

Figure 31 shows SEM observations and combined chemical mappings of the alkali activated fly ash binder after 28 days of curing. It especially focuses on the interface between a calcium-rich nodule labelled 1 and the surrounding matrix labelled 2.

Regarding the calcium-rich nodule, it displays a hollowed structure, especially in its centre, and as similarly observed previously by optical microscopy in section 4.4.2.1. In addition, those hollowed structures show dense black zones indicating the presence of filling resin and therefore porosity. Those structural characteristics strongly contrast with calcium nodules after 24 hours presenting a granular surface, and are attributed to the dissolution of calcium-rich phases over time leaving behind a porous body. It is supported by chemical mappings on Figure 31B&C showing a strong impoverishment in calcium and sulphur in the hollowed area with respect to nodules after 24 hours.

An enrichment in calcium and sulphur is seen in the outer part of the nodule suggesting a mechanism of dissolution of calcium and sulphur moving from the calcium nodules to the matrix. Moreover, few silicon supplied in that system by the alkaline solution is detected above the edges of the calcium nodule and inside implying that the alkaline solution penetrates through the calcium-nodule accelerating its dissolution. The coloration due to the silicon presence inside the nodule is few marked as unreactive quartz which corresponds to intensely coloured and well-defined edges spots on the silicon chemical mapping (Figure 31D) are present in the matrix and induces a rescaling of the silicon coloration.

Regarding the area surrounding the calcium nodule labelled 1, it is very massive and presents a low porosity compared to the binder after 24 hours. It corresponds to the area where new products are formed. Its chemical mappings show a high content of calcium and silicon which is in accordance with the physicochemical investigation that showed the formation of silicate chains combined with calcium over time. The wide diffusion of calcium into the matrix is clearly seen from Figure 31 when compared to the binder after 24 hours of curing for which calcium is contained and restrained to the nodule surface (see Figure 29 and Figure 30).

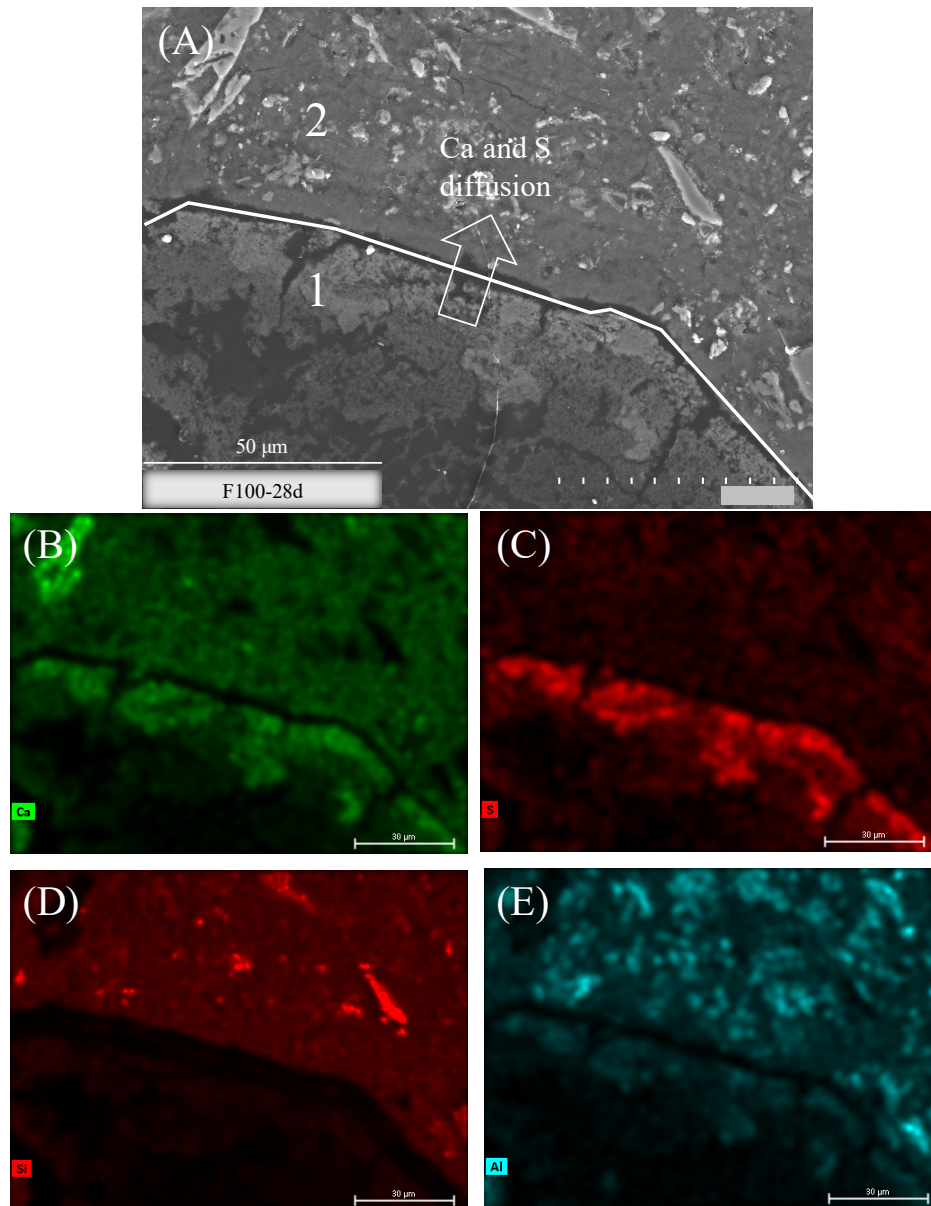


Figure 31: SEM observations of the alkali activated fly ash binder F100 at 28 days: (A) SEM micrograph, and chemical mappings of: (B) calcium, (C) sulphur, (D) silicon and (E) aluminium

Concerning sulphur elements, as well initially present in the nodule in the form of anhydrite CaSO_4 , its dissolution occurs in a lesser extent and seems stopped to the outer part of the nodule at 28 days (Figure 31C). The physicochemical evolution of this system studied in the previous chapter showed that dissolved sulphur combines with sodium to form thenardite Na_2SO_4 at 28 days. Consequently, the presence of thenardite is restrained to small areas around the calcium-rich particles, whereas silicate two-dimensional chains combined with calcium are widely spread all around the calcium nodules. The formation

of this thenardite crust limited around calcium nodules can be explained by the low amount of sulphur elements compared to calcium (see chemical composition of the raw fly ash in Table 1), that already all precipitated in this small area. The conjoint chemical mapping of sodium to localise thenardite is not shown here as sodium is a volatile element for which it is difficult to get a chemical mapping showing a reliable representativeness of sodium dispersion.

Finally, important crackings are observed around calcium-rich particle as seen on Figure 31 and are associated with shrinkage processes frequently observed for alkali activated materials (Lee et al., 2014; Fang et al., 2018).

Figure 32 shows the alkali activated fly ash binder at 28 days, and more particularly a calcium-rich reactive nodule labelled 1 surrounded by a dense matrix comprising both new products and non-reactive phases such as quartz or aluminium containing minerals.

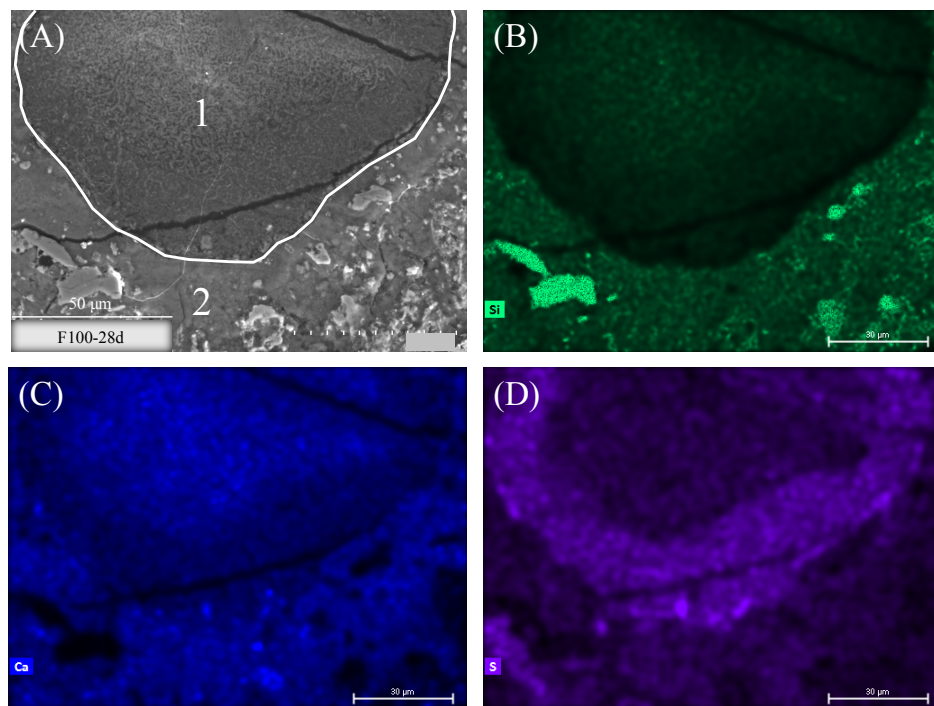


Figure 32: SEM observations of the alkali activated fly ash binder F100 at 28 days: (A) SEM micrograph, and chemical mappings of: (B) silicon, (C) calcium and (D) sulphur

However, in that case the extent of dissolution of the calcium nodule appears lower as the hollowed structure is not seen but rather a granular microstructure similar of those observed after 24 hours. Chemical mappings show that the dissolution of that nodule did

start as calcium is widely diffused into the matrix, and an enrichment in sulphur is once again seen in the outer part of the nodule. Nevertheless, the dissolution is at a different stage as calcium is still strongly detected in the centre of the nodule and no hollowed structure is noticed. Consequently, the extent of reaction of a calcium-rich nodule varies locally. A lesser porosity of the calcium nodule could for instance moderate its dissolution. Its size, its content in calcium and sulphur or else the amount of water locally available are also all parameters that may locally affect the extent of reaction.

Figure 33 shows micrographs of the alkali activated binder after 28 days, and more particularly the difference between microstructural changes occurring around a calcium rich particle identified as the dark reactive zones in optical microscopy, and around a glassy particle identified as the brown matrix in optical microscopy.

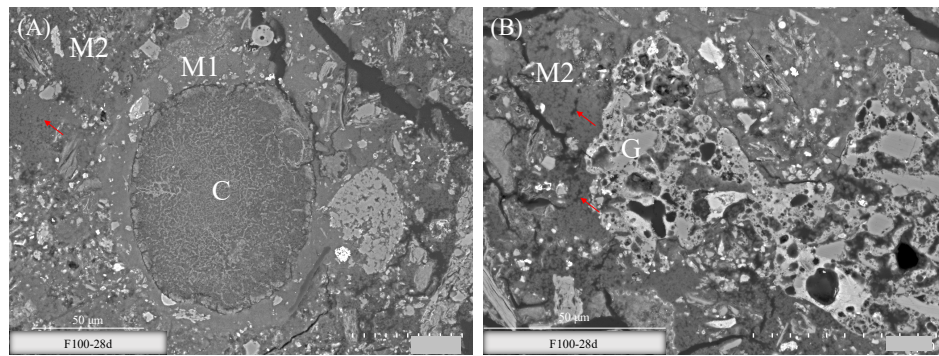


Figure 33: Comparing SEM microstructural changes of the alkali activated fly ash binder F100 at 28 days around: (A) a calcium-rich nodule labelled C, and (B) a particle from the vitreous phase labelled G; M1 = dense matrix; M2 = porous matrix

It is worth noting that although amorphous and extremely porous the vesicular glassy phases reaction is negligible as its vesicular structure remains similar to the one after 24 hours (see Figure 30A, particle labelled 1). This observation is in accordance with our previous investigation in chapter 3 about the physicochemical evolution of that system which shows that the vitreous phase mainly remains unreactive. It is well known that the rate of reaction of the aluminosilicate vitreous phases of fly ash at ambient temperature following alkaline activation is slow and takes several days (Provis and Deventer, 2009; Wardhono et al., 2015). Whereas the calcium-rich particles in our mixes are extremely and quickly reactive as the formation of new products containing calcium already starts after 24 hours as seen previously in Figure 29. Hence, the faster reaction of calcium-rich particles leads to the formation of very dense products (as seen in Figure 33A) freezing the system and preventing the later reaction of the aluminosilicate glassy phases.

Very massive and dense areas are observed around calcium-rich nodules (see Figure 33A), while a more porous matrix is seen around vesicular glassy phases (see Figure 33B). The comparison in Figure 33 hence evidences that there are different matrices forming the alkali activated treated soil: (i) a first circularly-shaped matrix identified around calcium-rich particles and presenting a high density labelled M1 on Figure 33A, and (ii) a more porous matrix less bonded labelled M2 on Figure 33A&B whose pores are shown by red arrows, and located around glassy phases of lower reactivity. A previous investigation of that system by Nuclear Magnetic Resonance in chapter 3 (see section 3.4.1.5) showed the signature of only one type of silicate chains combined with calcium and spreaded into the matrix as a new compound. Therefore, Scanning Electron Microscopy provides an additional information: although the atomic structure of the silicate chain remains similar, the arrangement of those phases in the matrix varies following the local environment. Similarly to the great heterogeneity of fly ash, the matrix formed is also highly heterogeneous.

4.4.2.3 Mercury Intrusion Porosimetry (MIP)

Figure 34A shows cumulative curves of mercury intrusion porosimetry tests of the alkali activated fly ash binder over time. The longer the curing time, the lower is the cumulative intrusion volume ratio implying a progressive decrease of the overall porosity over time, and in accordance with the general tendencies observed by SEM in section 4.4.2.2. It is owed to the progressive filling of pores by the new compounds formed i.e. calcium-silicate two-dimensional chains and thenardite.

Additionally, it is worth noted that the initial cumulative intrusion volume ratios are different following the curing time whereas the samples cured in their molds have not showed any volumetric variation over time. Therefore, this difference is due to pores that could not be measured by the Porosimeter i.e. pores whose size are lower than 7 nanometer which corresponds to the limit of detection or to newly formed ink-bottle pores inside the samples.

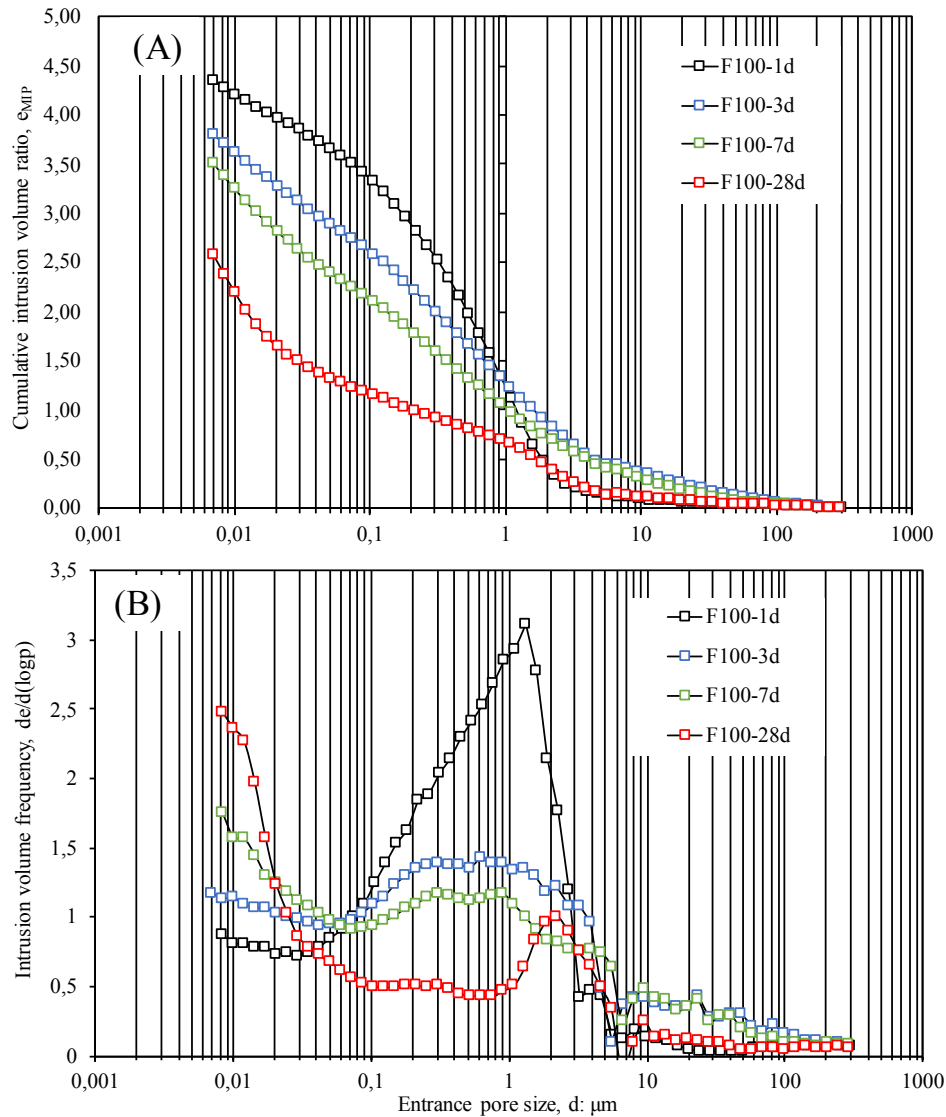


Figure 34: Comparing mercury intrusion porosimetry tests of the alkali activated fly ash binder F100 over time and in terms of (A) cumulative intrusion volume ratios, (B) intrusion volume frequency ratios as a function of entrance pore size

Figure 34B shows the frequency distributions of pore entrance diameters belonging to the alkali activated fly ash binder over time. Samples at 24 hours, 3 and 7 days all show one very broad modal pore sizes between 0.05 μm and 3 μm . However, from 24 hours to 7 days the frequency of those pores progressively decreases due to their filling by newly formed compounds. Whereas, at 28 days a narrower modal pore size at about 2 μm is observed. By analogy with SEM pictures, those remaining pores at 2 μm could correspond to either the size of the cracks seen around calcium particles and associated with shrinkage as previously observed on Figure 31, the porosity formed within calcium nodules after

their dissolution also seen on Figure 31, or else pores that have not been filled by new compounds within the more porous matrix previously identified and labelled M2 on Figure 33.

Finally, in the area of lower pore size i.e. below 20 nm the increase of frequency over time corresponds to the formation of a new class of pores inside the matrix. It is associated with the formation of the silicate two-dimensional chains combined with calcium, whose structure resembles those of Calcium-Silicate Hydrates (i.e. C–S–H phases commonly found in Portland cement) known for possessing an intrinsic porosity of a nanometer size (Muller, 2014). However, this small new class of pores cannot be fully probed by MIP technique whose detection limit in the small entrance pore size is of 7 nm.

4.4.3 Interaction between the alkali activated fly ash binder and kaolin

The following section aims at understanding the interaction between kaolin and the alkali activated fly ash binder previously described. The previous chapter focussing on the physicochemical evolution of the same mixes herein studied showed that kaolin was not very reactive during alkaline activation and did not modify the reaction sequence when compared to the one of the alkali activated fly ash binder alone. Accordingly, similar mechanisms of ions dissolution precipitation from the calcium-rich particles into the matrix leading to the formation of new products also occur in the alkali activated fly ash binder treated soil as previously described for the binder in section 4.4.2.2, and hence will not be detailed here.

Regarding the pore network structure, the previous chapter also showed that kaolinite platelets were homogeneously spread across the matrix. This section consequently aims at giving a deeper insight of the influence of kaolin on the microstructure with respect to the binder alone.

Figure 35 shows microstructural observations of the alkali activated fly ash binder treated soil over time by optical microscopy. Similarly to the alkali activated fly ash binder, after 24 hours of curing, dispersed dark spots corresponding to calcium-rich nodules are seen across the overall sample, whereas at 28 days larger dark zones encompassing the newly formed compounds have grown around those nodules. Hollowed greyish nodule structures at 28 days can also be distinguished as for the binder and associated with the dissolution of calcium-rich particles.

The widening of darker zones which indicates the extent of reaction is lesser than the binder and represents around $\frac{1}{4}$ of the sample. This is consistent with the proportions of aluminosilicate solid considering that half of fly ash containing the reactive calcium

nodules has been replaced by non-reactive kaolin in this soil-binder mixture. Consequently, the growth and development of new products into the available spaces does not seem influenced by the presence of kaolin.

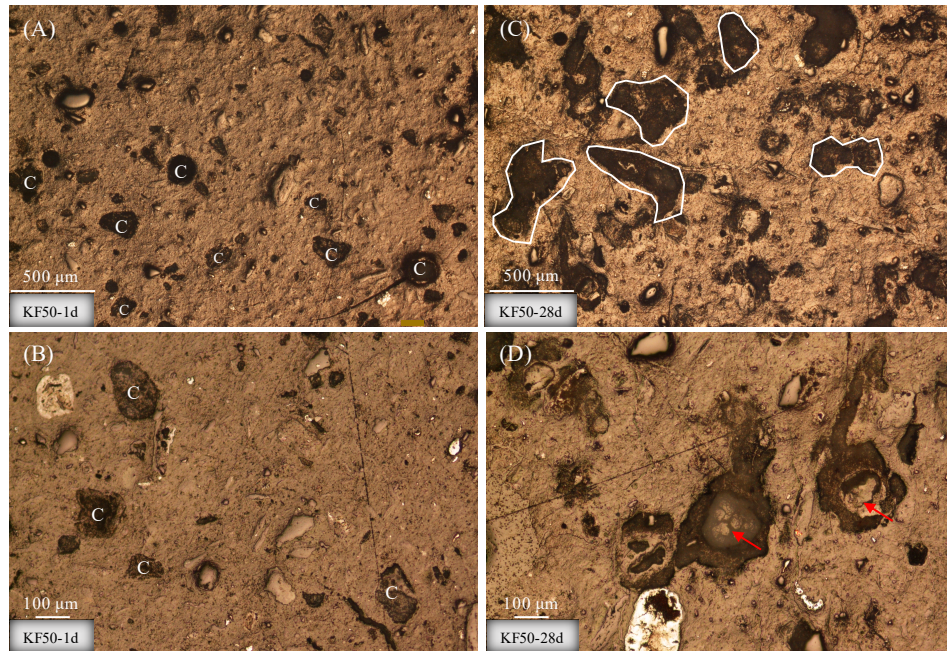


Figure 35: Optical microscopy images of the alkali activated fly ash binder treated soil KF50 (A) and (B) after 24 hours, (C) and (D) at 28 days, C=calcium-rich particle

Figure 36 shows micrographs of the alkali activated binder treated soil. After 24 hours crackings around and inside calcium nodules are seen (see particle C on Figure 36A), and associated to shrinkage similarly to the alkali activated fly ash binder at 28 days. The treated soil at 28 days however shows less marked crackings as shown on Figure 36B which focusses on the interface between a calcium-rich nodule labelled 1 and the surrounding dense matrix labelled 2. It is attributed to the presence of kaolinite acting as a filler at the periphery of the calcium-rich nodules (see red arrows on Figure 36B showing kaolinite platelets).

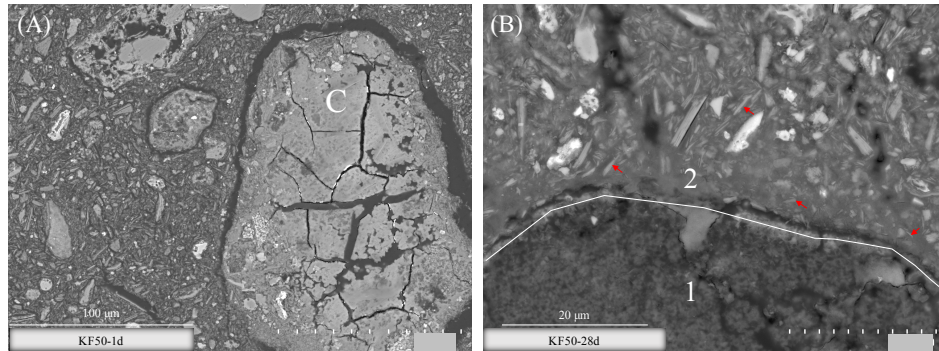


Figure 36: SEM micrographs of the alkali activated fly ash binder treated soil KF50 at (A) 24 hours and (B) 28 days

Figure 37A shows cumulative curves of mercury intrusion porosimetry tests of the alkali activated fly ash binder treated kaolin over time. Similarly to what was observed for the alkali activated binder, a decrease of the total porosity is detected over time.

In addition, the initial cumulative intrusion volume ratios are also different following the curing time and associated with pores not detected by the apparatus.

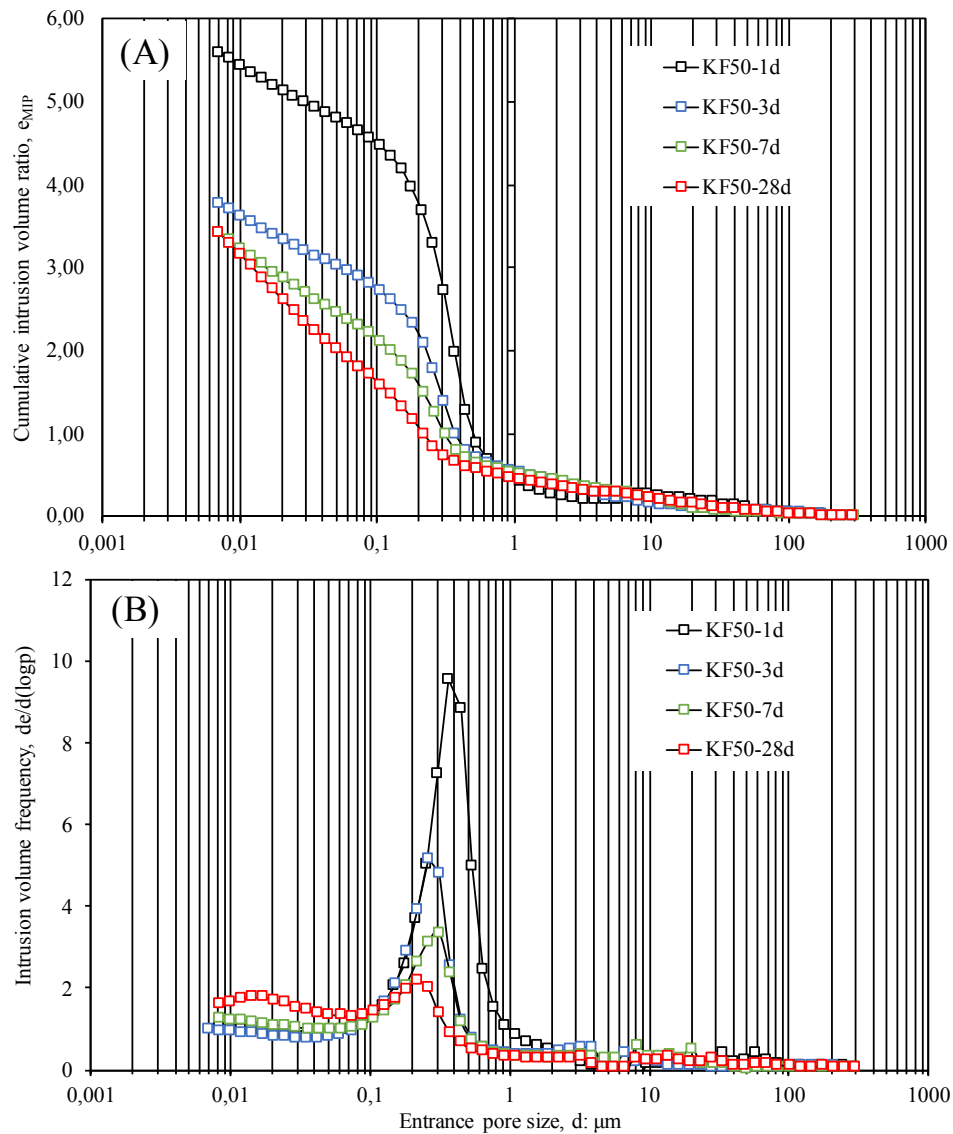


Figure 37: Comparing mercury intrusion porosimetry tests of the alkali activated fly ash binder treated soil KF50 over time and in terms of (A) cumulative intrusion volume ratios, (B) intrusion volume frequency ratios as a function of entrance pore size

Figure 37B shows the frequency distributions of pore entrance diameters belonging to the treated soil over curing time. Similarly to the alkali activated fly ash binder, the treated soil at 24 hours shows one modal pore sizes. Nevertheless, compared to the binder it is associated with a lower entrance pore size value around 0.4 μm and a much thinner peak. The non-presence of a wide class of pores between 0.05 μm and 3 μm at 24 hours as seen for the alkali activated fly ash binder is associated with the filling of the spaces between the coarse grains of fly ash by the small sized kalinite platelets. At 24 hours, kaolin

therefore leads the organisation of the system microstructure as the typical pattern of kaolin (i.e. a monomodal curve with a peak around $0.4\ \mu\text{m}$) is shaping the curve.

Increasing the curing time, the filling of largest pores around the peak is seen as for the binder and due to the progressive filling of those pores by the newly products formed. A little shift of the residual peak towards smaller entrance diameters is also observed.

Finally, the formation of a new class of pores in the area of lower pore size i.e. below 30 nm is observed between 7 and 28 days of curing. Similarly to the binder, it is associated with the intrinsic porosity of the newly formed silicate-calcium chains. The delay in detection compared to the binder is due to the lower amount of phases formed for that system.

4.4.4 Comparison with Portland cement

This last section focusses on a comparison with microstructural development in Portland cement for which the mechanisms involved appear alike. This comparison particularly helps at providing a better understanding of (i) how microstructures are formed and (ii) interpreting the short and long-term performances of the treated soil regarding the evolution of the binder over time.

4.4.4.1 Processes generating the microstructure

In cement systems, the dissolution of cement particles releases ions into the pore solution which then combine with water to form mainly Calcium Silicate Hydrates C–S–H (Muller, 2014). In a similar way, in our alkali activated binder, the dissolution of calcium-rich particles from fly ash releases calcium cations into the pore solution which then combine with water and silicon anions from the alkaline solution to form silicate two-dimensional chains combined with calcium. A former investigation by Nuclear Magnetic Resonance in the previous chapter (see section 3.4.1.5) nevertheless showed that the chains structure is slightly different from C–S–H, namely they are not well organized, of high length and may incorporate aluminium in a three-dimensional environment which has not been described in literature yet.

Secondly, it was reported for cement systems that the first Calcium Silicate Hydrates C–S–H cover cement grains and further grow into the available space. All cement grains are therefore surrounded by a shell of C–S–H (Scrivener, 2004). Again similarly in this study,

optical microscopy images clearly show the development and growth of new products around calcium-rich reactive particles suggesting a similar mechanism.

Furthermore, Scrivener (2004) shows that as the cement grains dissolve, this might leave a hollow shell (Scrivener, 2004). The various extent of reaction of individual cement grains depends on their sizes: small cement grains hydrate completely in the first stages and remain as hollow shells of hydration product; whereas big grains further hydrate which forms denser hydration products and which fill in the gap between shell and grain (Muller, 2014). In this study it is also noticeable that calcium-rich reactive phases react at different rates: some completely dissolve after 28 days leaving a hollow shell while other remain with their initial structure and still contain calcium. Consequently, and similarly to what is described in the literature, depending on the calcium nodule size, the local products formed slightly differ which could lead to local variation of the inherent material properties.

4.4.4.2 Pore network characteristics

Regarding the pore network characteristics of cement systems, two populations of pores are generally distinguished: (i) capillary pores which correspond to space not being filled by solid products of hydration, and (ii) very small pores called gel pores associated to the intrinsic porosity of Calcium Silicate Hydrates C-S-H. Over time, while chemical reactions proceed the population of capillary pores decreases whereas the population of gel pores increases, which may lead to the formation of disconnected spaces (Jennings et al., 2008). Our alkali activated binder shows similar tendencies that is a progressive decrease of intermediate pores or capillary pores while a new class of pores associated with silicate-calcium chain products is detected using Mercury Intrusion Porosimetry.

4.4.4.3 Macroscopic behaviour according to the microstructure evolution

Since both the processes generating the microstructure and the evolution of the pore network over time of our alkali activated binder are similar to cement systems, a similar influence of the microstructure on the short and long-term performances can be expected.

Changes in the pore network strongly influence transport properties that govern the rate of all major deterioration processes and the service life of building materials (Wong et al., 2006). Namely the formation of gel pores inside the capillary spaces tends to decrease the connectivity of the pore network inhibiting the transport of aggressive substances such as

acids, carbonate or chloride through concrete and therefore enhancing the material durability (van Deventer et al., 2010; Muller, 2014).

Finally, despite the great inhomogeneity of the reactive fly ash the growth and widening of new products appear to occur homogeneously across the sample at a millimetric scale in our alkali activated materials which would benefit the formation of a homogeneously reinforced material.

4.5 Conclusions

The development of a novel binder that is an alkali activated calcium-rich fly ash for clay soil stabilisation was investigated. The study of its microstructural evolution showed that structural changes occur around calcium-bearing minerals from fly ash which constitute the reactive phases, and whose dissolution leads to the formation of new compounds on its surface first and then growing into the available space. Capillary pore spaces are progressively filled by new compounds (i.e. thernadite and silicate-calcium chains) over time. Whereas the newly formed silicate-calcium chains possess an intrinsic porosity of nanometric size conducting to the formation of a new class of small pores over time. Different heterogenous matrices of various porosity and arrangement are however observed across the material and owed to the high heterogeneity of fly ash whose particles locally react differently.

The interaction between the binder and kaolin showed that small sized kaolinite platelets fill the spaces between coarser grains from fly ash. Kaolin is therefore leading the microstructural organisation, that is, the pore network is characterised by pores ranging in lower size compared to the binder. Nevertheless, the microstructural changes remain similar over time i.e. filing of capillary pores and appearance of nanometric pores from silicate-calcium chains.

The observed microstructural evolution is very similar to the one of cement system and should therefore conducts to akin performances that is an increase in strength and ability to resist to aggressive substances due to changes in transport properties. However, regarding the complexity of both cement and alkali activated systems which are multi-components systems, a coupling of those microstructural observations with mechanical performances and transport properties is of further interest. Namely, a complementary three-dimensional characterisation of the pore network using for instance microtomography would greatly help to assess the connectivity and tortuosity of the pore network which are primordial parameters to understand properly transport properties and therefore durability. Using micro-indentation coupled with Scanning Electron Imaging would also allow to measure local hardness variations following the extent of reaction of calcium particles and therefore help to apprehend how significant are the local microstructural variations for the mechanical performances at a macroscopic scale.

4.6 References

- Askeland, D.R., Fulay, P.P., Wright, W.J., 2011. *The science and engineering of materials*, 6th ed. ed. Cengage Learning, Stamford, CT.
- Buchwald, A., Kaps, C., Hohmann, M., 2003. Alkali-activated binders and pozzolan cement binders—complete binder reaction or two sides of the same story, in: *Proceedings of the 11th International Conference on the Chemistry of Cement*. Portland Cement Association Durban, South Africa, pp. 1238–1246.
- Chemeda, Y., 2015. Effect of hydrated lime on kaolinite surface properties and its rheological behaviour. Université de Nantes.
- Clemens, H., Mayer, S., Scheu, C., 2008. Microstructure and Properties of Engineering Materials. *Neutrons Synchrotron Radiat. Eng. Mater. Sci. Fundam. Appl.* 1–20.
- Cristelo, N., Glendinning, S., Fernandes, L., Pinto, A.T., 2012. Effect of calcium content on soil stabilisation with alkaline activation. *Constr. Build. Mater.* 29, 167–174. <https://doi.org/10.1016/j.conbuildmat.2011.10.049>
- Cristelo, N., Glendinning, S., Teixeira Pinto, A., 2011. Deep soft soil improvement by alkaline activation. *Proc. Inst. Civ. Eng. - Ground Improv.* 164, 73–82. <https://doi.org/10.1680/grim.900032>
- Fang, G., Bahrami, H., Zhang, M., 2018. Mechanisms of autogenous shrinkage of alkali-activated fly ash-slag pastes cured at ambient temperature within 24 h. *Constr. Build. Mater.* 171, 377–387. <https://doi.org/10.1016/j.conbuildmat.2018.03.155>
- Jennings, H.M., Bullard, J.W., Thomas, J.J., Andrade, J.E., Chen, J.J., Scherer, G.W., 2008. Characterization and Modeling of Pores and Surfaces in Cement Paste: Correlations to Processing and Properties. *J. Adv. Concr. Technol.* 6, 5–29.
- Lawrence, M., Jiang, Y., 2017. Porosity, Pore Size Distribution, Micro-structure, in: Amziane, S., Collet, F. (Eds.), *Bio-Aggregates Based Building Materials*. Springer Netherlands, Dordrecht, pp. 39–71. https://doi.org/10.1007/978-94-024-1031-0_2
- Lee, N.K., Jang, J.G., Lee, H.K., 2014. Shrinkage characteristics of alkali-activated fly ash/slag paste and mortar at early ages. *Cem. Concr. Compos.* 53, 239–248. <https://doi.org/10.1016/j.cemconcomp.2014.07.007>
- Muller, A.C.A., 2014. Characterization of porosity & CSH in cement pastes by 1H NMR. École Polytechnique Fédérale de Lausanne, Suisse.
- Nath, S.K., Maitra, S., Mukherjee, S., Kumar, S., 2016. Microstructural and morphological evolution of fly ash based geopolymers. *Constr. Build. Mater.* 111, 758–765. <https://doi.org/10.1016/j.conbuildmat.2016.02.106>
- Provis, J.L., Deventer, J.S.J. va., 2009. *Geopolymers Structure, processing, properties and industrial applications*, Woodhead Publishing in materials. Woodhead, Cambridge.

- Rios, S., Cristelo, N., Viana da Fonseca, A., Ferreira, C., 2016. Structural Performance of Alkali-Activated Soil Ash versus Soil Cement. *J. Mater. Civ. Eng.* 28, 4015125. [https://doi.org/10.1061/\(ASCE\)MT.1943-5533.0001398](https://doi.org/10.1061/(ASCE)MT.1943-5533.0001398)
- Scrivener, K.L., 2004. Backscattered electron imaging of cementitious microstructures: understanding and quantification. *Cem. Concr. Compos.* 26 8 935–945.
- Scrivener, K.L., Kirkpatrick, R.J., 2008. Innovation in use and research on cementitious material. *Cem. Concr. Res.* 38, 128–136. <https://doi.org/10.1016/j.cemconres.2007.09.025>
- Shi, C., Krivenko, P.V., Roy, D.M., 2006. Alkali-activated cements and concretes. Taylor & Francis, London ; New York.
- Silva, R.A., Oliveira, D.V., Miranda, T., Cristelo, N., Escobar, M.C., Soares, E., 2013. Rammed earth construction with granitic residual soils: The case study of northern Portugal. *Constr. Build. Mater.* 47, 181–191. <https://doi.org/10.1016/j.conbuildmat.2013.05.047>
- Singhi, B., Laskar, A.I., Ahmed, M.A., 2016. Investigation on Soil–Geopolymer with Slag, Fly Ash and Their Blending. *Arab. J. Sci. Eng.* 41, 393–400. <https://doi.org/10.1007/s13369-015-1677-y>
- Tenn, N., Allou, F., Petit, C., Absi, J., Rossignol, S., 2015. Formulation of new materials based on geopolymer binders and different road aggregates. *Ceram. Int.* 41, 5812–5820. <https://doi.org/10.1016/j.ceramint.2015.01.010>
- van Deventer, J.S.J., Provis, J.L., Duxson, P., Brice, D.G., 2010. Chemical Research and Climate Change as Drivers in the Commercial Adoption of Alkali Activated Materials. *Waste Biomass Valorization* 1, 145–155. <https://doi.org/10.1007/s12649-010-9015-9>
- van Deventer, J.S.J., San Nicolas, R., Ismail, I., Bernal, S.A., Brice, D.G., Provis, J.L., 2015. Microstructure and durability of alkali-activated materials as key parameters for standardization. *J. Sustain. Cem.-Based Mater.* 4, 116–128. <https://doi.org/10.1080/21650373.2014.979265>
- Wardhono, A., Law, D.W., Strano, A., 2015. The Strength of Alkali-activated Slag/fly Ash Mortar Blends at Ambient Temperature. *Procedia Eng.* 125, 650–656. <https://doi.org/10.1016/j.proeng.2015.11.095>
- Wilkinson, A., Haque, A., Kodikara, J., 2010. Stabilisation of clayey soils with industrial by-products: part A. *Proc. Inst. Civ. Eng. - Ground Improv.* 163, 149–163. <https://doi.org/10.1680/grim.2010.163.3.149>
- Wong, H.S., Buenfeld, N.R., Head, M.K., 2006. Estimating transport properties of mortars using image analysis on backscattered electron images. *Cem. Concr. Res.* 36, 1556–1566.
- Zhang, M., Guo, H., El-Korchi, T., Zhang, G., Tao, M., 2013. Experimental feasibility study of geopolymer as the next-generation soil stabilizer. *Constr. Build. Mater.* 47, 1468–1478. <https://doi.org/10.1016/j.conbuildmat.2013.06.017>

**Use of alkali activated fly ash binder for
kaolin clay soil stabilisation: Mechanical
behaviour**

Chapter 5 is in preparation for submission. Additional work might be needed before paper submission.

Samples preparation, one-dimensional compression tests and shear tests were carried out at the University of Strathclyde. Mercury Intrusion Porosimetry analyses were performed at the University of Cassino. Nuclear Magnetic Resonance were performed at the Institute of Materials Jean Rouxel.

The Candidate performed one-dimensional compression tests, collected the data, conceived and designed the analysis and wrote the paper. Direct shear tests were carried out together with Valentina Saravo in the context of her bachelor thesis. Sebastiana Dal Vecchio from the University of Cassino performed Mercury Intrusion Porosimetry experiments. Giacomo Russo from the University of Cassino and Southern Lazio helped for the analysis and interpretation of MIP data. He also corrected the paper. Alessandro Tarantino helped in designing the experimental strategy and interpretation of results.

5.1 Abstract

This study examines the use of a calcium-rich fly ash from coal combustion binder activated by a sodium-based alkaline solution for kaolin treatment and as a substitute to usual high-carbon footprint stabilisers such as lime and Ordinary Portland Cement. The global aim is to explore the feasibility of this binder as a potential soil stabiliser by conducting a multi-scale analysis that conjointly explores the physicochemical evolution of the system, its microstructure and its mechanical performance. The present work is devoted to this latter aspect of the research. To this end, an experimental study about the mechanical behaviour of the treated samples at different curing times by means of one-dimensional compression test and direct shear test has been carried out.

An insight into the mechanical properties evidences the relevant improvement of mechanical performance of treated samples. Increasing the curing time, the overall stiffness of the treated soil increases, as well as the yield stress. In terms of shear resistance, the treated soil progressively develops a peak of shear resistance over time, which is similar to the characteristic response of cemented soils. All those improvements are associated with the formation of a binding phase identified as an amorphous silicate consisting of chains combined with calcium and whose formation essentially occurs within 28 days.

A further insight in microstructural changes induced by loads on treated samples evidences that both plastic and elastic strains are consequences of size variation in the larger pores range.

Finally, compared with the effects of traditional binders, similar tendencies of improvement are observed for the alkali activated binders evidencing its good potential for soil treatment.

5.2 Introduction

Works on alkali activated binder treated soils are recent and constitute a novel domain of application. Consequently, very few studies on clay soil treatment using this type of binders have been conducted (Wilkinson et al., 2010; Singhi et al., 2016). The present work therefore aims to assess the feasibility of using this novel binder for soil improvement in terms of mechanical properties.

To study the workability of using a class of material for a novel application, several parameters are significant to explore such as the composition, microstructure and processing which all determine the performances and cost of a material (Askeland et al., 2011). Our project as a whole was hence designed to develop a detailed comprehension of alkali activated treated soil across various scale levels. Two scale levels have been investigated in the two previous chapters, and considering the same system herein studied but on reconstituted samples. At first, the particle level was examined. It gave an information about the reactivity of the phases initially present and an understanding of the chemical composition and crystal structure of the new phases formed in the treated soil. Notably, it showed that calcium-containing phases from fly ash represented the reactive phases, and whose dissolution following alkaline activation leads to the formation of amorphous silicate consisting of chains and combined with calcium (Chapter 3). The structure of those newly formed chains resembles the one of Calcium Silicate Hydrate C–S–H commonly found in Portland cement, and therefore a similar type of mechanical improvement than Portland cement is expected for the alkali activated binder treated kaolin. In a second stage, the resulting microstructural organization of the material on a nanometer to centimeter length scale was examined. It corresponds to the arrangement of solid phases within the material. Remarkably, it showed that the dissolution of reactive calcium-rich phases leads to the formation of new compounds that first cover the grain surfaces and then further grow into the available space resulting in a decrease of the overall porosity over time.

The present work therefore constitutes the third level of investigation that focusses on the macroscopic level. This study was designed in two stages in order to investigate the effect of the binder on the soil mechanical behaviour. Namely, an initial stage focusses on the oedometer test which gives an assessment of one-dimensional stiffness of the alkali activated binder treated soil. An investigation of the effects of loads on the microstructure of treated samples was also performed by Mercury Intrusion Porosimetry analyses. While a second stage focusses on the investigation of shear strength of the alkali activated binder treated soils. In addition, along the whole study a conjoint understanding of those mechanical data in view of the knowledge gained about the physicochemical and microstructural evolution of the system was carried out.

5.3 Material and methods

5.3.1 Materials

A Polish fly ash derived from hard coal and coal slime combustion in fluidised bed boiler was used. Its chemical analysis is given in Table 1, and consists primarily of SiO_2 , Al_2O_3 and CaO . The fly ash contains, approximately, 52% of particles sized lower than $45\ \mu\text{m}$ and 41% lower than $10\ \mu\text{m}$.

Speswhite kaolin provided by Imerys Minerals UK, and whose chemical composition is given in Table 1 was used. It is mainly constituted of kaolinite (95%) and secondarily of muscovite (4%) (Chemed, 2015). The kaolin contains, approximately, 100 % of particles sized lower than $10\ \mu\text{m}$ and 80 % lower than $2\ \mu\text{m}$. Its specific gravity is $G_s = 2.60$. The liquid and plastic limits are respectively 70 % and 32 % giving a plastic index of 38 % (Vitale et al., 2016).

A unique alkaline solution was used: a sodium silicate with a mass ratio $\text{SiO}_2/\text{Na}_2\text{O}$ of 1.7 and a dry mass percentage of 44%; supplied by Woellner Group and named GEOSIL 34417.

5.3.2 Sample preparation

Sample preparation was designed in order to mimic real field conditions encountered in embankment construction. To mimic the first step of soil mixing, the alkaline solution i.e. silicate and water were stirred together for one hour and then sprayed on the aluminosilicate powders i.e. fly ash and kaolin previously mixed together as well. It gives a wet powder. As a preliminary study, only two types of mixes were studied and named KF10 and KF20. KF10 is the alkali activated binder treated soil whose solid phase is made of 90% of kaolin and 10% of fly ash in mass, while KF20 contains 80% of kaolin and 20% of fly ash in mass. The proportion of added fly ash was kept low in order to be closer to field conditions for which the content of Portland cement added to the soil is comprised between 7 to 12 %. The liquid and plastic limits of the mix labelled KF20 are respectively 60 % and 35 % giving a plastic index of 25 %.

In order to obtain similar initial condition to compacted soil in the field, the wet powder obtained was statically compacted into a mold at a vertical stress of 600 kPa for one hour. The void ratio at the end of compaction was $e = 0.72$ for the treated soil KF10, and $e = 0.83$ for the raw kaolin.

Once the compaction loads were removed the sample was cured for 1, 7, 14, 28, 60 or 90 days at 20 °C inside their molds in order to avoid any volumetric expansion during curing. Finally, samples within their molds were packed under vacuum to avoid carbonation during curing.

For one-dimensional compression test this mold was the oedometer ring, whereas for direct shear test the mold was a designed 3D printed plastic mold. This plastic mold was designed in order to cure several samples and use the shear box at the same time. It was designed in Autodesk Fusion 360 and printed with the Ultimaker 2 Extended 3D printer. The mold was made of two parts: (i) a base that maintains the mold (see Figure 38A), and (ii) a cover (see Figure 38B) that is inserted inside the base and attached to it with screws (see Figure 38C). The samples were compacted inside the cover, that was later removed and packed under vacuum.

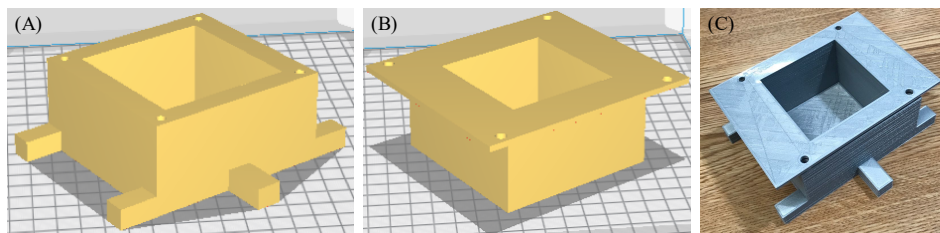


Figure 38: 3D printed mold (A) design of the base, (B) design of the cover and (C) assemblage of the mold

The initial water content was fixed to 28% for all the samples, which corresponds to the optimum moisture content determined by Proctor compaction test. Additionally, the mass ratio of alkaline solution to fly ash was fixed to 50% for all the samples, giving the initial molar ratios (considering that kaolin is unreactive): Si/Al = 2.0, Si/Na = 3.5 and Al/Na = 1.8. The Al/Na ratio was not fixed to one because of the presence of calcium ions in high quantity in our system playing a role of charge compensation as well as sodium.

5.3.3 Methods

One-dimensional compression test

Oedometer tests were performed on compacted samples in standard oedometer cells. Tests were performed in saturated conditions. After saturation, vertical stress was conventionally applied in successive steps ($\Delta\sigma_v/\sigma_v = 1$) up to a vertical stress of 2220 kPa.

Samples were allowed to consolidate until measured axial strains are approximately close to the expected maximum, and in order to maintain the full test duration within 1 day, avoiding curing inside the oedometer cell.

Mercury Intrusion Porosimetry (MIP)

MIP tests were carried out on samples removed from the oedometer cell at a given vertical stress in order to capture microstructural features of samples induced by loading along the compressibility curve. MIP tests were performed on freeze dried samples by a double chamber Micromeritics Autopore III apparatus. In the filling apparatus (dilatometer) samples were outgassed under vacuum and then filled by mercury allowing increase of absolute pressure up to ambient one. Using the same unit the intrusion pressure was then raised up to approximately 200 kPa by means of compressed air. The detected entrance pore diameters range between 134 μm and 7.3 μm (approximately 0.01 MPa - 0.2 MPa for a mercury contact angle of 139°). After depressurisation to ambient pressure, samples were transferred to high-pressure unit, where mercury pressure was increased up to 205 MPa following a previously set intrusion program. The smallest detected entrance pore diameter was about 7 nm. Corrections to pore-size distribution due to compressibility of intrusion system were applied performing a blank test.

Direct shear test

Direct shear tests were performed according to ASTM D 3080-90 (ASTM D 3080-90, 1994) on compacted samples in a standard shear box. Cured samples were transferred from a 3D printed mold to the shear box in a centred position using a load frame. Samples were fully saturated and vertical displacements were monitored. After saturation, a normal pressure of 100 kPa was applied in steps and until consolidation was completed. Shear displacement was then applied to a rate of displacement of 0.04 mm/min.

5.4 Results and discussion

5.4.1 One-dimensional compression

Oedometer tests were performed on raw and treated compacted kaolin samples. The initial and final conditions of the samples have been reported in Table 5.

Table 5: Initial and final conditions of oedometer samples

Sample ID	e_0	w_0 (%)	S_0 (%)	e_f	w_f (%)	S_f (%)
Kaolin	1.54	58.97	100.00	1.21	46.32	100.00
KF10 - 1 day	1.57	60.14	100.00	1.28	49.31	100.00
KF10 - 7 days	1.49	57.09	100.00	1.25	48.13	100.00
KF10 - 14 days	1.48	56.88	100.00	1.24	47.77	100.00
KF10 - 28 days	1.48	56.74	100.00	1.25	47.97	100.00
KF10 - 60 days	1.48	56.68	100.00	1.25	48.12	100.00
KF10 - 90 days	1.44	55.10	100.00	1.23	47.12	100.00

Figure 39 shows compressibility curves of the raw kaolin and the fly ash-based alkali activated binder treated kaolin as a function of curing time. It evidences the reduction of the overall volumetric strains as a function of curing time implying that the alkali activated treated soil becomes stiffer with time. More specifically, from 1 to 7 days the improvement remains similar. Whereas at 14 days an intermediary behaviour is observed and at 28 days the maximum improvement is detected. In fact, from 28 to 90 days the curves display an almost similar behaviour signifying that the major improvement is effective and achieved after a curing time of 28 days.

Furthermore, regarding the oedometer curve at 28 days, the yield stress indicating the transition from a reversible to irreversible behaviour can clearly be identified at around 700 kPa. Yield stress is supposed to be the stress at which bonds from the binding agent start to break, inducing a more compressible behaviour of the sample for higher applied stresses (i.e. a steeper slope of the compressibility curve). At lower curing times i.e. 1 and 7 days the yielding point is however fairly identifiable, and no range of small deformation is visible but rather a constantly steep curve. Therefore, there is a clear shift of the yield

stress over time to higher values. It implies that the addition of the alkali activated binder to the soil enlarges the range of stress to which the soil is showing a reversible behaviour.

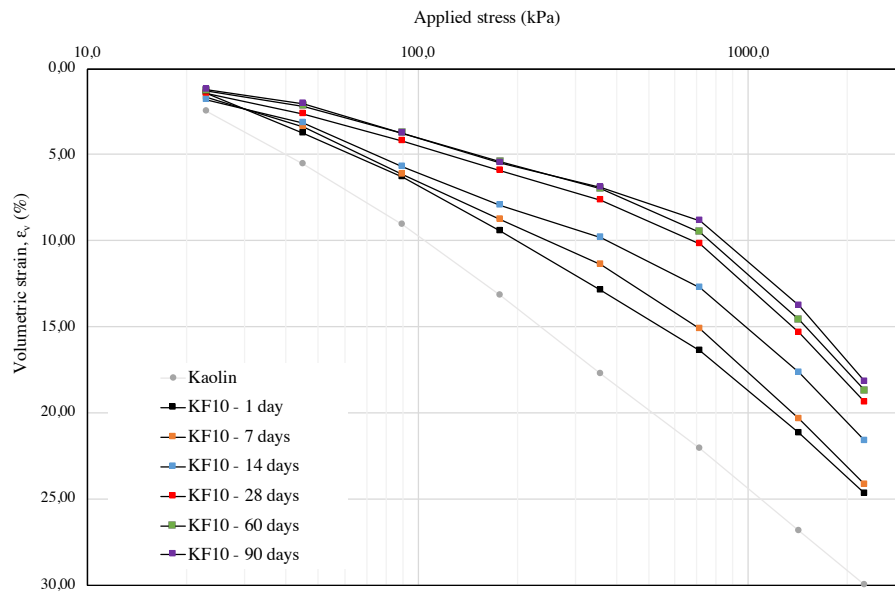


Figure 39: One-dimensional compression tests on the raw and alkali activated binder treated kaolin (KF10) as a function of time

Table 6 Comparison of Compressibility index C_c before and after major yield

Sample ID	Compressibility index C_c (-) before yield	Compressibility index C_c (-) after yield
KF10 - 1 day	0.51	0.45
KF10 - 7 days	0.22	0.49
KF10 - 14 days	0.17	0.50
KF10 - 28 days	0.14	0.51
KF10 - 60 days	0.13	0.51
KF10 - 90 days	0.13	0.54

Figure 39: One-dimensional compression tests on the raw and alkali activated binder treated kaolin (KF10) as a function of time

Table 6 shows a comparison of the compressibility index before and after major yield. It outlines that the decrease over time in compressibility occurs before yield. After yield,

once the binding agent starts to break the compressibility remains very similar whatever is the curing time. The improvement brought by the binding agent is therefore effective before yield.

Finally, compared to the raw kaolin the treated soil at 28 days of curing displays cumulative volume strains twice less, implying an overall increase of its stiffness after the treatment.

In order to better understand the effect of loads on the microstructure of the treated soil, mercury intrusion porosimetry analyses were performed at 28 days on treated samples submitted to increasing load in the oedometer cell.

Three stress levels for which important variations in volumetric strain are seen were selected as shown in Figure 40, and in order to capture the major microstructural changes occurring under loads. The first stress level selected corresponds to a pre-yielding stress where bonds from the binder are supposed to be still present, while a second stress level corresponds to a stress at yielding, and finally a third one corresponds to a post-yielding state where a destructuration stage is clearly identifiable.

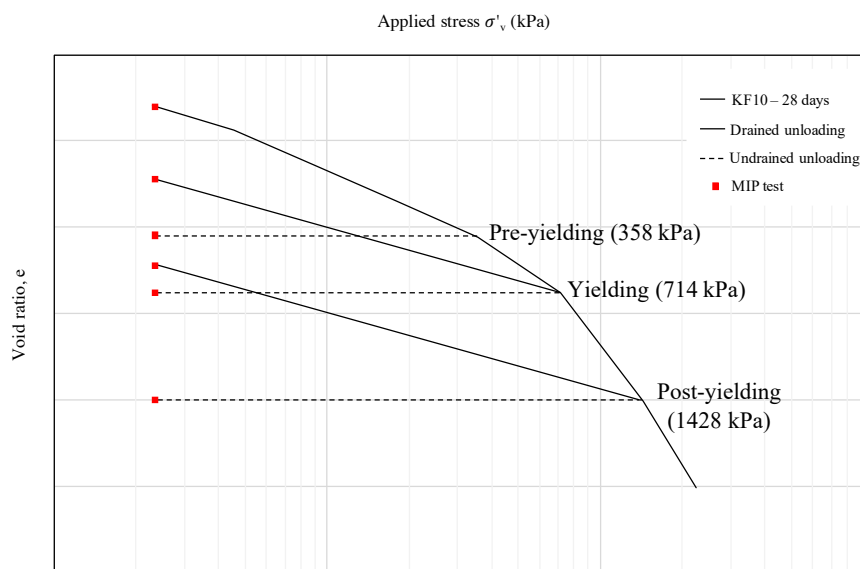


Figure 40: Schematic illustration of MIP samples preparation for one-dimensional loads induced microstructural effects analysis

Two different samples for each stress level were prepared, as suggested by Pedrotti and Tarantino (2017). After reaching the target applied load, the first sample was quickly unloaded without allowing any recovering of volume strains, generating undrained

conditions. The unloading was performed in one single step. The sample was rapidly removed from the oedometer and sealed in plastic bag preventing water loss until the freeze-drying was performed. The second sample was unloaded under drained conditions, allowing the rebound of the structure and the recovering of elastic strains. Undrained loading allows an insight on the effects of loads on microstructure, since the final condition of the sample before and after the unloading stage are very similar to each other. The described preparation procedure strategy has been sketched in Figure 40.

With reference to drained unloading of alkali activated fly ash binder treated samples, Figure 41 shows the pore entrance diameters frequency distributions for different stress levels. Samples show a bimodal distribution of entrance pore diameters. As widely accepted (e.g. Delage et al., 1996; Tarantino and De Col, 2008; Russo and Modoni, 2013), microstructure of compacted treated samples is characterized by an aggregate structure, with smaller pores corresponding to intra-aggregates pores, and larger pores corresponding to inter-aggregates pores. The most significant changes of microstructure induced by applied loads occur in the inter-aggregate porosity. The larger pores within the range of $0.4 \mu\text{m} - 10 \mu\text{m}$ show in fact a progressive reduction of frequency as the stress level increases without any significant change of modal size (located around $1.0 \mu\text{m}$). Whereas smaller pores, with modal size around $0.15 \mu\text{m}$, are not affected by the applied loads. Hence, the drained unloading allows to highlight the plastic strain characterised by the progressive reduction of the larger pores population induced by loads. This reduction does not affect the modal pore size but just their frequency.

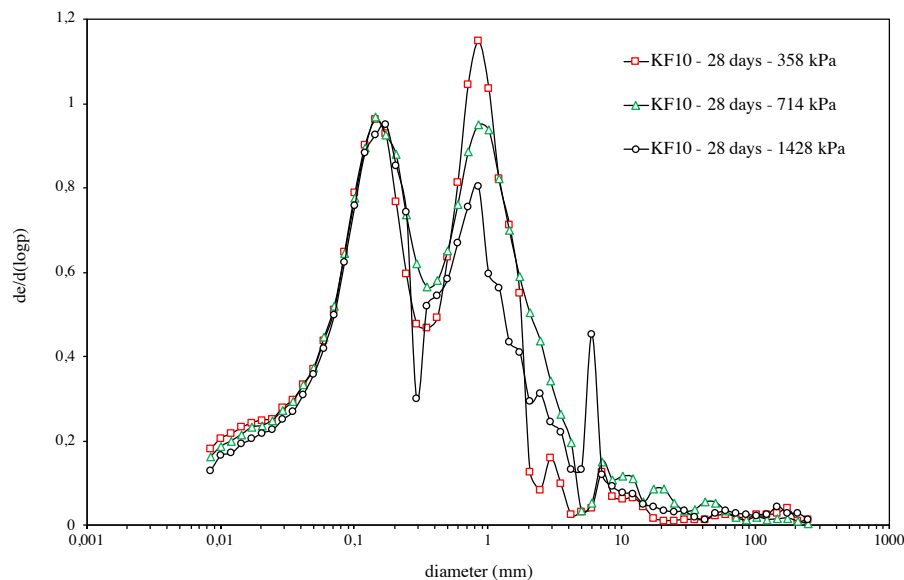


Figure 41: Comparison between frequency distributions of entrance pore sizes tests of the alkali activated fly ash binder treated soil KF10 at 28 days as a function of the applied stress and for a drained unloading

Further insights on the effects of loads on microstructure of treated samples have been allowed by comparing MIP results on drained and undrained unloading samples at different stress levels. In Figure 42A pore sizes frequencies of drained and undrained unloaded samples at pre-yield stress level (i.e. $\sigma'_v = 358$ kPa) have been compared. The undrained unloading evidences a reduction of inter-aggregate pores size frequency induced by applied load without any significant modal size variation; the reduction is reversible, as evidenced by recovering occurring upon drained unloading. At yield stress level (i.e. $\sigma'_v = 714$ kPa), the pore size distribution of treated sample after undrained unloading does not show any significant reduction of inter-aggregate pores frequency, but an appreciable shift of inter-aggregate pores modal size towards smaller dimensions, as detected by comparison with drained unloading sample. Inter-aggregate pores decrease their dimension without changing their distribution, and recover the load induced strains upon unloading (i.e. rebounding) evidencing that at yield stress the destructuration (i.e. bonding breakage) stage is not affecting the structure of treated samples. From Figure 42C, increasing the applied stresses at post-yield level (i.e. $\sigma'_v = 1428$ kPa), a similar shift of the inter-aggregate modal pore size towards smaller dimensions has been detected for undrained unloading sample. The decrease of frequency of inter-aggregate pores could be linked to the partial destructuration of the treated samples which induces local collapse of larger pores upon drained unloading, also evidenced by the lower void ratio detected by MIP pertaining to the post-yield stress level drained unloading sample with respect to undrained unloading sample, as reported in Table 7.

Table 7: Comparison of initial void ratios (i) e back-calculated from the oedometer test and (ii) e_{MIP} measured by the mercury intrusion porosimeter

	e	e_{MIP} – undrained unloading	e_{MIP} – drained unloading
KF10 - 28 days - 358 kPa	1.29	1.34	1.45
KF10 - 28 days - 714 kPa	1.22	1.48	1.58
KF10 - 28 days - 1428 kPa	1.10	1.41	1.39

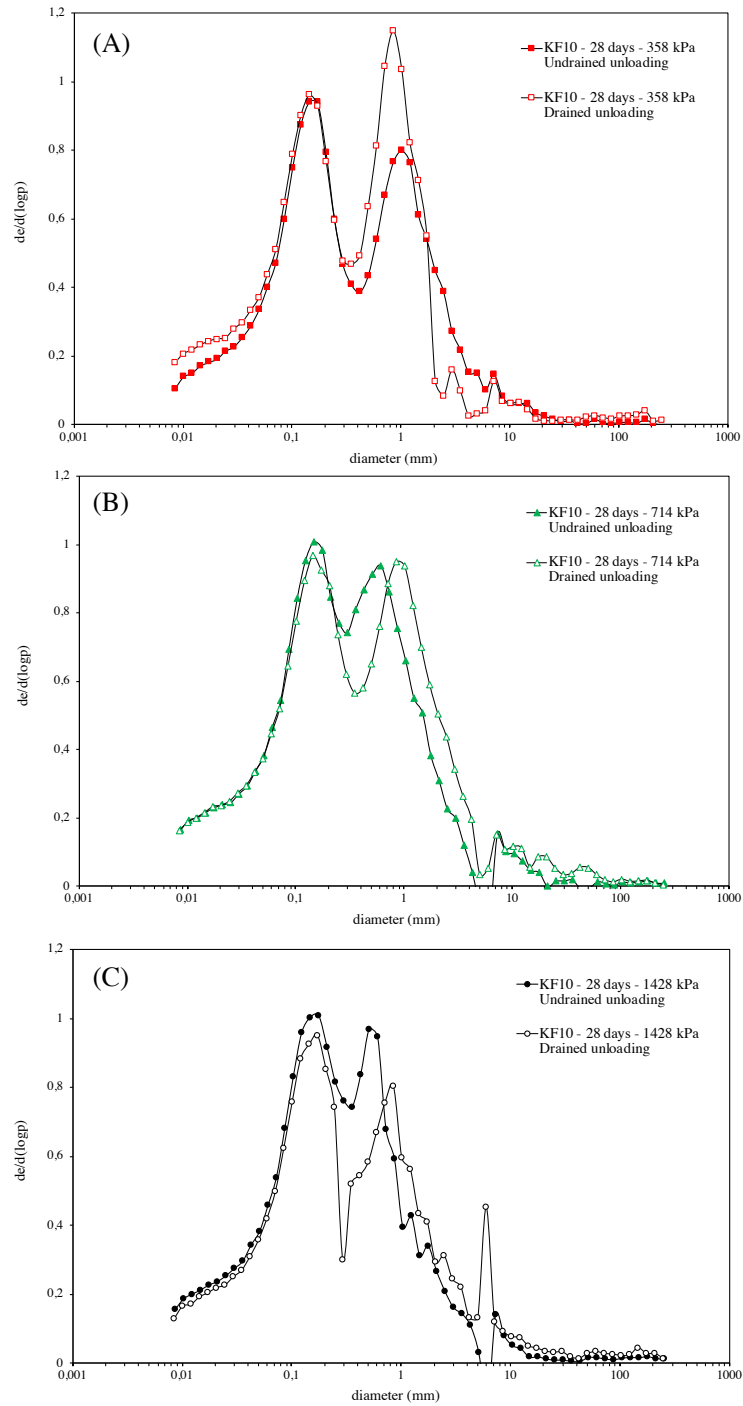


Figure 42: Comparison between frequency distributions of entrance pore sizes for drained and undrained unloading of the alkali activated fly ash binder treated soil KF10 at 28 days and at: (A) pre-yield stress level (358 kPa), (B) yield stress (714 kPa) and (C) post-yield stress (1428 kPa)

5.4.2 Shear strength

Direct shear tests were performed on raw and treated compacted kaolin samples. The initial and final conditions of the samples have been reported in Table 8.

Table 8: Initial and final conditions of shear box samples

Sample ID	e_0	w_0 (%)	S_0 (%)	e_f	w_f (%)	S_f (%)
Kaolin	1.60	61.56	100.00	1.29	49.65	100.00
KF10 - 1 day	1.70	65.07	100.00	1.37	52.49	100.00
KF10 - 7 days	1.70	65.20	100.00	1.39	53.54	100.00
KF10 - 28 days	1.54	59.07	100.00	1.36	52.31	100.00
KF20 - 7 days	1.76	67.40	100.00	1.38	51.91	100.00

Figure 43A&B show shear behaviour of the raw kaolin and the fly ash-based alkali activated binder treated soil KF10 as a function of time for a vertical confining stress of 100 kPa. Figure 43A particularly displays stress-strain curves. It shows that the raw kaolin presents a slight peak reaching a shear strength of 50 kPa and followed by a little softening, induced by compaction. The alkali activated treated samples KF10 at 1 and 7 days display a very similar behaviour than the raw kaolin implying that a negligible improvement of the soil shear strength occurs until 7 days. Whereas at 28 days the initial stiffness is higher at low strains. In addition, a clear peak is distinguished whose shear strength is largely higher and reaching 72 kPa. This higher stiffness and shear resistance are given by bonding provided by the alkali activated binder. Finally, the softening phase observed after reaching the maximum shear stress is more marked and clearly visible at 28 days. It is due to the destructuration stage of the structure leading to a strong decrease of the shear resistance.

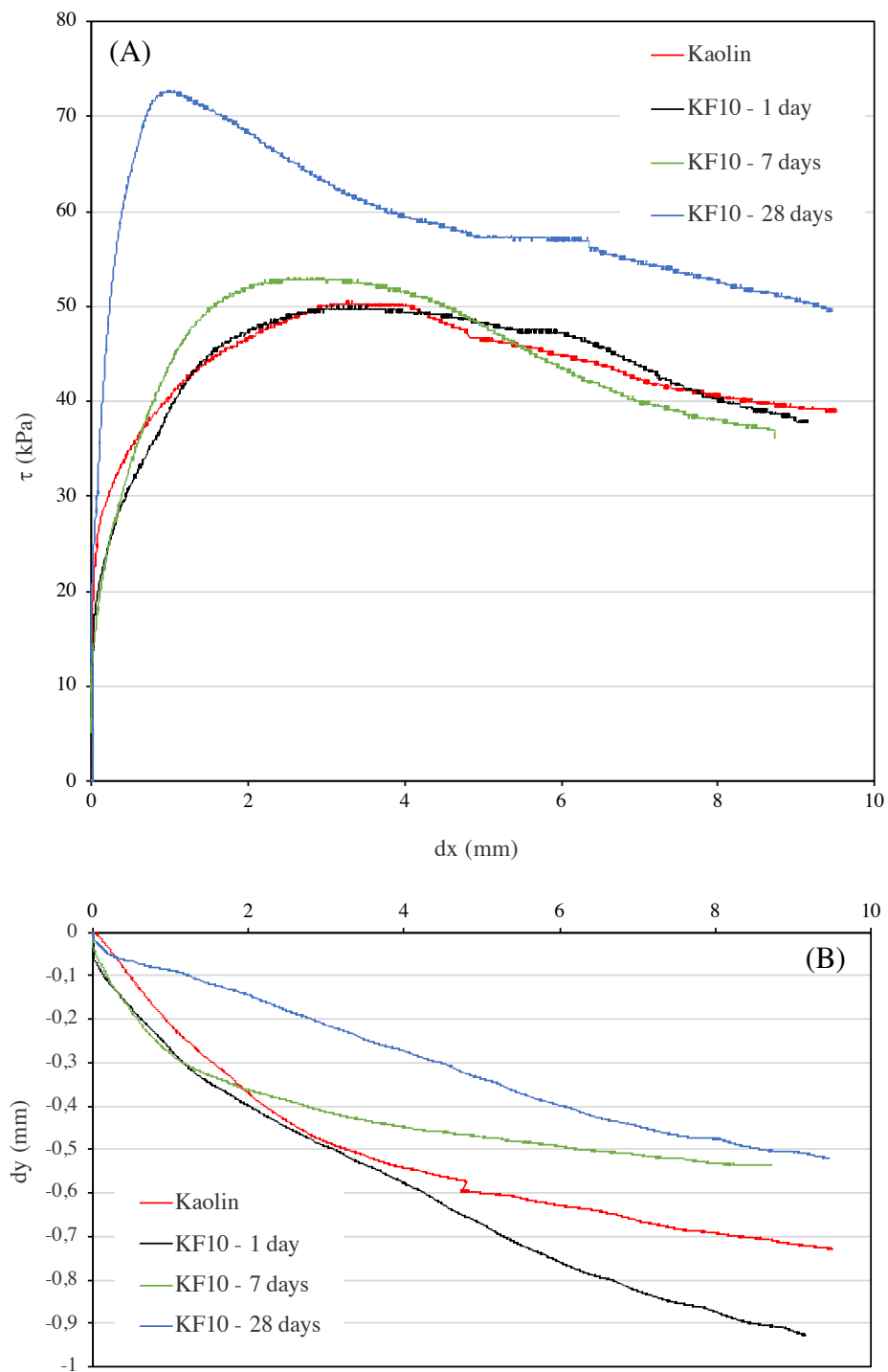


Figure 43: Direct shear test results ($\sigma'_v = 100$ kPa) on raw kaolin and alkali activated binder treated samples KF10 as a function of time (A) stress-strain curves and (B) associated volume changes

Consequently, and similarly to what observed from the oedometer tests in section 5.4.1 the improvement of the shear resistance is significant and effective after 28 days.

Figure 43B additionally displays volume changes against displacement. A contractive behaviour is observed for all samples i.e. the volume decreases with increasing shear.

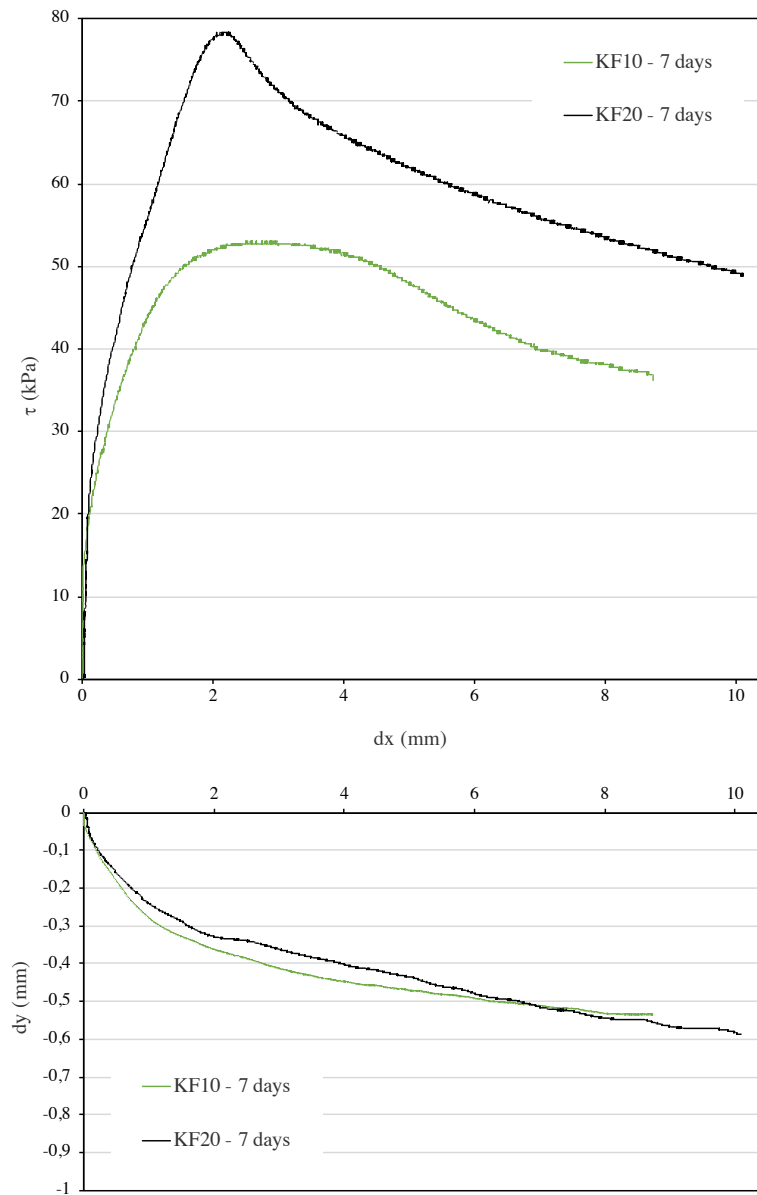


Figure 44: Comparison of direct shear tests of the alkali activated binder treated soils KF10 and KF20 at 7 days

Figure 44 shows a comparison of the shear behaviours of the alkali activated binder treated samples KF10 and KF20 after 7 days of curing. By comparison the alkali activated soil KF20 containing a higher content of reactive fly ash shows a higher stiffness and slightly lower volume change. Notably its stress-strain curve is very similar to the one of KF10 at 28 days i.e. the presence of a clear peak and a shear strength higher than 70 kPa. Increasing the content of binder hence leads to a faster effective improvement namely

within 7 days for KF20 instead of 28 days for KF10 due mainly to the higher amount of binding agents developing in the system.

5.4.3 Link between the microscopic and macroscopic scales

Mechanical testing shows that major improvements of the mechanical behaviour occur within 28 days, attesting of the successful formation of a binder over time. The formation of this binder introduces bondings between particles originating in an evolution of the macroscopic behaviour. Namely, this bonding is responsible of a progressive reduction of compressibility and increase of yield stress within 28 days. In fact, those observations strongly match with the observed physicochemical evolution showing that reactions essentially occur within 28 days, and hence that the new compounds responsible of bonding are formed during that time interval (Chapter 3). This is showed in Figure 45 which displays ^{29}Si MAS-NMR spectra of the raw fly ash and the alkali activated fly ash binder at 28 days and 6 months. A comparison of the spectrum of the raw fly ash with the spectra of the alkali activated fly ash binder over time clearly indicates the appearance of a new resonance located at -85 ppm, and associated with the formation of the binding phase. More specifically, it corresponds to Q^2 -type silicon environments in chain structure i.e. the formation of silicon chains combined with calcium for this system (3.4.1.5), and whose structure resembles the one of Calcium Silicate Hydrates encountered in Portland Cement. From 28 days to 6 months this resonance associated with the binding phase does not change neither in amplitude nor in chemical shift value indicating a negligible evolution of the binding phase in terms of both chemistry and atomic structure during that time interval, and explaining the achievement of an effective improvement of the mechanical response of the treated soil after 28 days of curing time.

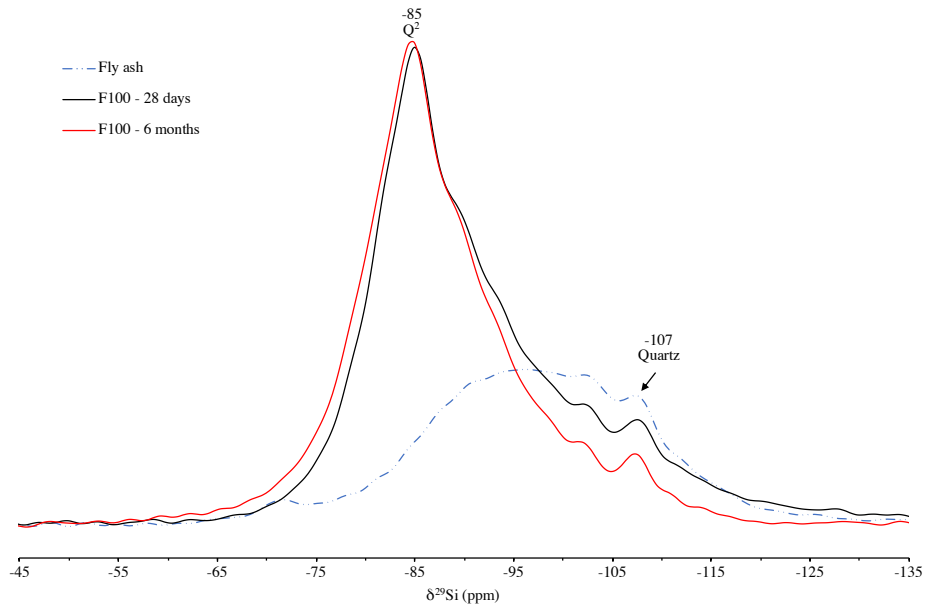


Figure 45: ^{29}Si MAS-NMR spectra of the raw fly ash and the binder F100 at 28 days and 6 months

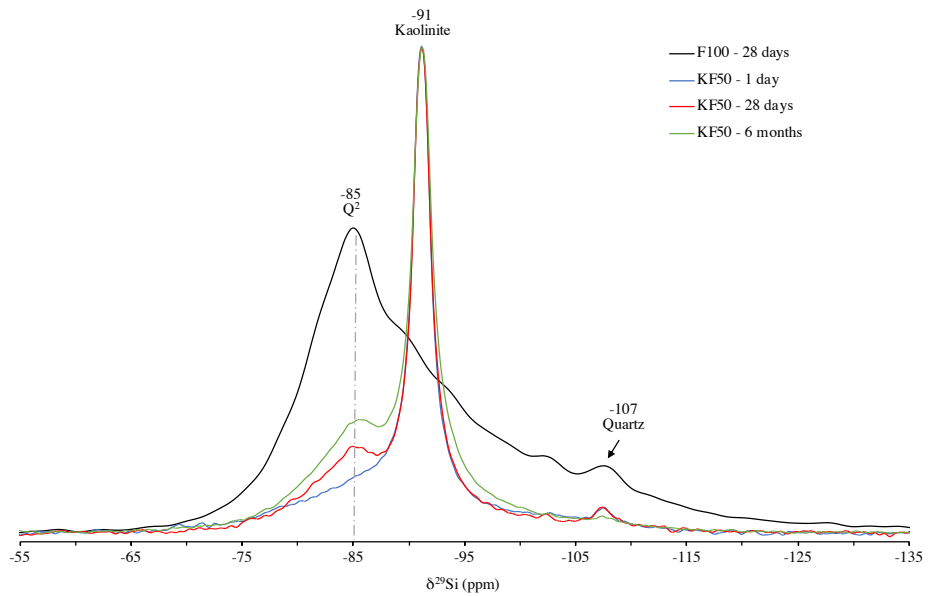


Figure 46: Comparison of ^{29}Si MAS-NMR spectra of the alkali activated binder F100 at 28 days and the alkali activated kaolin KF50 at 1 and 28 days

Figure 46 additionally shows a comparison of ^{29}Si MAS-NMR spectra of the alkali activated fly ash binder at 28 days formerly presented in Figure 45, and the treated soil

KF50 at 1 and 28 days. It is worth seeing that the formation of the new resonance located at -85 ppm and associated with the binding phase is also present for the treated soil evidencing the development of similar reactions for the binder and soil-binder mixes. This new resonance is less marked for the soil-binder mixture as the content of reactive fly ash is lesser and therefore fewer new compounds are formed. In addition, it shows that the resonance associated with kaolinite at -91 ppm does not undergo any modification over time showing its negligible reactivity. The binding phase solely therefore constitutes the main actor of the observed mechanical improvement.

Oedometer tests furthermore evidence the progressive evolution of the mechanical improvement over time. This progressive extent was also observed in 0 by Optical microscopy. It showed the local widening of the treated part comprising the new binding phase over time and around reactive calcium-rich particles. This local expansion through the matrix progressively involves more and more particles and fills the porosity of the material leading to the herein observed mechanical improvement.

Bonding is also responsible of a progressive increase of shear strength observed by the development of a resistance peak over time. This resistance peak is associated with a contractive behaviour upon shearing. However, when dealing with dense materials the feature of a peak stress is usually associated with a dilative behaviour i.e. an expansion of the volume during shearing (Head, 1994). By contrast, the contractive behaviour observed in our alkali activated binder treated soil hence suggests that the observed resistance peak is due solely to the presence of the binding phase. Upon shearing the breakage of the bonding would favour a contractive behaviour. Nevertheless, the vertical stress having been set up to 100 KPa i.e. largely below yield, those results should be further validated experimentally by performing additional direct shear tests at higher vertical stresses i.e. 700 KPa and above.

Direct shear test additionally shows that the mechanical improvement is more effective as the content of fly ash is higher. In fact, the improvement is more effective when increasing the amount of fly ash from 10 to 20 %. Our previous study about the physicochemical evolution of that system showed that the products formed in terms of atomic structure remain similar whatever the proportion of added binder (3.4.2). Therefore, the high shear strength reached earlier when the amount of binder is higher is due to the same newly formed binding phase but in a larger amount.

5.5 Conclusions

The development of a novel binder that is an alkali activated calcium-rich fly ash for clay soil stabilisation was explored. The study of its resistance to compression and shear forces both shows that the relevant improvement of mechanical response is achieved after 28 days for 10 % of added binder.

When subjected to one-dimensional compression the treated soil shows a relevant increase of stiffness compared to the raw kaolin. The addition of the alkali activated binder also leads to an increase of the yield stress which reaches 700 kPa at 28 days. The range of stresses to which the soil is subjected to limited strains under reversible behaviour is hence largely increased by the binder development and maintained until the yield stress of 700 kPa. Beyond that stress level the newly formed bonding agent breaks leading to a destructure stage. Furthermore, an investigation of the microstructural changes of the treated soil induced by loads evidences how elastic and plastic strains are associated to changes of dimension and frequency of inter-aggregates pores.

Treated soil progressively develops a shear resistance over time clearly visible after 28 days of curing and associated to a contractile behaviour.

Those mechanical results are in accordance with the physicochemical evolution of the system that showed a reaction sequence development essentially occurring within 28 days from the dissolution of reactive compounds from fly ash to the formation of the binding phase. The observed improvements of the mechanical behaviour are hence a result of the formation of a binding phase creating bonding between soil particles.

This study confirms a positive feasibility potential of using fly ash-based alkali activated binder for clay soil stabilisation. A deeper understanding of the mechanical properties is hence of interest in view of suitable geotechnical applications.

5.6 References

- Askeland, D.R., Fulay, P.P., Wright, W.J., 2011. *The science and engineering of materials*, 6th ed. ed. Cengage Learning, Stamford, CT.
- ASTM D 3080-90, 1994. Standard test method for direct shear test of soils under consolidated drained conditions. *Annu. Book ASTM Stand.* 04.08., 290–295.
- Buchwald, A., Kaps, C., Hohmann, M., 2003. Alkali-activated binders and pozzolan cement binders—complete binder reaction or two sides of the same story, in: *Proceedings of the 11th International Conference on the Chemistry of Cement*. Portland Cement Association Durban, South Africa, pp. 1238–1246.
- Chemeda, Y., 2015. Effect of hydrated lime on kaolinite surface properties and its rheological behaviour. *Université de Nantes*.
- Cristelo, N., Glendinning, S., Fernandes, L., Pinto, A.T., 2012. Effect of calcium content on soil stabilisation with alkaline activation. *Constr. Build. Mater.* 29, 167–174. <https://doi.org/10.1016/j.conbuildmat.2011.10.049>
- Cristelo, N., Glendinning, S., Teixeira Pinto, A., 2011. Deep soft soil improvement by alkaline activation. *Proc. Inst. Civ. Eng. - Ground Improv.* 164, 73–82. <https://doi.org/10.1680/grim.900032>
- Delage, P., Audiguier, M., Cui, Y.-J., Howat, M.D., 1996. Microstructure of a compacted silt. *Can. Geotech. J.* 33, 150–158. <https://doi.org/10.1139/t96-030>
- Head, K.H., 1994. *Manual of Soil Laboratory Testing Volume 2: Permeability, Shear Strength and Compressibility Tests*. Second Edition, ELE International Limited.
- Pedrotti, M., Tarantino, A., 2017. An experimental investigation into the micromechanics of non-active clays. *Géotechnique* 1–18.
- Provis, J.L., van Deventer, J.S.J. (Eds.), 2014. *Alkali Activated Materials, RILEM State-of-the-Art Reports*. Springer Netherlands, Dordrecht.
- Rios, S., Cristelo, N., Viana da Fonseca, A., Ferreira, C., 2016. Structural Performance of Alkali-Activated Soil Ash versus Soil Cement. *J. Mater. Civ. Eng.* 28, 4015125. [https://doi.org/10.1061/\(ASCE\)MT.1943-5533.0001398](https://doi.org/10.1061/(ASCE)MT.1943-5533.0001398)
- Russo, G., Modoni, G., 2013. Fabric changes induced by lime addition on a compacted alluvial soil. *Géotechnique Lett.* 3, 93–97. <https://doi.org/10.1680/geolett.13.026>
- Scrivener, K.L., Kirkpatrick, R.J., 2008. Innovation in use and research on cementitious material. *Cem. Concr. Res.* 38, 128–136. <https://doi.org/10.1016/j.cemconres.2007.09.025>
- Shi, C., Krivenko, P.V., Roy, D.M., 2006. *Alkali-activated cements and concretes*. Taylor & Francis, London ; New York.
- Silva, R.A., Oliveira, D.V., Miranda, T., Cristelo, N., Escobar, M.C., Soares, E., 2013. Rammed earth construction with granitic residual soils: The case study of northern

Portugal. Constr. Build. Mater. 47, 181–191.
<https://doi.org/10.1016/j.conbuildmat.2013.05.047>

Singhi, B., Laskar, A.I., Ahmed, M.A., 2016. Investigation on Soil–Geopolymer with Slag, Fly Ash and Their Blending. Arab. J. Sci. Eng. 41, 393–400.
<https://doi.org/10.1007/s13369-015-1677-y>

Tarantino, A., De Col, E., 2008. Compaction behaviour of clay. Géotechnique 58, 199–213.

Tenn, N., Allou, F., Petit, C., Absi, J., Rossignol, S., 2015. Formulation of new materials based on geopolymer binders and different road aggregates. Ceram. Int. 41, 5812–5820.
<https://doi.org/10.1016/j.ceramint.2015.01.010>

Vitale, E., Deneele, D., Russo, G., Ouvrard, G., 2016. Short-term effects on physical properties of lime treated kaolin. Appl. Clay Sci. 132–133, 223–231.
<https://doi.org/10.1016/j.clay.2016.04.025>

Wilkinson, A., Haque, A., Kodikara, J., 2010. Stabilisation of clayey soils with industrial by-products: part A. Proc. Inst. Civ. Eng. - Ground Improv. 163, 149–163.
<https://doi.org/10.1680/grim.2010.163.3.149>

Conclusions

This study had a twofold purpose. Firstly, it aimed at developing an alkali activated binder suitable for the particular application of soil stabilisation and the understanding of its reactivity and general features. Secondly, it aimed at investigating the interaction between the developed binder and the soil selected that is kaolin. In addition, the research strategy was approached by developing a multi-scale study in order to manage the system as a whole for any future application.

The multi-scale study herein conducted evidences that the particle, microstructural and mechanical levels are derived from one another as changes occur within a similar timeframe for all scale levels. Especially the following conclusions can be drawn (also summarized in Figure 47):

At particle level, kaolin soil being mainly unreactive the physicochemical evolution of the binder and soil-binder mixture are similar that is:

- The reaction sequence essentially occurs within 28 days;
- Calcium-containing phases derived from fly ash are the reactive phases, while the vitreous phase from fly ash remains mainly unreactive;
- The new compounds formed are thenardite Na_2SO_4 , and an amorphous silicate consisting of chains combined with calcium probably incorporating three-dimensional four-fold aluminium environments and whose structure resembles the one of Calcium Silicate Hydrate encountered in Portland cement.

At microstructural level, similar tendencies of microstructural evolution are seen for the binder and the soil-binder mixture that are:

- Microstructural changes mainly occur around the reactive calcium-containing phases derived from fly ash;
- The dissolution of calcium-rich phases leads to the formation of new compounds that first cover the grain surfaces and then further grow into the available space resulting in a spreading of the binding phase through the material matrix;
- The evolution of the pore network over time is characterized by a progressive filling of capillary pores by new compounds while small nanometric pores are being formed over time and associated with the newly formed amorphous silicate-calcium chains;
- Different heterogenous matrices of various porosity and arrangement are formed across the material and owed to the high heterogeneity of fly ash whose particles locally react differently.

At a macroscopic level:

- The relevant improvement of mechanical response of the treated soil is achieved after 28 days of curing time corresponding to the time required for the chemical reactions to occur;
- The addition of the alkali activated binder to the soil leads to an increase of both the compressive strength and yield stress over time. Especially, a stiffness twice higher than the original kaolin is measured for 10% of added binder;
- An increase of the shear resistance also occurs with the progressive development of a resistance peak over time, associated with a contractive behaviour upon shearing.

Those observed general features at each scale level closely resemble those of Portland cement and hence strongly suggest a positive feasibility potential of using alkali activated materials in the particular application of soil treatment. In addition, the knowledge of the binder evolution at different scale levels also helps building confidence about the performance of the material formed and its behaviour over time.

Some further developments are worth noted to strengthen the confidence of using alkali activated binder for soil stabilisation:

- A new compound formed is an amorphous silicate consisting of chains combined with calcium. Because of the presence of calcium, this new compound can easily be carbonated at the air leading to a potential decrease of mechanical strength. It would be hence of interest to verify the durability of the treated soil subjected to a curing at the air. Another new compound is thenardite Na_2SO_4 . Thenardite is a highly soluble salt in water. Hence, it would also be important to check the durability of the material subjected to wetting-drying cycles.
- Fly ash is a highly inhomogeneous industrial waste that is within a similar batch or regarding its country origin. Therefore, it is highly important to understand the impact of the fly ash source on the reactivity and properties of the treated soil. A key point for the future could be to distinguish classes of fly ash for which the reactivity and mechanical improvement remains in a similar range. This study aimed at providing a point of reference to compare other systems comprising different fly ashes or other reactive aluminosilicate with the final purpose to generalise those processes following the selected reactive precursor.
- To begin with this study considered solely kaolin as a soil. It would be of great interest to verify the behaviour of the treated soil selecting soils of different mineralogical composition.

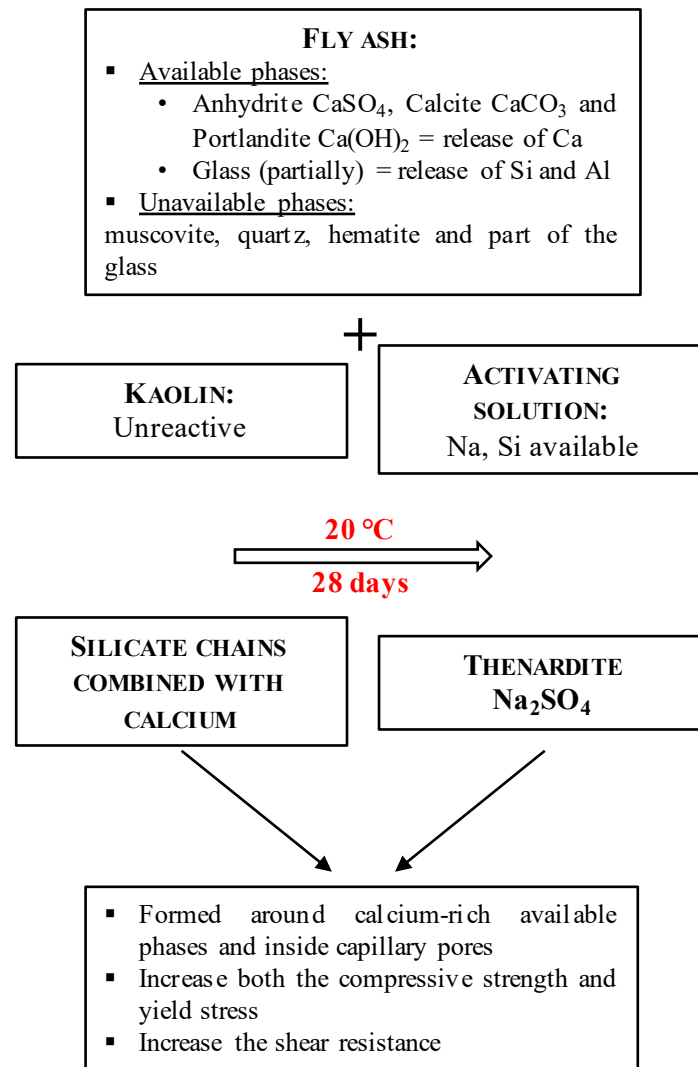


Figure 47 Conceptual model of alkaline activation of a calcium-rich fly ash for kaolin treatment

List of Figures

Figure 1: Components of alkali activated material and geopolymer products	8
Figure 2: Conceptual model for geopolymerisation from Duxson et al. (2007)	10
Figure 3: Polycondensation reaction of monomers leading to the formation of K–A–S–H type phases (Davidovits, 2017)	13
Figure 4: Proposed structural model for K-Poly(sialate-siloxo) Geopolymer (Davidovits, 1994)	13
Figure 5: Local environments of silicon described by the Q _n notation	15
Figure 6: Si-NMR of alkali activated material vs. geopolymer product (Davidovits, 2017)	16
Figure 7: Al-NMR of geopolymer product (Davidovits, 2017)	17
Figure 8: Schematic representation of (a) 1:1 layer, (b) 2:1 layer type clay	27
Figure 9: XRD of raw fly ash and fly ash-based alkali activated material F100 as a function of curing time; A=anhydrite; C=calcite; F=feldspar; H=hematite; M=muscovite; P=portlandite; Q=quartz; T=thenardite	45
Figure 10: DTG curves of raw fly ash and fly ash-based alkali activated material F100 as a function of curing time	46
Figure 11: FTIR of raw fly ash and fly ash-based alkali activated material F100 as a function of curing time in the CO ₃ ²⁻ stretching vibrations range	47
Figure 12: FTIR of raw fly ash and fly ash-based alkali activated material F100 as a function of curing time in the SO ₄ ²⁻ stretching vibrations range; 681, 616 and 596 cm ⁻¹ = anhydrite CaSO ₄ ; 639 and 617 cm ⁻¹ = thenardite Na ₂ SO ₄	47
Figure 13: SEM observations of a calcium-rich nodule from the alkali activated fly ash at 1 day: (A) SEM micrograph, (B) chemical composition (wt. %) of areas 1 and 2, (C) and (D) chemical mappings of calcium and sulphur respectively	48
Figure 14: SEM micrographs of the alkali activated fly ash binder F100 (A) at 1 day and (B), (C) and (D) at 28 days; C=calcium nodules; Q=quartz; arrows=glass	49
Figure 15: ²⁷ Al MAS-NMR spectra of the raw fly ash and alkali activated fly ash at 28 days	50

Figure 16: ²⁹ Si MAS-NMR spectra of the raw fly ash and alkali activated fly ash at 28 days.....	52
Figure 17 pH curves of the fly ash-based alkali activated material F100 as a function of curing time	53
Figure 18: FTIR of the raw kaolin and alkali activated kaolin (A) KF50 and (B) KF20 as a function of curing time in the OH stretching vibrations range.....	54
Figure 19: XRD of the alkali activated kaolin KF50 as a function of curing time; A=anhydrite; C=calcite; F=feldspar; H=hematite; K=kaolinite; M=muscovite; P=portlandite; Q=quartz; T=thenardite.....	55
Figure 20: XRD of the alkali activated kaolin KF20 as a function of curing time; A=anhydrite; C=calcite; F=feldspar; H=hematite; K=kaolinite; M=muscovite; P=portlandite; Q=quartz; T=thenardite.....	55
Figure 21 SEM micrographs of the alkali activated kaolin KF50 (A) at 1 day and (B), (C) and (D) at 28 days; C=calcium nodules; Q=quartz; red arrows=glass; blue arrows=kaolinite platelets.....	56
Figure 22: ²⁷ Al MAS-NMR spectra of the alkali activated fly ash F100 at 28 days and alkali activated kaolin KF50 at 1 and 28 days.....	57
Figure 23: ²⁷ Al MAS-NMR of the alkali activated kaolin KF20 at 1 and 28 days	58
Figure 24: ²⁹ Si MAS-NMR spectra of the alkali activated fly ash F100 at 28 days and alkali activated kaolin KF50 at 1 and 28 days.....	59
Figure 25: ²⁹ Si MAS-NMR of the alkali activated kaolin KF20 at 1 and 28 days	59
Figure 26 Comparison of the pH curves as a function of curing time for the treated soils KF50 and KF20	60
Figure 27: SEM micrographs of the raw fly ash; C=calcium-rich particle; F=feldspar; G=glass; Q=quartz.....	77
Figure 28: Optical microscopy images of the alkali activated fly ash binder F100 (A) and (B) after 24 hours, (C) and (D) at 28 days; C=calcium-rich particle....	78
Figure 29: SEM observations of the alkali activated fly ash binder F100 after 24 hours of curing: (A) SEM micrograph, and chemical mappings of: (B) calcium, (C) sulphur, (D) silicon and (E) sodium.....	80
Figure 30: SEM observations of the alkali activated fly ash binder F100 after 24 hours of curing: (A) SEM micrograph, and chemical mappings of: (B) calcium, (C) sulphur, (D) silicon and (E) aluminium	81
Figure 31: SEM observations of the alkali activated fly ash binder F100 at 28 days: (A) SEM micrograph, and chemical mappings of: (B) calcium, (C) sulphur, (D) silicon and (E) aluminium	83
Figure 32: SEM observations of the alkali activated fly ash binder F100 at 28 days: (A) SEM micrograph, and chemical mappings of: (B) silicon, (C) calcium and (D) sulphur.....	84

Figure 33: Comparing SEM microstructural changes of the alkali activated fly ash binder F100 at 28 days around: (A) a calcium-rich nodule labelled C, and (B) a particle from the vitreous phase labelled G; M1 = dense matrix; M2 = porous matrix	85
Figure 34: Comparing mercury intrusion porosimetry tests of the alkali activated fly ash binder F100 over time and in terms of (A) cumulative intrusion volume ratios, (B) intrusion volume frequency ratios as a function of entrance pore size	87
Figure 35: Optical microscopy images of the alkali activated fly ash binder treated soil KF50 (A) and (B) after 24 hours, (C) and (D) at 28 days, C=calcium-rich particle	89
Figure 36: SEM micrographs of the alkali activated fly ash binder treated soil KF50 at (A) 24 hours and (B) 28 days	90
Figure 37: Comparing mercury intrusion porosimetry tests of the alkali activated fly ash binder treated soil KF50 over time and in terms of (A) cumulative intrusion volume ratios, (B) intrusion volume frequency ratios as a function of entrance pore size	91
Figure 38: 3D printed mold (A) design of the base, (B) design of the cover and (C) assemblage of the mold	103
Figure 39: One-dimensional compression tests on the raw and alkali activated binder treated kaolin (KF10) as a function of time	106
Figure 40: Schematic illustration of MIP samples preparation for one-dimensional loads induced microstructural effects analysis	107
Figure 41: Comparison between frequency distributions of entrance pore sizes tests of the alkali activated fly ash binder treated soil KF10 at 28 days as a function of the applied stress and for a drained unloading	108
Figure 42: Comparison between frequency distributions of entrance pore sizes for drained and undrained unloading of the alkali activated fly ash binder treated soil KF10 at 28 days and at: (A) pre-yield stress level (358 kPa), (B) yield stress (714 kPa) and (C) post-yield stress (1428 kPa)	110
Figure 43: Direct shear test results ($\sigma'_v = 100$ kPa) on raw kaolin and alkali activated binder treated samples KF10 as a function of time (A) stress-strain curves and (B) associated volume changes	112
Figure 44: Comparison of direct shear tests of the alkali activated binder treated soils KF10 and KF20 at 7 days	113
Figure 45: ^{29}Si MAS-NMR spectra of the raw fly ash and the binder F100 at 28 days and 6 months	115
Figure 46: Comparison of ^{29}Si MAS-NMR spectra of the alkali activated binder F100 at 28 days and the alkali activated kaolin KF50 at 1 and 28 days	115
Figure 47 Conceptual model of alkaline activation of a calcium-rich fly ash for kaolin treatment	123

List of Tables

Table 1: Chemical composition (wt. %) of raw fly ash and kaolin	42
Table 2: Samples composition wt. %.....	43
Table 3: Average elemental composition (wt. %) of F100 and KF50 denser areas at 28 days.....	50
Table 4: Compared reactivity sequences of kaolin treated either by lime, or a mix of lime and fly ash or an alkali activated fly ash	61
Table 5: Initial and final conditions of oedometer samples	105
Table 6 Comparison of Compressibility index C_c before and after major yield	106
Table 7: Comparison of initial void ratios (i) e back-calculated from the oedometer test and (ii) e_{MIP} measured by the mercury intrusion porosimeter	109
Table 8: Initial and final conditions of shear box samples	111